SECTION 4

ANALYSIS OF NEW PROJECT CONCEPTS/IDEAS

CONTENTS

4.1 MODULAR INTERGRADED SOLAR/THERMAL FLAT PLATE COLLECTOR

Soteris A. Kalogirou, Georgios Florides, Andreas Savvides, Constantinos Christofi, Charalambos Tsioutis, Constantions Vassiliades, Rafaela Agathokleous, Gregoris Panayiotou

4.1.1 Concept

Existing building materials can act as the back plate of a flat plate collector. An integrated water or air collector can thus be built on a building façade or roof. Using copper pipes and water as a circulating medium, or air in ducts, the falling solar energy can be absorbed and transformed into heat. The units are proposed to provide additional thermal insulation to the building, whilst producing useful amounts of hot water or air that could be used for the occupant needs and comfort.

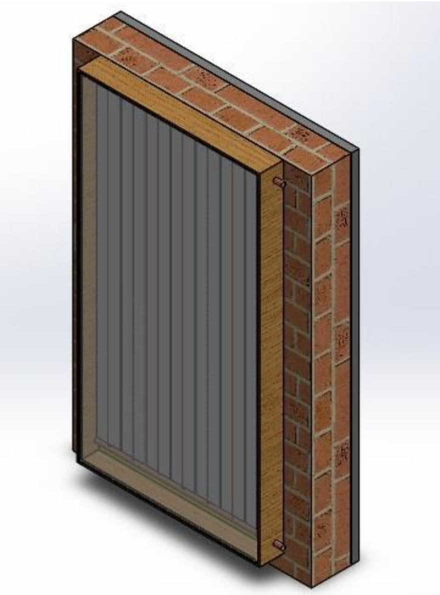

(a)

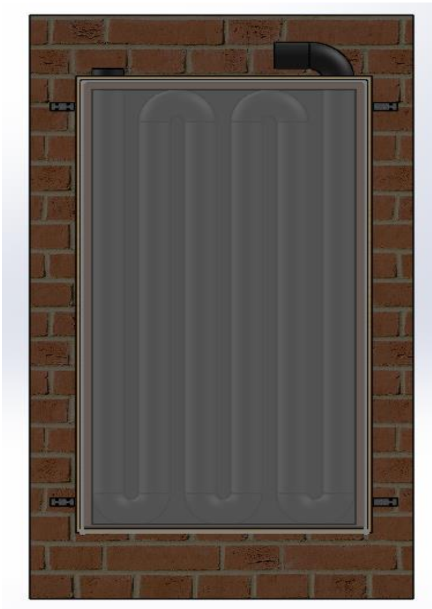

(b)

Figure 4.1.1. Image of the prototypes utilising the building materials as a back plate and providing (a) hot water and (b) air for the occupant needs.

The constructed unit utilises the face of an existing brick wall where an extra insulation is placed on the front face of the wall.

In the case of the hot water collector, a conventional copper plate with copper pipes is positioned in front of the insulation and the unit is framed in a wooden box and covered with glass. Using the same operating principle as a flat plate collector the unit heats domestic hot water by catching and storing solar energy. The working Heat Transfer Fluid (HTF) is water, that can be stored in an insulating vessel and be used when needed. It can also be used as a circulating fluid of the heat exchanger of a hot water cylinder.

In the case of the hot air collector, the hot air can be circulated either directly in a room to race its temperature or blended with the air in a duct system. A visualization of both systems are shown in Figure 4.1.1.

4.1.2 Application

The modular façade integrated Solar/Thermal Flat plate collector, as all other similar BISTS, is designed to:

- Reduce building cooling loads in warm climates and heat loss in cool climates by providing additional insulation to the building fabric

- Provide direct thermal energy generated on site by either heating water or air and therefore lower the power requirements of the building

- Reduce the carbon footprint of the building by using renewable energy

The units being modular can be used in the façade or roof of a building. These units can be used across a range of domestic and commercial building structures and typologies, substituting common envelope elements in both existing and new structures.

4.1.3 Physical description

4.1.3.1 Physical description and detailing

Engineering drawings were prepared for full size modules taking into account available construction and engineering material specifications and dimensions. The drawings were followed and the prototypes were fabricated according to specifications. Figure 4.1.2 shows the four prototype units mounted onto a building wall.

Figure 4.1.2a, shows the integrated hot water collector. The unit was enclosed in a wooden frame, with dimensions 1.72 m x 0.92 m and 120 mm deep, that was mounted on a vertical brick wall 1.8 m x 1.2 m x 200 mm thick, facing south and covered with 40 mm plaster on the backside. In the frame an insulating layer of glass wool, 30 mm thick, was placed on the wall. The absorbing plate consists from seven, 1.6 m x 0.15 x 0.4 mm thick, corrugated copper strips on which 7 copper pipes of 15 mm in diameter were welded. The absorber was placed in front of the insulation and covered with a 5 mm glass. In this case the system was connected to a hot water cylinder allowing the system to work with natural convection.

Figure 4.1.2b shows the integrated hot air collector utilising an aluminium foil duct. The unit was enclosed in a wooden frame, with inside dimensions 1.72 m x 0.92 m and 170 mm deep, that was mounted on a vertical brick wall 1.8 m x 1.2 m x 200 mm thick, facing south and covered with 40 mm plaster on the backside. In the frame an insulating layer of glass wool, 30 mm thick, was placed on the wall. In front of the insulation was placed an absorbing mild steel plate, 0.4 mm thick, and 5 loops of aluminum tube (6 running lengths) of 100 mm in diameter and painted black. The enclosing frame was covered with a 5 mm glass. Additionally, the system was connected to a two speed air fan for extracting the air of the collector.

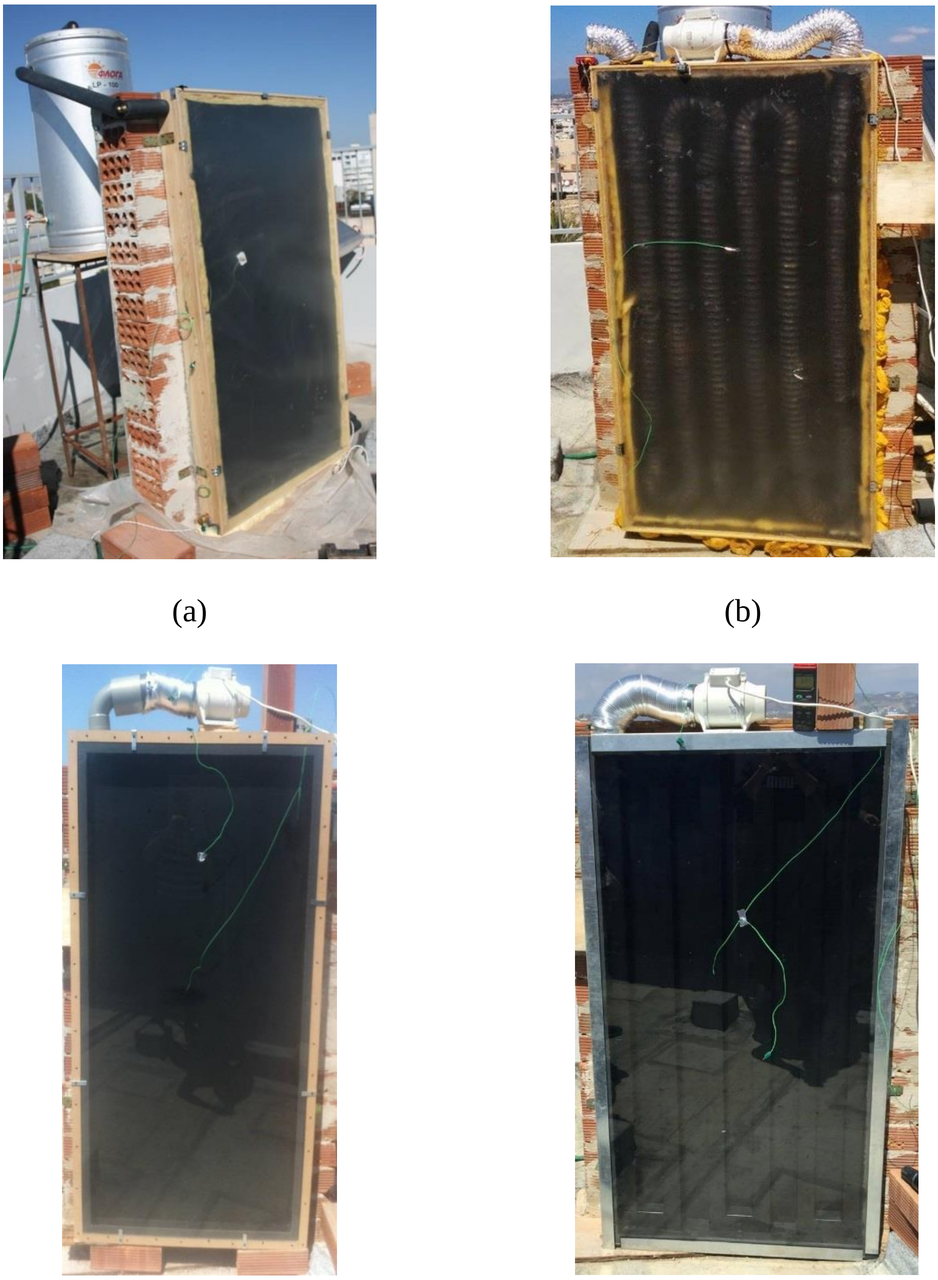

(a) (b)

(c) (d)

Figure 4.1.2. Prototype constructions, (a) integrated hot water collector (b) integrated hot air collector utilising an aluminium foil duct (c) integrated hot air collector with internal metal separators (d) integrated hot air collector with a mild steel square tube duct.

Figure 4.1.2c shows the integrated hot air collector with internal metal separators. The unit was enclosed in a wooden frame, with inside dimensions 1.735 m x 0.94 m and 76.6 mm deep, that was mounted on a vertical brick wall 1.8 m x 1.2 m x 200 mm thick, facing south and covered with 40 mm plaster on the backside. In the frame an insulating layer of glass wool, 50 mm thick, was placed on the wall. In front of the insulation was placed a mild steel plate, 1.0 mm thick. On the plate seven vertical mild steel separators were glued with high temperature silicone. In this way 8 linked compartments were created, forming a continuous tube. On top, an absorbing mild steel plate 0.6 mm thick was glued with high temperature silicone. The absorbing plate was then painted black. The enclosing frame was covered with a

5 mm glass. The sites of the wooden frame in this case, were also insulated. Additionally, the system was connected to a two speed air fan for extracting the air of the collector.

Figure 4.1.2d shows the integrated hot air collector with a mild steel square tube duct. The unit was enclosed in a wooden frame, with inside dimensions 1.635 m x 0.84 m and 76.6 mm deep, that was mounted on a vertical brick wall 1.8 m x 1.2 m x 200 mm thick, facing south and covered with 40 mm plaster on the backside. In the frame an insulating layer of glass wool, 50 mm thick, was placed on the wall. In front of the insulation was placed a mild steel absorber plate, 0.5 mm thick. On the plate a continuous welded pipe, made of six vertical mild steel runs of square tube 6 cm x 6cm x 1.5mm thick, were placed. The absorbing plate and the tube was then painted black. The enclosing frame was covered with a 5 mm glass. Additionally, the system was connected to a two speed air fan for extracting the air of the collector.

4.1.3.2 Engineering drawings

A series of engineering construction drawings are shown in Figure 4.1.3.

(a) Integrated hot water collector

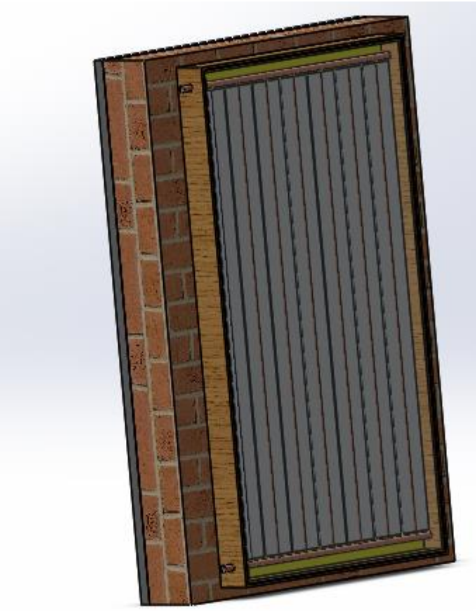

Assembly drawing

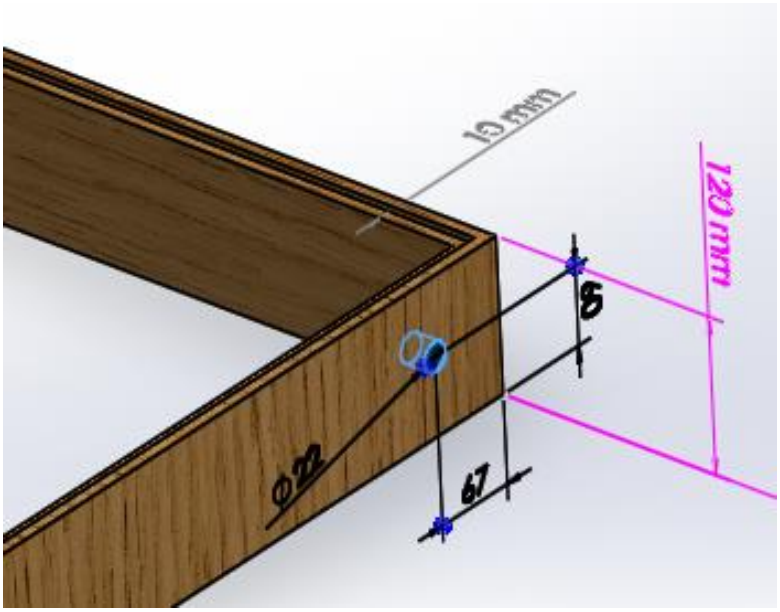

Detail of wooden frame (dimensions in mm)

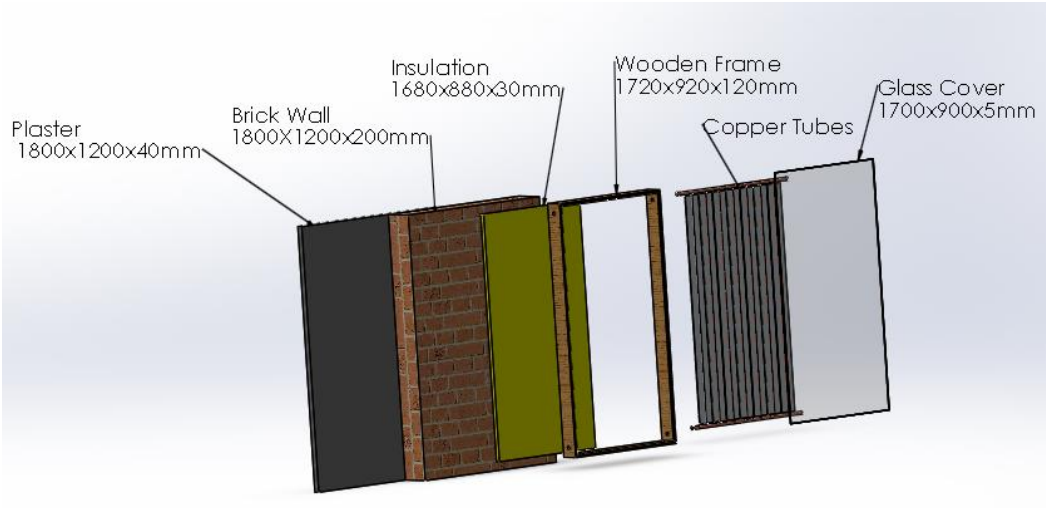

Expanded assembly showing details

(b) integrated hot air collector utilising an aluminium foil duct

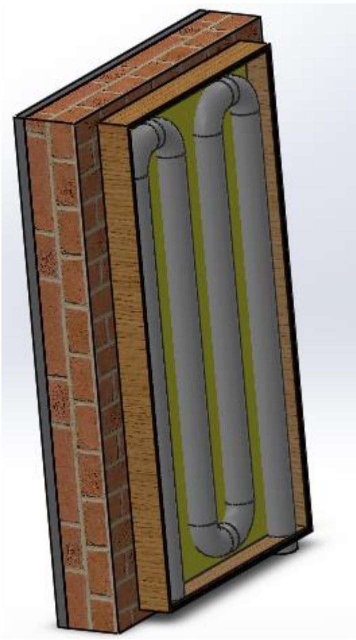

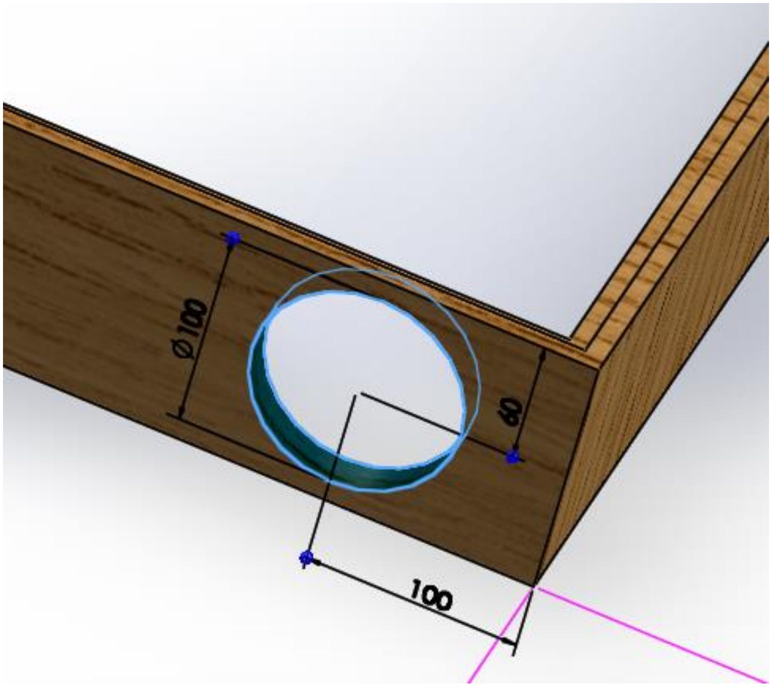

Assembly drawing

Detail of wooden frame (dimensions in mm)

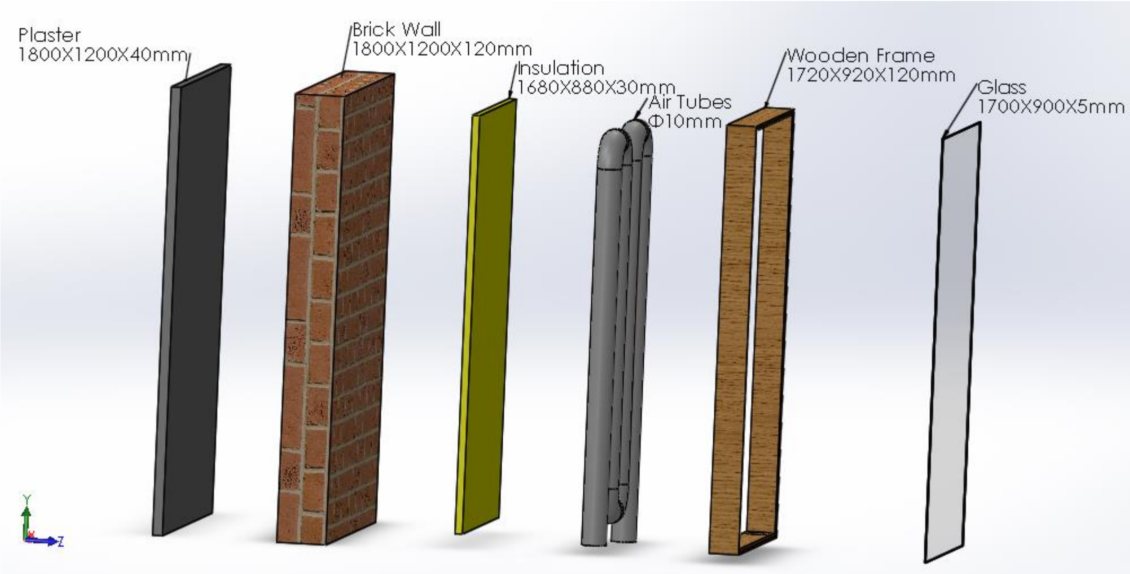

Expanded assembly showing details

(c) integrated hot air collector with internal metal separators

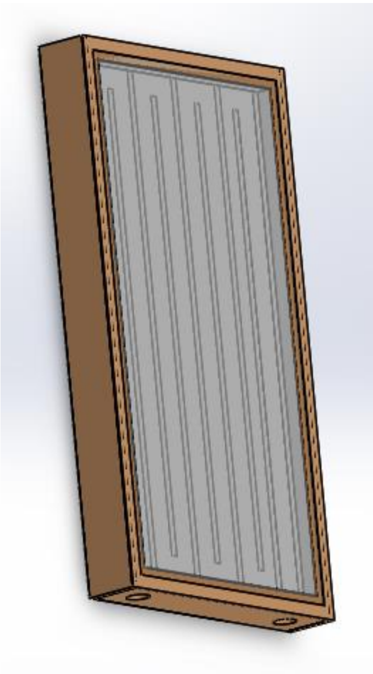

Assembly drawing

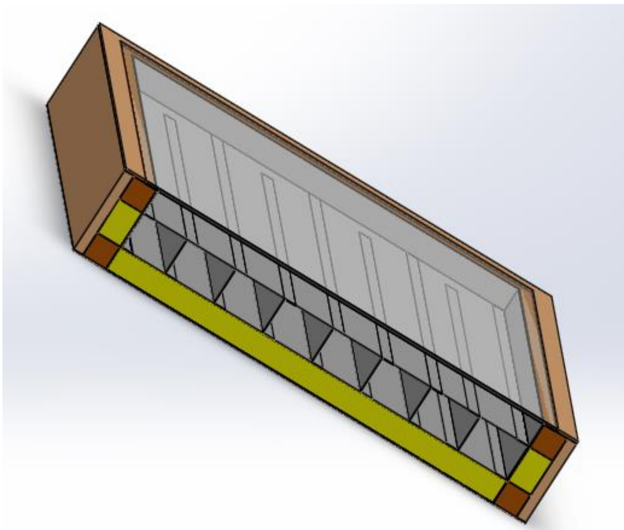

Section through the middle, showing separators in position, with insulation and top glass

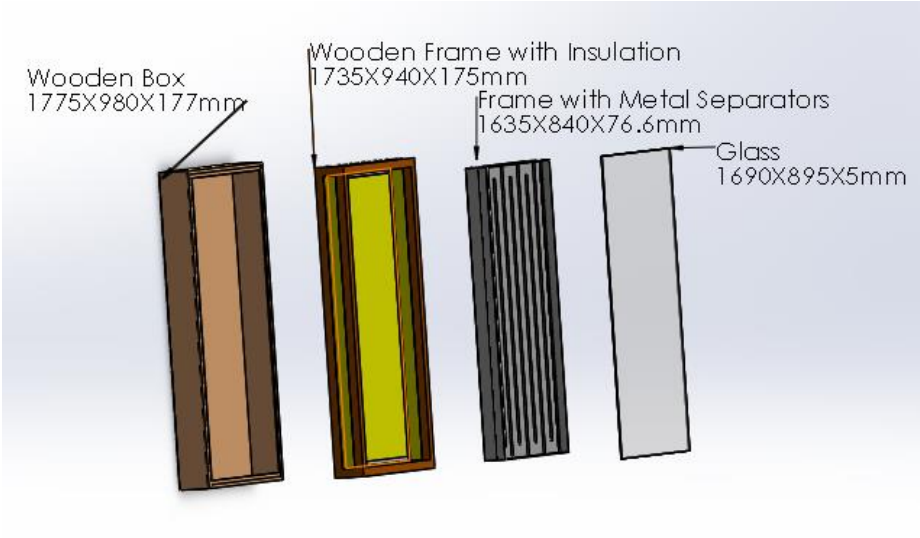

Figure 4.1.3. Expanded assembly showing details.

4.1.3.3 Materials

The full size prototype units constructed and tested at the Cyprus University of Technology can accept a number of modifications in order to suit specific building constructions and product requirements. The presented units though, consist of the following material components:

(a) Integrated hot water collector

- Frame
  - Wood, 1.72 m x 0.92 m x 15 mm thick
  - Peripheral insulation, glass wool 30 mm
  - Fixed on the wall with 4 galvanised steel angle brackets
- Enclosed construction
  - Backside insulation, glass wool 30 mm
  - 7 absorbing corrugated copper strips 1.6 m x 0.15 x 0.4 mm thick, on which 7 copper pipes 15 mm in diameter were welded.
  - Copper heater and riser 22 mm in diameter.
  - Matt black absorber paint on front surface (spray applied)
- Cover
  - 5 mm low iron glass
- Insulated hot water tank
  - capacity 100lt

- Miscellaneous
    - Screws and bolds
    - Sealants (1 tube of silicon)
    - Copper pipe 22mm in diameter
    - 22 mm Copper pipe compression fittings
    - Copper pipe insulation - Armaflex Class O Tube Black 2m x 25mm x 28mm

(b) Integrated hot air collector utilising an aluminium foil duct

- Frame
    - Wood, 1.72 m x 0.92 m x 15 mm thick
    - Peripheral insulation, glass wool 30 mm
    - Fixed on the wall with 4 galvanised steel angle brackets
- Enclosed construction
    - Backside insulation, glass wool 30 mm
    - Mild steel plate 1.7 m x 0.885 x 0.4 mm thick
    - 5 loops of aluminum tube (6 running lengths and 11m in total) of 100 mm in diameter, painted black
    - Matt black absorber paint on front surface (spray applied)
- Cover
    - 5 mm low iron glass
- Air fan
    - Power 25 Watts
    - Air mass flow 0.019 kg/s

Miscellaneous

- Screws and bolds
- Sealants (1 tube of polyurethane foam)

(c) Integrated hot air collector with internal metal separators

- Frame
    - Wood, 1775 x 980 x 177 mm, 20mm thick
    - Peripheral insulation, glass wool 50 mm
    - Fixed on the wall with 4 galvanised steel angle brackets
- Enclosed construction
    - Backside, glass wool 50 mm
    - Mild steel back plate 1635 x 840 x 1mm
    - 7 separator Length1561mm, Π-Section 25 x 75 x 25mm, 0.8 mm thick plate.
    - Mild steel top plate 1631 x 836 x 0.6mm
    - Matt black absorber paint on front surface (spray applied)
- Cover
    - 5 mm glass of dimensions 1690 x 895mm
- Air fan
    - Power 25 Watts
    - Air mass flow 0.019 kg/s
- Miscellaneous
    - Screws and bolds
    - Sealants
    - High temperature silicone

(d) Integrated hot air collector with a mild steel square tube duct

- Frame
    - Wood, 1.72 m x 0.92 m x 15 mm thick
    - Peripheral insulation, glass wool 30 mm
    - Fixed on the wall with 4 galvanised steel angle brackets
- Enclosed construction
    - Backside insulation, glass wool 30 mm
    - Mild steel plate 1.7 m x 0.885 x 0.4 mm thick

- Mild steel square tube 6 cm x 6 cm x 1.5 mm thick, (6 running lengths and 11m in total), painted black
- Matt black absorber paint on front surface (spray applied)

- Cover
  - 5 mm low iron glass
- Air fan
  - Power 25W
  - 240 V
  - Air mass flow 0.019 kg/s
- Miscellaneous
  - Screws and bolds
  - Sealants

4.1.4 Physical fabrication

4.1.4.1 Fabrication process

The full size prototypes were mainly constructed from ready made parts found easily in the market. In a few cases, as for example in the case of the production of the mild steel plate of the integrated hot air collector utilising an aluminium foil duct, an industrial scale cutting and bending machine was used. In other cases, a cutting band saw and a welding machine were needed for the fabrication of the absorbing square tube. The prototype units were completed to specifications as detailed in the engineering drawings. Figures 4.1.4 to 4.1.7 detail the collectors' fabrication.

Figure 4.1.4. Positioning the ready-made absorbing plate in the integrated hot water collector.

Figure 4.1.5. Positioning the aluminium foil duct in the integrated hot air collector utilising an aluminium foil duct.

Figure 4.1.6. Fixing the internal metal separators in the integrated hot water collector with internal metal separators.

Figure 4.1.7. Painting black the integrated hot air collector with a mild steel square tube duct.

4.1.4.2 Assembly process

Once all parts were placed inside the frames and when needed were painted black, thermocouples were positioned at the appropriate places for monitoring the system temperatures. Finally, the units were sealed with the glass covers. Pyranometers and air flow meters were also placed in the right places for carrying out the performance tests. Figure

4.1.8, shows the monitoring instruments in position for testing the performance of the integrated hot air collector utilising an aluminium foil duct.

Figure 4.1.8. Pyranometer, air flow meter and temperature sensors in position for testing the performance of the integrated hot air collector utilising an aluminium foil duct.

4.1.5 Modular configuration

4.1.5.1 Unit size and dimensions

The complete units have a finished rectangular module size of approximately 1.7m x 0.9m. All connection ports are designed with access at the unit sides. The final mounting bracketing arrangement is to be determined.

4.1.5.2 Modularisation and up-scaling

The operation of the building integrated flat plate collectors was conceived to be modular with the configuration of the units in either series or parallel. Figure 4.1.9, shows an example of how a set of two coloured flat plate collector array can change the appearance of a building facet and Figure 4.1.10, shows one of the possible interconnections of the building integrated flat plate collectors. The full-scale systems could provide heat tailored to a building load and occupant needs.

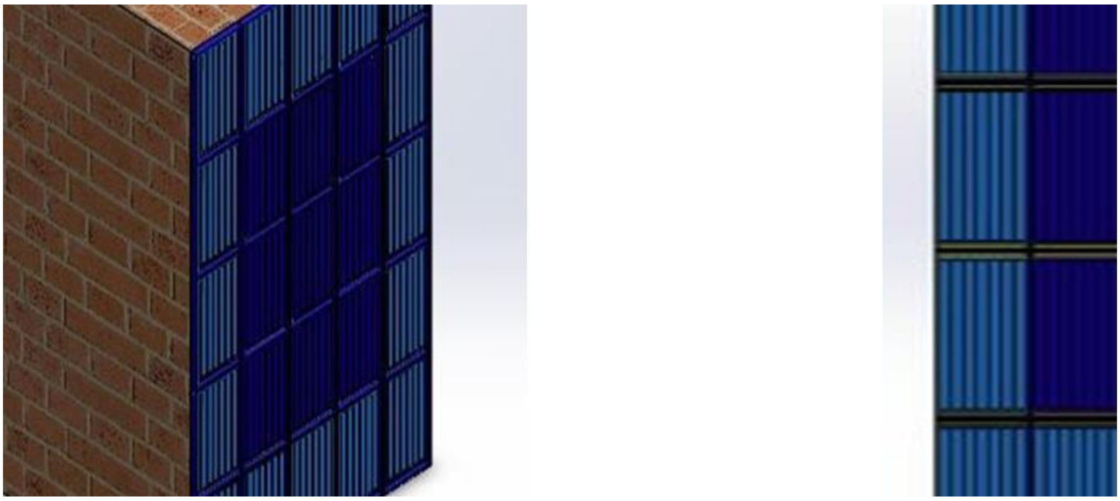

Figure 4.1.9. A system of two coloured flat plate collectors covering a building facet (side and front view).

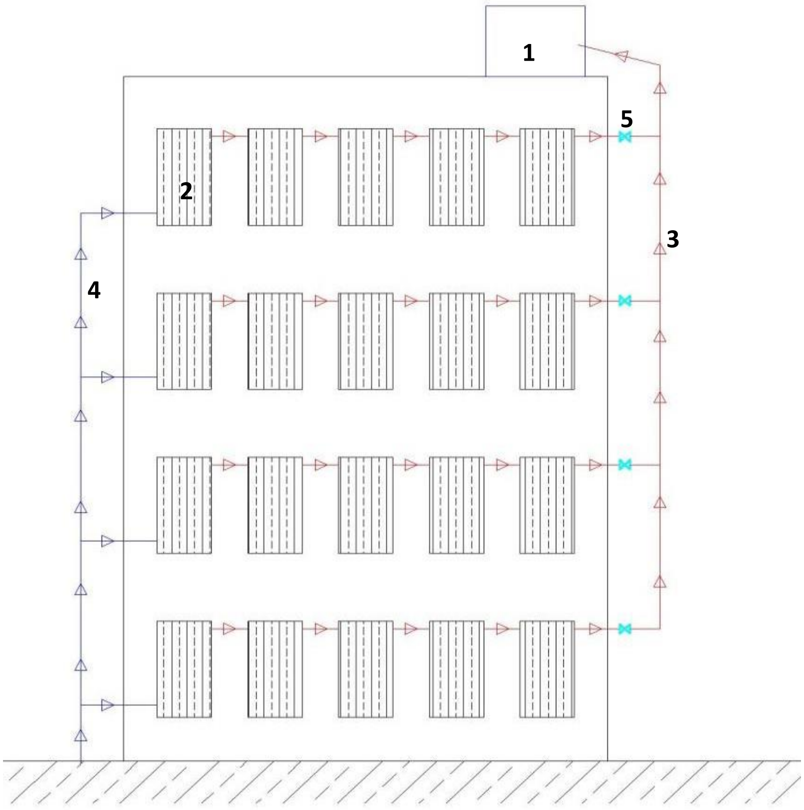

Figure 4.1.10. One of the possible interconnections of the building integrated flat plate collectors.

4.1.6 Product development

To commercialise the building integrated flat plate collectors is not difficult because of the large scale production of the common flat plate collectors. Readymade components can easily be found and the tailored-made parts can simply be manufactured with standard industrial processes. Various materials can also be interchanged (e.g. the wooden frame with plastic or aluminium material) without affecting the efficiency.

4.1.7 Physical mounting/installation

4.1.7.1 Structural integration

The system's building integration is done by the mounting of the system on the static body and the masonry of the building. Thus, the structural efficiency of the walls and the system itself is secured. Moreover, the masonry accommodates the system's piping.

4.1.7.2 Section Detailing

The system is mounted or placed within the building's masonry in such a manner that it becomes a part of it, as shown in Figures 4.1.11 and 4.1.12. The construction is such that it can accommodate a conventional opening (e.g. window), in the position of which, the system's module is placed. The back of the system is closed with conventional masonry, in order not to be perceived internally by the users of the building. In selected internal locations, control points are placed.

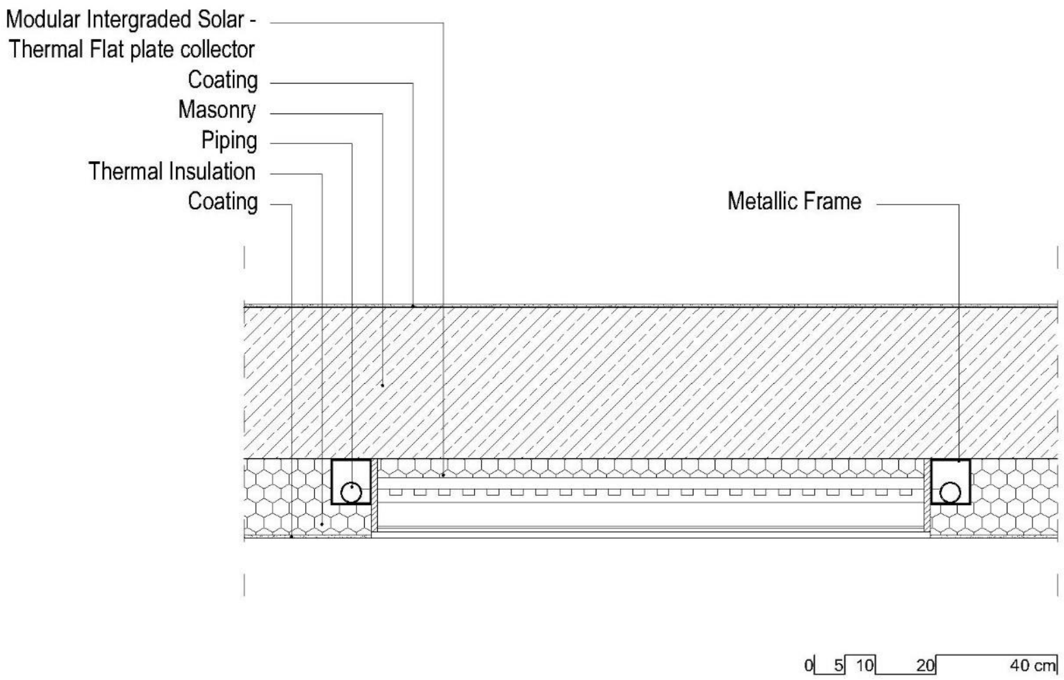

Figure 4.1.11. Horizontal section detail.

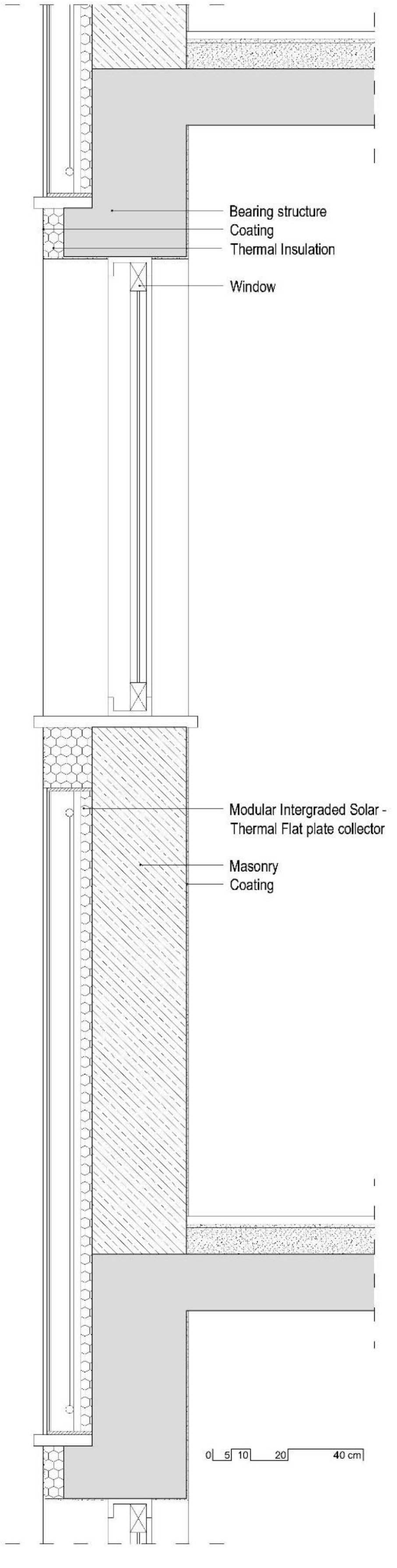

Figure 4.1.12. Vertical Section.

4.1.7.3 Weather proofing and specific conditions influence

The mounting of the system is done in such a way that its thermal insulation is a continuation of the building's insulation, ensuring its adequacy for weather conditions. At the same time, this configuration provides the maximum possible insulation because the combination of the system with the insulation of the shell reduces to a minimum the geometrical thermal bridges. The positioning of a second wall behind the system (Figures 4.1.11 and 4.1.12) ensures the continuity of the shell thus providing the necessary fire safety. Furthermore, the continuity of the shell provides the necessary soundproofing.

4.1.7.4 Services interconnection

Regarding services interconnection, they will connect to the system through a metal frame which is placed on the side of the module (Figure 4.1.11). In relation to the piping between two modules that are placed within a distance and in relation to the pipes that will start from the system to go to the machinery space, they will pass in the conventional way (through the walls) as with any other building piping.

4.1.7.5 Relevant regulations

The full integration of the system in the building walls and its interconnection with the conventional systems and piping, along with the fact that its construction and building integration takes into account all the above, makes its use viable without violating any potential regulations.

4.1.8 In situ artist impression

4.1.8.1 Images and perspectives

Figure 4.1.13 shows how the system could be integrated in a small ground floor building layout.

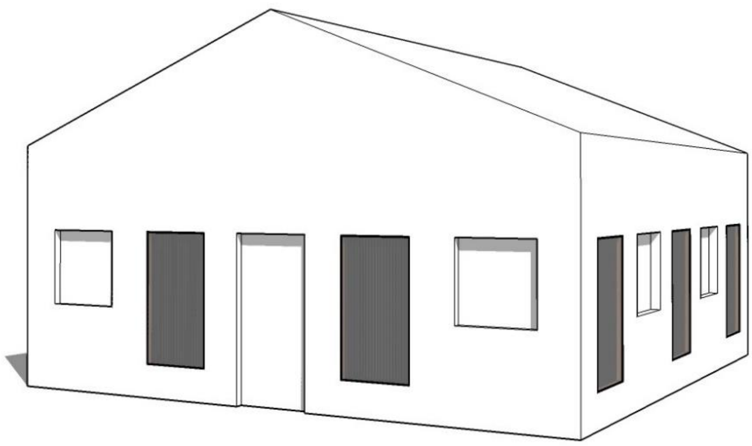

Figure 4.1.13. Integration on small building.

Figures 4.1.14, 4.1.15 and 4.1.16 show possible building integrations of the system in multi-storey buildings, where there are several solutions.

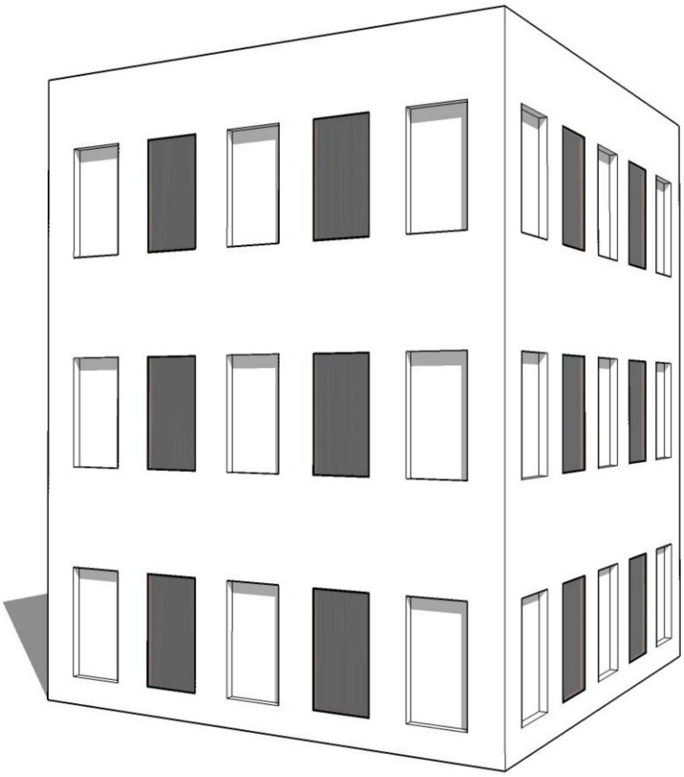

Figure 4.1.14. Integration on a multi-storey building.

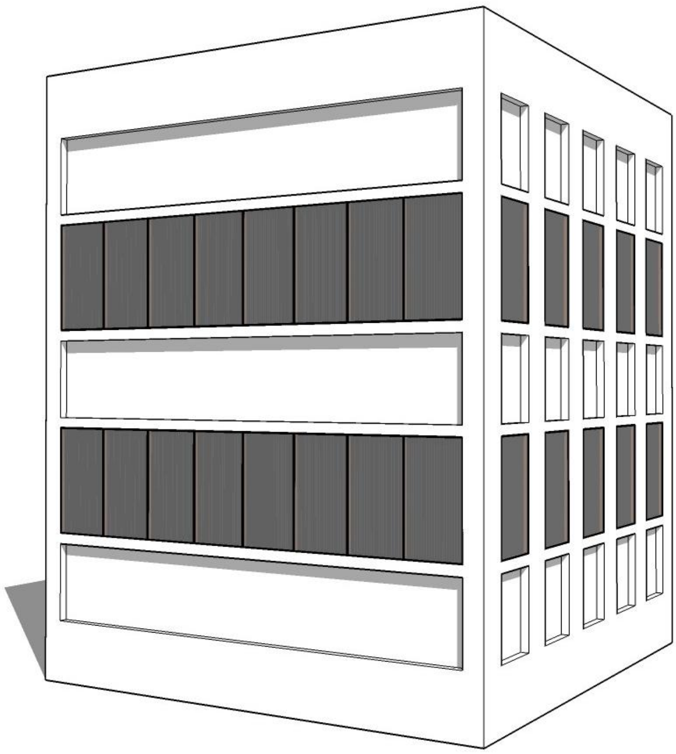

Figure 4.1.15. Integration on a multi-storey building.

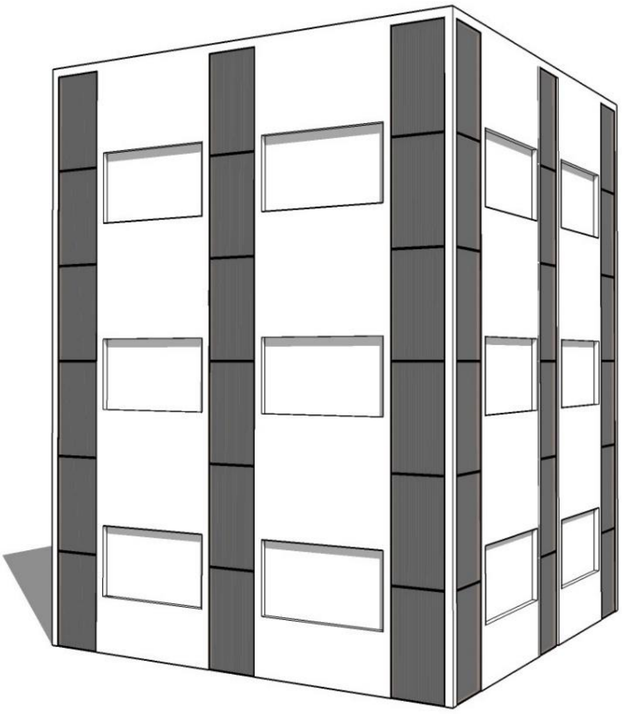

Figure 4.1.16. Integration on a multi-storey building.

4.1.8.2 Influence on aesthetics, appearance, empathy

The building integration (as shown in Figures 4.1.13, 4.1.14, 4.1.15, 4.1.16, 4.1.17) of this system can follow the basic design principles of the building in which it is integrated. Its square shape helps it to replace openings while the creation of multiple-module sequences can be placed in horizontal or vertical arrays which can be easily integrated into a building's design principles.

Figure 4.1.17. Realistic visualization of the system integrated on a multi-storey building.

4.2 HYBRID PHOTOVOLTAIC/SOLAR THERMAL (HYPV/T) FAÇADE MODULE

Mervyn Smyth, Ahmed Besheer[1], Aggelos Zacharopoulos, Jayanta D. Mondol, Adrian Pugsley[1], Andreas Savvides[2], Constantinos Vassiliades[2]

4.2.1 Concept

The innovative modular HyPV/T façade concept integrates a novel cascade thermal diode configuration in an Integrated Collector/Storage (ICS) solar water heater with PV cells into a single multi-functional facade element (Figure 4.2.1). It builds upon research conducted over 12 years, combining innovative solar technologies with building architecture. Installed on a building façade, the unit is proposed to provide additional thermal insulation, whilst producing useful amounts of hot water and generating electricity.

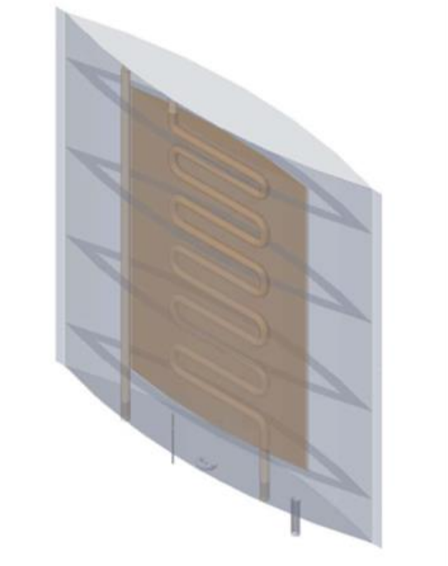

Figure 4.2.1. Image of the prototype HyPVT unit based on an elliptical profile.

The unit is a step improvement and advancement on prior art based on a thermal diode ICS solar water heater, using the same operating principle to pre-heat domestic hot water by catching and storing solar energy. The innovative thermal diode promotes solar collection during the day but reduces thermal losses at night whilst incorporating an integrated PV module. The design is based on two structural vessels, arranged to create a cavity between the walls of the inner (thermal storage) and outer (solar absorbing) vessels. In this instance, the vessels are flat and rectangular, allowing for solar radiation to be captured effectively during the solar day and aid easier façade integration. The cavity contains a liquid/vapour phase change material as the working Heat Transfer Fluid (HTF) which is maintained at a sub-atmospheric pressure. The HTF is in direct contact with the solar absorbing surface of the outer vessel (and effective wetted surface area). During collection periods solar radiation incident on the outer (absorbing surface) vessel, causes the HTF to evaporate at low

[1] Non COST member but worked on this project.

[2] Contributed only to the architectural integration demonstrations.

temperature thus producing a vapour. The vapour fills the cavity and condenses on contact with colder inner (thermal storage) vessel surface with the collected thermal energy transferred to the water store through latent heat exchange. Condensed water runs down the vessel wall to the HTF reservoir, upon which the produce of evaporation/condensation is repeated. During non-collection periods no heat transfer takes place as the HTF temperatures are not high enough to cause evaporation. The inner store is now thermally isolated from the outer vessel, thus retaining the stored heat for longer periods.

4.2.2 Application

The modular façade integrated HyPVT solar collector is designed to:

- Reduce heat loss in cool climate conditions and reduce cooling loads in warm climate conditions by adding an additional insulating element to the building fabric

- Provide an energy saving by augmenting the thermal energy and power requirement of the building by direct on site generation

- Integrate renewable energy technology to comply with current building regulations and reduces carbon footprint

The multi-functionality of the unit provides a unique product concept. The unit is predominately seen to be a modular system for use in façade mounted applications (note: an inclined version is being developed). The unit can be used across a range of building structure buildings.

4.2.3 Physical description

4.2.3.1 Physical description and detailing

A full size prototype design was developed and engineering drawing prepared. The drawings were supplied to fabrication specialists and the prototype HyPVT unit completed to specification. Figure 4.2.2 details the prototype unit complete with PV module. The unit was designed with elliptical (Egyptian eye) profile, with dimensions 1m x 1m and 150mm deep, to provide an inherent structural strength to withstand the forces put upon the vessel under evacuation. The basic unit was made from an external 1.2mm thick SS 304 outer vessel supported by an internal exo-skeleton. The inner (thermal storage) vessel was of a similar elliptical profile with a volume of 27 litres under no vacuum and of 28.1 litres when under vacuum. A value of 30 litres per m^2 is deemed suitable for ICS type solar water heaters by much of the presented literature.

Figure 4.2.2. Prototype HyPVT unit with PV panel ready for testing.

The HyPV/T collector unit is proposed to be encased in a weather tight enclosure. The sides and back are made from white acrylic capped ABS and along with a 50mm thick insulating layer, form the outer unit casing. The aperture front is made from clear (UV treated) PETG which is a suitable transparent aperture material.

4.2.3.2 Engineering drawings

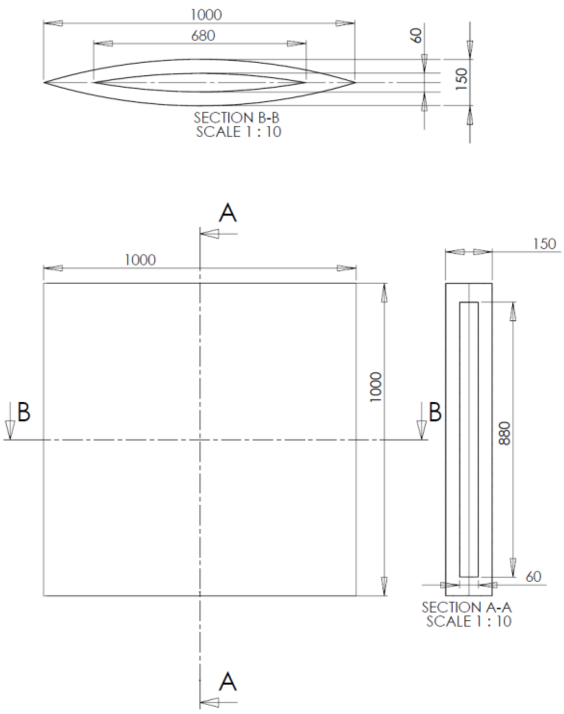

4.2.3.3 Materials

The full size prototype unit fabricated, assembled and tested at Ulster University is still in its infancy in terms of product design. A number of design enhancements and developments, along with DfM process are ongoing. The presented unit however, consists of the following material components:

Vessels

- Outer Vessel
    - 2 off 1m x 1m x 1.2mm 304 grade Stainless Steel sheet (TIG welded together)
    - 2 off end plates 1m x 0.075 x 1.2mm 304 grade Stainless Steel sheet (TIG welded together)
    - Internal structural support approx. 1m x 0.2m 1.2mm 304 grade Stainless Steel sheet (TIG welded together)
    - Thermal diode and HTF (IP protection)
    - Matt black absorber paint on front surface (spray applied)

<u>or</u>

- - Keratherm KP 98 bonding paste (brush applied if using PV option)

- Inner Vessel
    - 2 off 0.68m x 0.88m x 1.2mm 304 grade Stainless Steel sheet (TIG welded together)
    - 2 off end plates 0.68m x 0.075 x 1.2mm 304 grade Stainless Steel sheet (TIG welded together)
    - Internal structural support approx. 0.68m x 0.15m 1.2mm 304 grade Stainless Steel sheet (TIG welded together)
- Tank plumbing fittings
    - Approx. 0.6m long 15mmØ Stainless Steel pipe (TIG welded)
    - 4 off compression fittings to suit
    - 3 off 15mmØ isolating valves
    - Approx. 0.1m long 6mmØ Stainless Steel evacuation pipe (TIG welded)
    - 1 off 6mmØ evacuation isolating valve
    - Approx. 1m long 15mmØ flexible overflow hose

PV Panel (optional) - Solbian Sun Power Flexible Marine Solar (SP-112Q) module

- Peak Power Pmax 112W
- Nº of Cells 36
- Rated Voltage V_{mp} 19.7V
- Open Circuit Voltage V_{oc} 24V
- Rated Current Imp 5.7A
- Short Circuit Current I_{sc} 6.1A
- Dimensions mm 855 x 800
- Thickness mm 2
- Weight Kg 1.6

Casing element

- 1.1m x 1.1m x 0.25m deep outer back casing made from 3mm thick white acrylic capped ABS sheet (vacuum formed)
- 1.1m x 1.1m 2mm thick clear (UV treated) PETG transparent aperture casing
- Insulation (approx. 1.1m x 1.1m x 50mm thick Extruded Polystyrene Foam (XPS) (Blue Board)
- Screws (approx. 20 off 4mm self-taping screws)
- Sealants (approx. ¼ tube of silicon)

Mounting element

- Brackets (TBD)
- Screws and bolts (TBD)

4.2.4 Physical fabrication

4.2.4.1 Fabrication process

A full size prototype was fabricated in-house were possible with specialist fabrication included if needed. The prototype HyPVT unit was completed to specification as detailed in the engineering drawings. Figures 4.2.3 and 4.2.4 detail the vessel's fabrication.

Both the inner and outer vessels were fabricated from 1.2mm thick 304 grade Stainless Steel sheet. The various elements were cut from full size sheets and formed to the exact requirements. The front and back sheets of the inner vessel were initially tack (TIG) welded together, along with any structural elements and pipe connections. Once the vessel was checked, the vessel was fully welded. The same process was carried out for the outer vessel, and before the front panel was put in place, the inner vessel was fixed inside and secured. Again, after checking, the unit was fully welded. Once the unit was finished, the welds and surfaces were cleaned using a pickling paste.

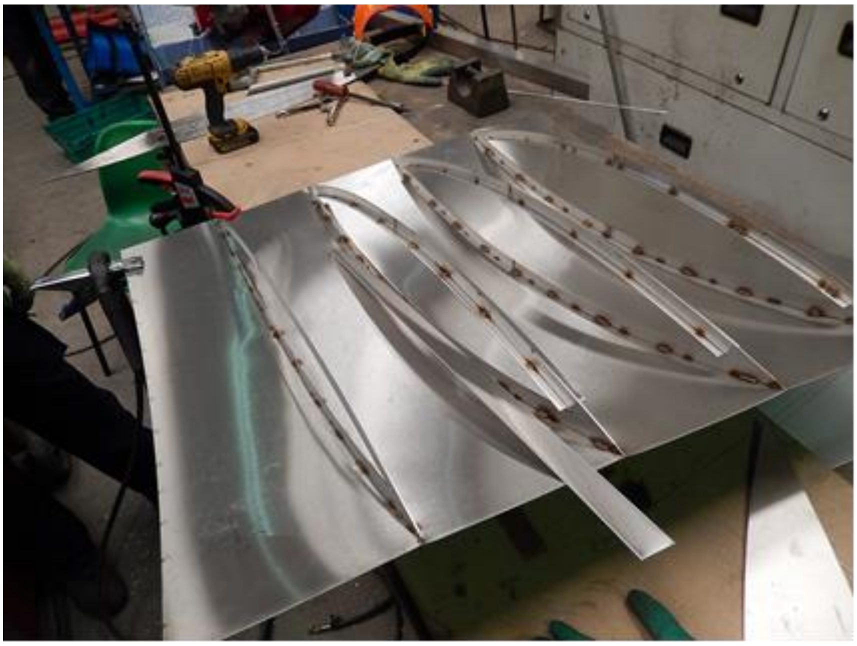

Figure 4.2.3. Fabrication process of the prototype HyPVT unit.

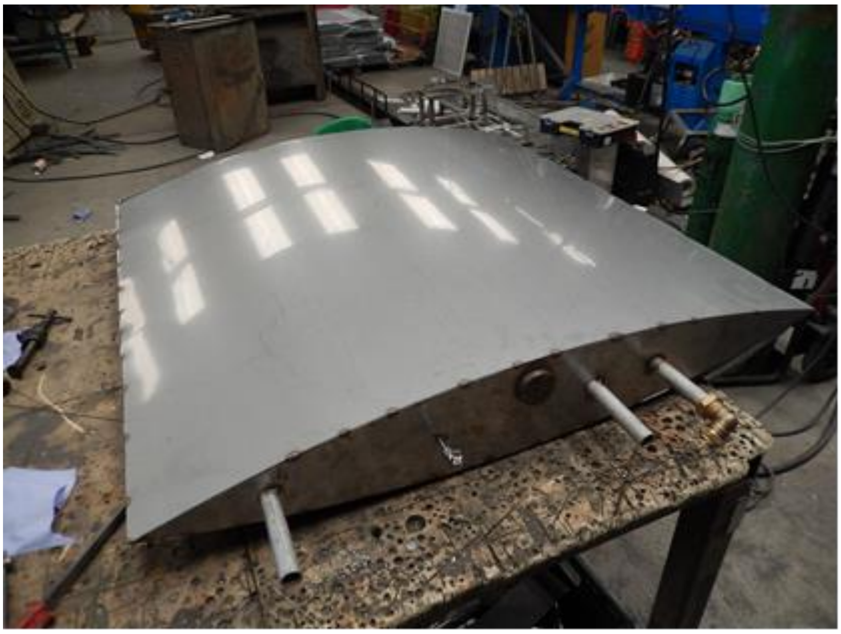

Figure 4.2.4. Final assembled prototype HyPVT vessel prior to welding and spraying.

The outer casing element was made from a vacuum formed sheet of 3mm thick white acrylic capped ABS sheet. An initial template was produced and a local specialist created the final unit. The outer transparent aperture casing was made from 2mm thick clear (UV treated) PETG sheet that was cut to suit the back casing dimensions.

4.2.5 Assembly process

Once the vessel and casing elements were fabricated, the various items were assembled. Depending upon the function, the outer absorbing surface of the vessel was either coated with sprayed matt black absorber paint finish (for solar thermal only) or Keratherm KP 98 bonding paste (brush applied) if using the PV/T option. At this stage all vessel fittings and valves were attached. The vessel was now placed into the outer casing, complete with back insulation. The vessel and insulation were secured using screw brackets and glue, respectively and all joints effectively sealed using the silicon. The front aperture cover was then inserted and fixed using the silicon gasket and screws. Figure 4.2.5 details the vessel (in solar thermal form) in a temporary casing prior to performance testing under a solar simulator.

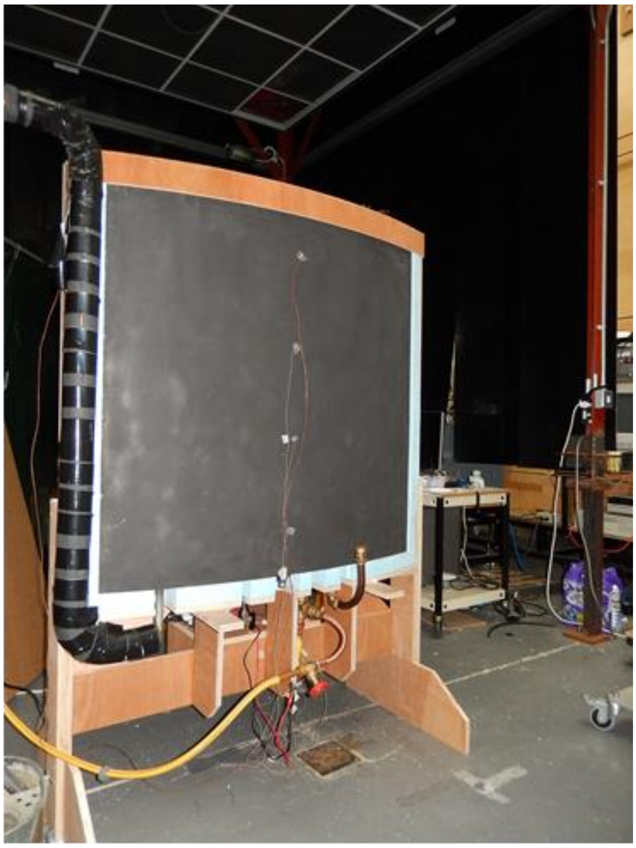

Figure 4.2.5. Prototype HyPVT unit in solar thermal option ready for testing.

4.2.6 Modular configuration

4.2.6.1 Units size and dimensions

The complete unit has a finished rectangular module size of 1.1m x 1.1m and 0.25m deep. All connection ports are designed with access at the unit base. The final mounting bracketing arrangement is to be determined.

4.2.6.2 Modularisation and upscaling

The operation of the HyPVT system was always conceived to be modular and the configuration of units in either series or parallel (both electrically and thermally) was key to its wider deployment. Figure 4.2.6 indicates the evolution from a single small scale demonstrator unit through to the full size prototype and then on to the envisaged modular array. Scaled up, the system could provide power and heat tailored to a building load. The potential to be operated in conjunction with a heat pump was also considered whereupon collected/stored heat quality could be improved via the use of the heat pump powered by the PV array.

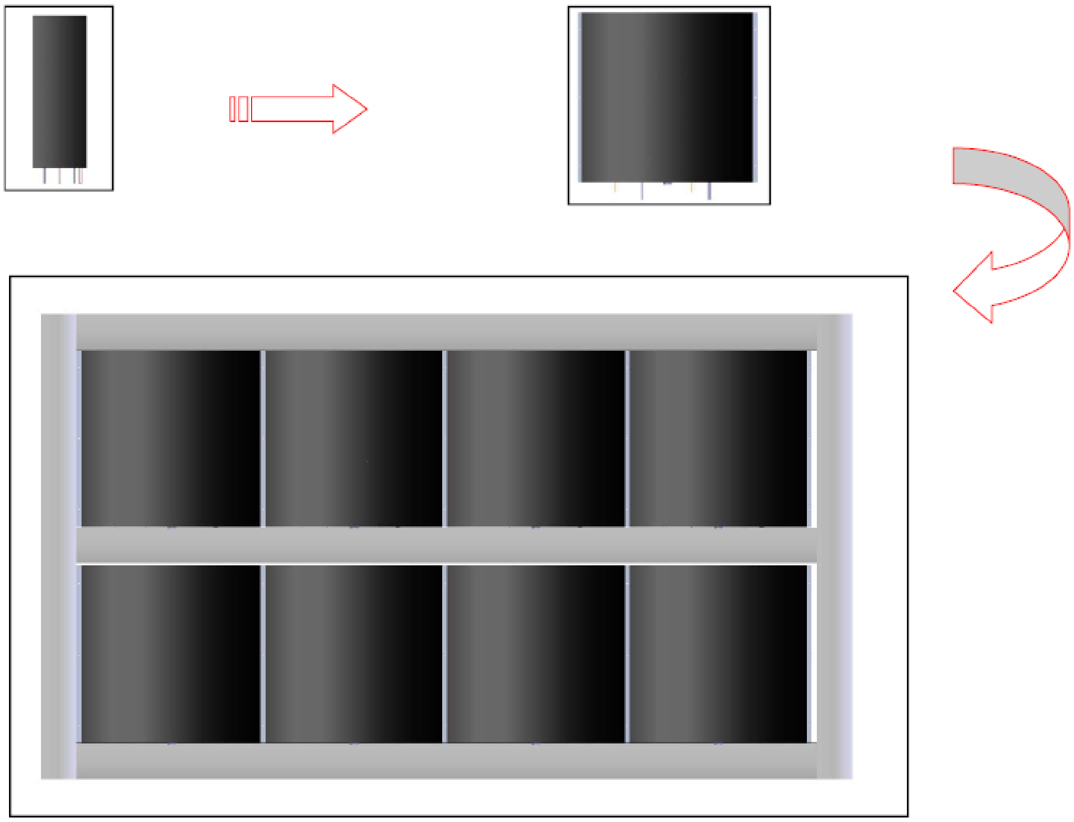

Figure 4.2.6. HyPVT modular concept.

4.2.6.3 Product development

To date, several concepts are being pursued to commercialise the HyPVT unit, these include optimising component design to improve performance and cost effectiveness, streamlining the fabrication and assembly process through Design for Manufacture (DfM), evaluating mass manufacturing options and seeking commercial partnerships. This work is ongoing.

4.2.7 Physical mounting/installation

4.2.7.1 Structural integration

The system's building integration is done by the accession of its surrounding metal frame on the static body of the building. This framework provides the structural efficiency of the wall to which it belongs, and also accommodates the system's piping.

4.2.7.2 Section Detailing

The system is placed within the building's masonry in such a manner that it becomes a part of it, as shown in Figures 4.2.7 and 4.2.8. The construction is such that it can accommodate a conventional opening (e.g. window), in the position of which, the system's module is placed. The back of the system is closed with conventional masonry, in order not to be perceived internally by the users of the building. In selected internal locations, control points are placed.

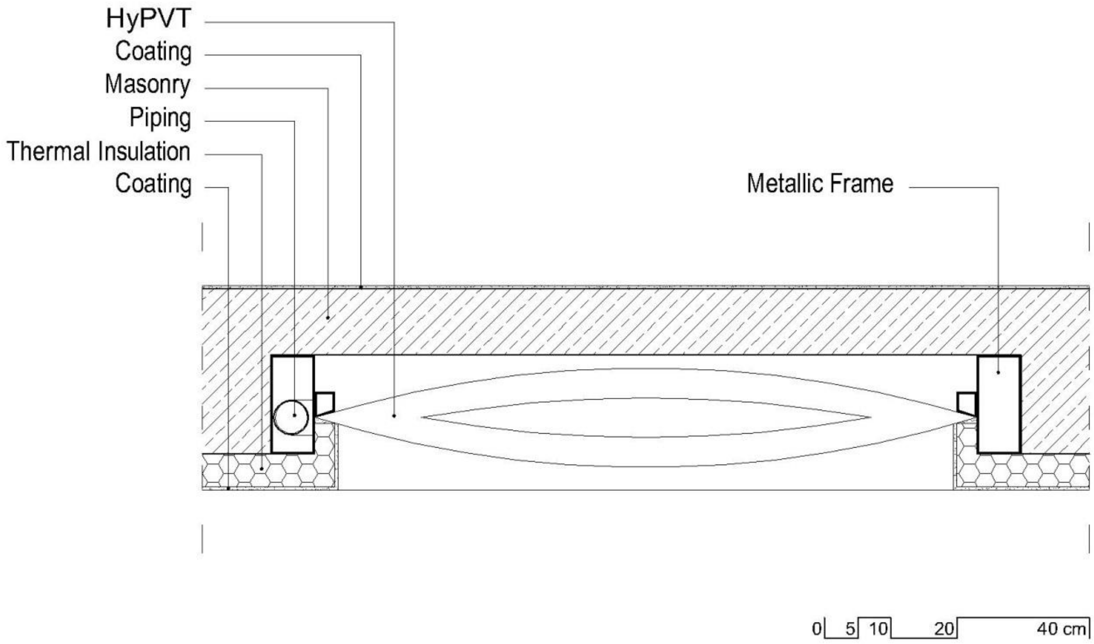

Figure 4.2.7. Horizontal Section.

4.2.7.3 Weather proofing and specific conditions influence

The installation of the system is in such a way that the external thermal insulation and contingent waterproofing cover 1-2 cm of the perimeter of it, ensuring its adequacy for weather conditions. At the same time, this overlap provides maximum insulation because the combination of the system (which is vacuum formed) with the insulation of the shell reduces to a minimum the geometrical thermal bridges. The positioning of a second wall behind the system (Figure 4.2.7) ensures the continuity of the shell thus providing the necessary fire safety. Furthermore, the continuity of the shell provides the necessary soundproofing.

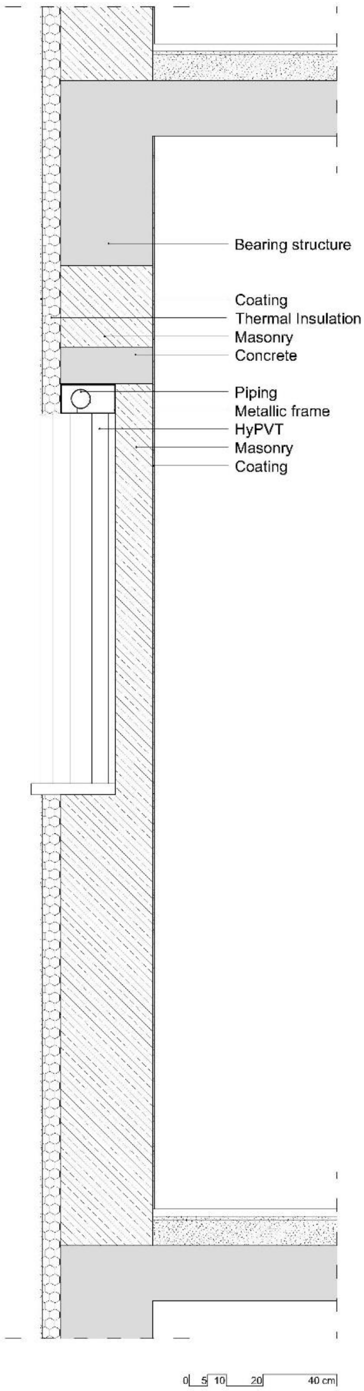

Figure 4.2.8. Vertical Section.

4.2.7.4 Services interconnection

Regarding services interconnection, they will connect to the system through the metal frame which also acts as a static carrier of the opening (Figures 4.2.7 and 4.2.8). In relation to the piping between two modules that are placed within a distance and in relation to the pipes that will start from the system to go to the machinery space, they will pass in the conventional way (through the walls) as with any other building piping.

4.2.7.5 Relevant regulations

The full integration of the system in the building walls and its interconnection with the conventional systems and piping, along with the fact that its construction and building integration takes into account all the above, makes its use viable without violating any potential regulations.

4.2.8 In situ artist impression

4.2.8.1 Images and perspectives

Figure 4.2.9 shows how the system could be integrated in a small ground floor building layout.

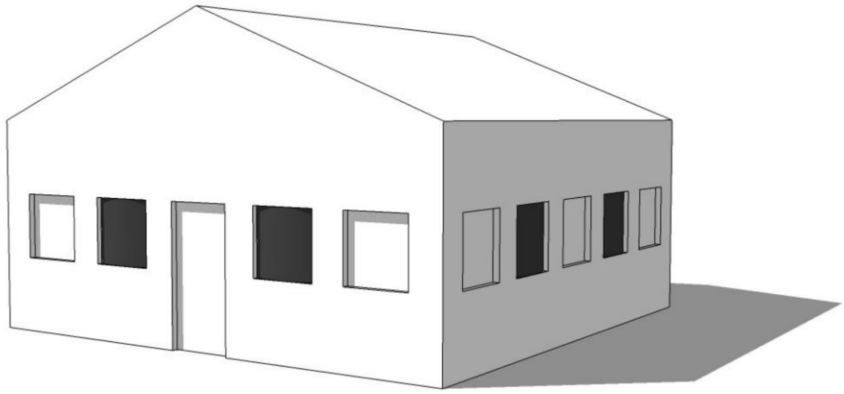

Figure 4.2.9. Integration on small building.

Figures 4.2.10, 4.2.11 and 4.2.12 show possible building integrations of the system in multi-storey buildings, where there are several solutions.

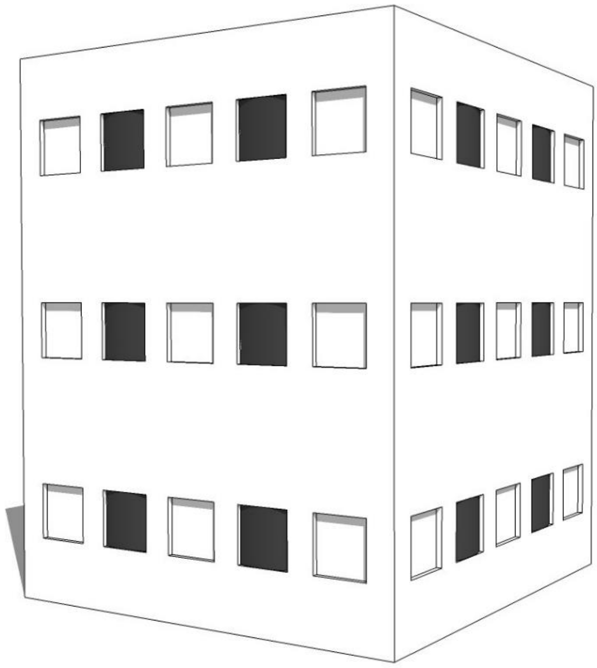

Figure 4.2.10. Integration on a multi-storey building.

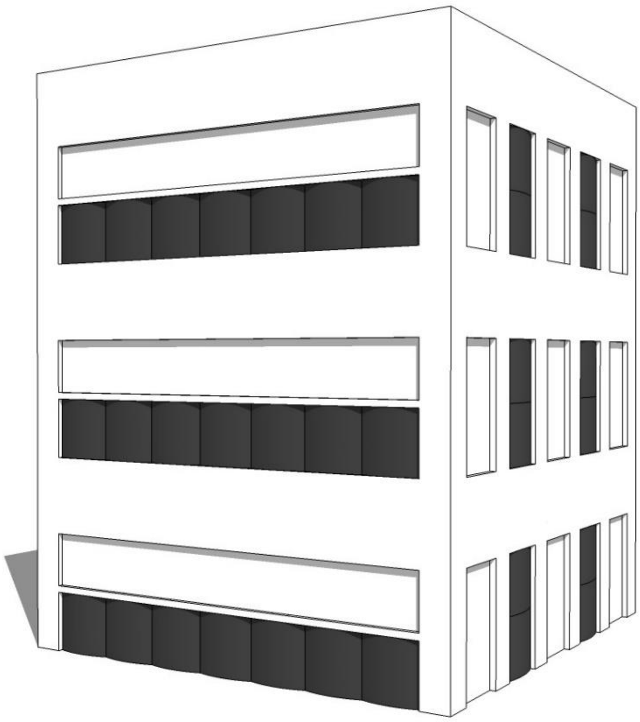

Figure 4.2.11. Integration on a multi-storey building.

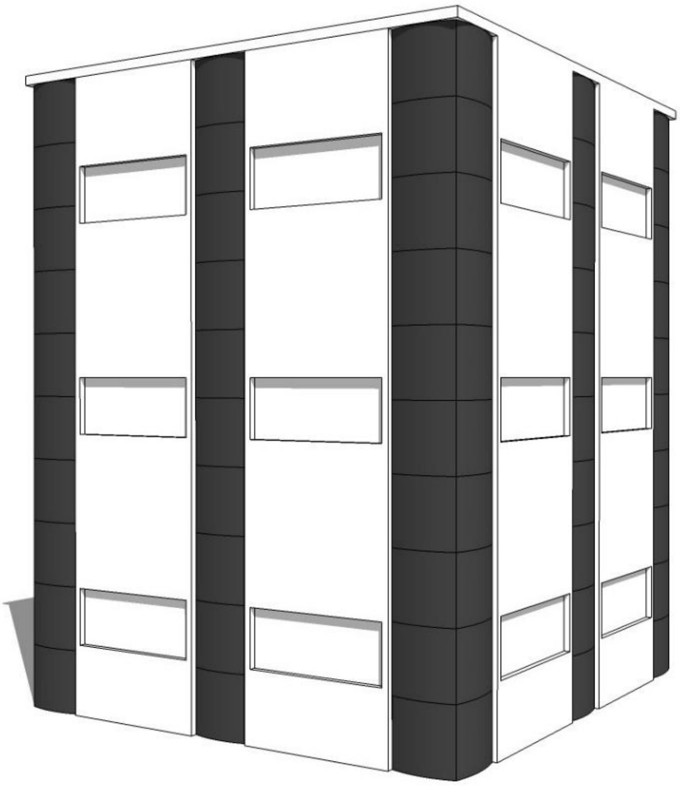

Figure 4.2.12. Integration on a multi-storey building.

4.2.8.2 Influence on aesthetics, appearance, empathy

The building integration (as shown in Figures 4.2.9, 4.2.10, 4.2.11, 4.2.12, 4.2.13) of this system can follow the basic design principles of the building in which it is integrated. Its square shape helps it to replace openings while the creation of multiple-module sequences can be placed in horizontal or vertical arrays which can be easily integrated into a building's design principles.

Figure 4.2.13. Realistic visualization of the system integrated on a multi-storey building.

4.3 CONCENTRATING PHOTOVOLTAIC/THERMAL GLAZING (COPVTG)

Aggelos Zacharopoulos, Trevor J. Hyde, Jayanta D. Mondol, Iurii Lytvyn[3], Mervyn Smyth, Andreas Savvides[4], Constantinos Vassiliades[4]

4.3.1 Concept

Many modern buildings (commercial and domestic) incorporate large glazed areas following architectural expression, providing improved daylighting and wellbeing for their occupants. However conventional fenestration systems have poor insulating properties (compared to traditional constructional elements) resulting in excessive heat loss during cold conditions and increased cooling loads during warmer, sunnier conditions. Integrating advanced glazing with renewable energy generation technologies whilst controlling daylight penetration can create comfortable building internal spaces while ensuring lower energy bills and associated carbon emissions.

Transparent concentrating lens for PV façade building integration have been developed to enable increased electricity generation per unit area of PV material compared to conventional PV panels. Prototype transparent concentrating PV lens were fabricated and experimentally characterised. The results demonstrated that by using the concentrating lens, almost double the amount of electricity per unit of PV material can be generated compared to conventional PV panels. Daylighting control is possible by tailoring the concentrating lens design to allow incident solar radiation to enter the building at different times during the day. By combining the concentrating lens with a flat glass pane into a double glazing unit and evacuating the cavity, convective heat losses can be eliminated.

The Concentrating PV/Thermal Glazing (CoPVTG) façade technology combines glazing based solar concentrating elements coupled with PV/Thermal absorbers. It can provide solar generated electricity and heated air through the PV/T absorbers while insulating the building thermally. The glazing based concentrating elements are designed to allow the sunlight to enter the building and provide natural daylight when required while redirecting it onto the PV/T absorbers to generate electricity/heat when solar gains need to be minimised to reduce cooling demands.

The technology consists of a double glazing panel where the outside pane of glass is shaped into a series of concentrating lens. A thin layer of photovoltaic cells is placed at the focus of the concentrating lens to act as PV/T absorber. The inner pane of glass is a conventional flat pane. Forced air flow between the two glass panes can be used to remove waste heat from the back of the PV and use for space heating or pre-heating purposes. To increase the thermal insulation properties of the technology a third (optional) flat glass pane can be used in front of the concentrating lens pane and the resulting cavity can be filled up with inert gases such as argon or evacuated to eliminate convective heat loss (Figure 4.3.1).

Depending on the design of the concentrating lens, a part of the incident solar radiation can reach the PV/T absorbers generating electricity and waste heat while the rest can travel

[3] Non COST member

[4] Contributed only to the architectural integration demonstrations

through the unit to provide daylight to the building interior. Using total internal reflection (TIR), the lens design can produce a seasonal effect with more light allowed into the building at low incidence angles (i.e. in the winter months) and less light at high incidence angles (i.e. in the summer). Figure 4.3.2 demonstrates how by using TIR different amounts of light can be collected onto the PV/T absorbers or transmitted through the glazing unit depending on the incident angle of the solar radiation.

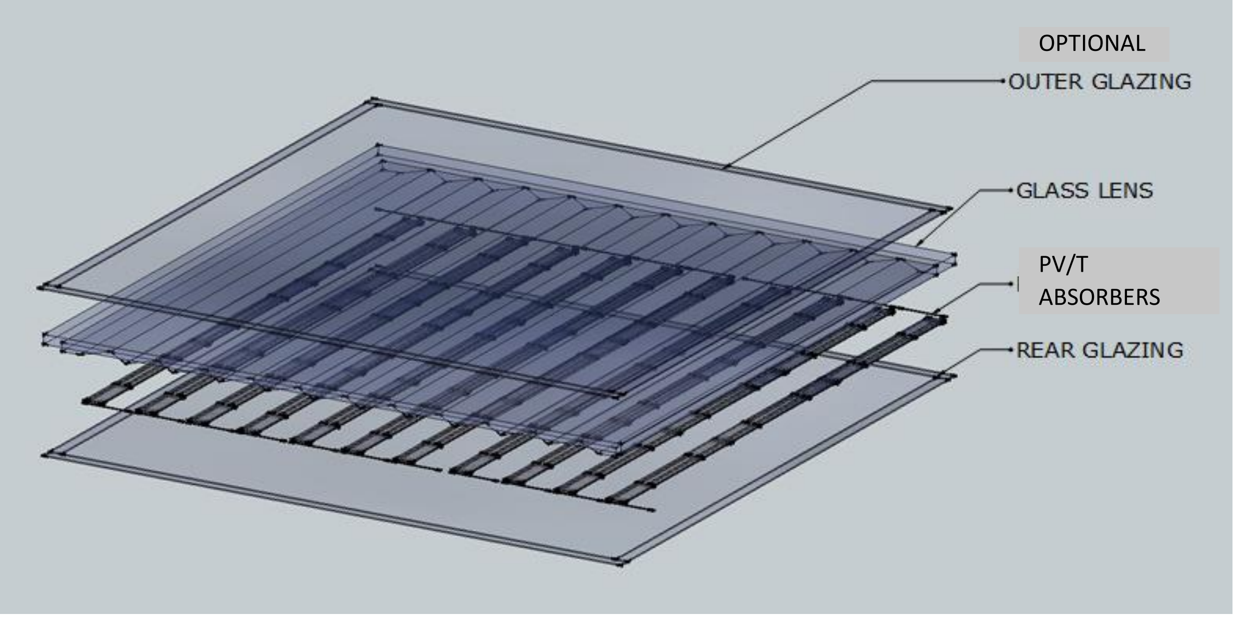

Figure 4.3.1. The CoPVTG technology combining concentrating glass lens with PV/T absorber elements.

For a 30º incidence angle the PV cells receive the beam radiation light which is directly incident on them. The remaining radiation is refracted through the lens and transmitted to the back of the unit. At a 55º incidence angle all beam solar radiation is reflected onto the PV/T absorbers by TIR at the back of the glass lens. The few rays missing the absorber at the bottom of the unit are due to edge-effects related to the size of the concentrating glass pane. Depending on the design of the concentrating lens there is a critical incidence angle that switches “on” or “off” the TIR of the solar radiation at the back of the glass lens. Glass lens that can control daylight transmission to the rear of the unit (i.e. into the building) for a specified range of incidence angles of solar radiation can be designed for a given building and geographic location.

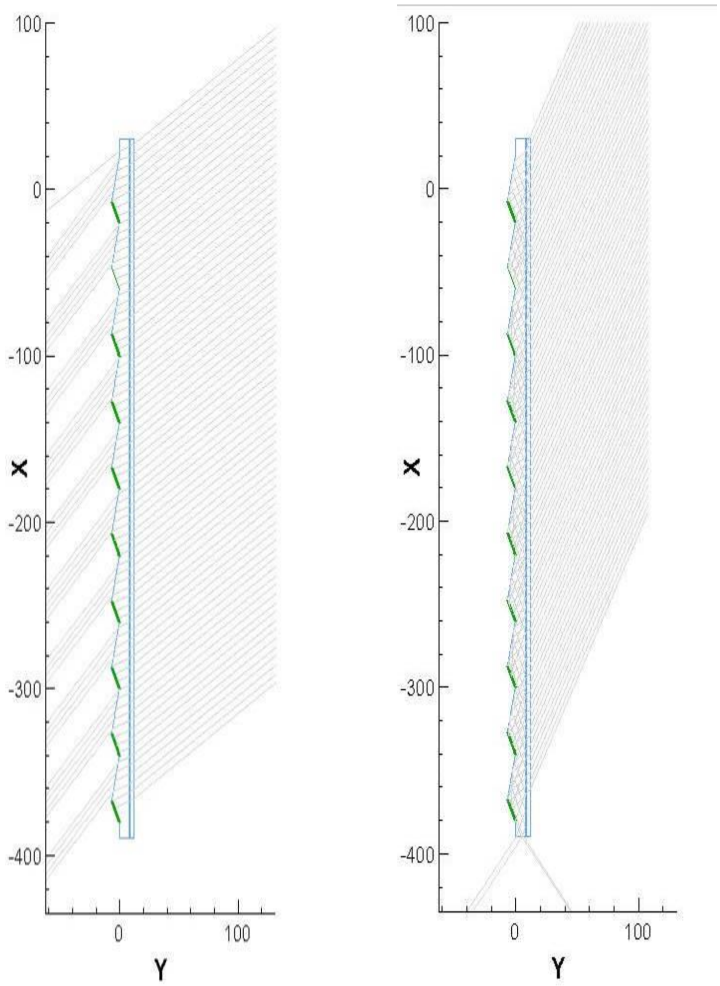

Figure 4.3.2. Ray trace diagrams demonstrating the control of light transmittance through the CoPVTG by TIR at the concentrating lens. Light incident at 30º (left) and 55º (right) from the perpendicular to the surface of the glazing.

4.3.2 Application

As a modular multifunctional building component based on conventional double glazing, the CoPVTG is designed to be compatible with traditional façade structures and fenestration framing arrangements, facilitating direct integration into new and retrofit building applications.

The multi-functionality of the unit provides a unique product concept. And is predominately seen to be a modular system for use in façade mounted applications for commercial building types.

4.3.3 Physical description

4.3.3.1 Physical description and detailing

A prototype 500mm x 500 mm CoPVTG unit was fabricated using an outer 15 mm (max) thickness concentrating lens pane and an inner 4 mm thickness flat glass pane (Figure 4.3.3). A 25 mm cavity was formed between two glass panes using appropriate size spacers which accommodated the air inlet and outlets at the bottom and top of the cavity respectively (Figure 4.3.3a). 33 multi-crystalline PV cells conFigured as 11 strips of 3 cells each were bonded at the focus of the concentrating lens using opti-clear silicon resin. Green coloured cells were used (C-Cell range by LOF Solar) to achieve better aesthetics. A UPVC window frame was used to mount the fabricated CoPVTG unit (Figure 4.3.3a). The frame had a slot cut out along its top and bottom to allow the air to flow through the unit. The air was supplied by flow and return header ducts with slots cut identical to that of the window frame allowing a clear passage of air. The fabricated CoPVTG inserted into the PVC window frame is illustrated in Figure 4.3.3b.

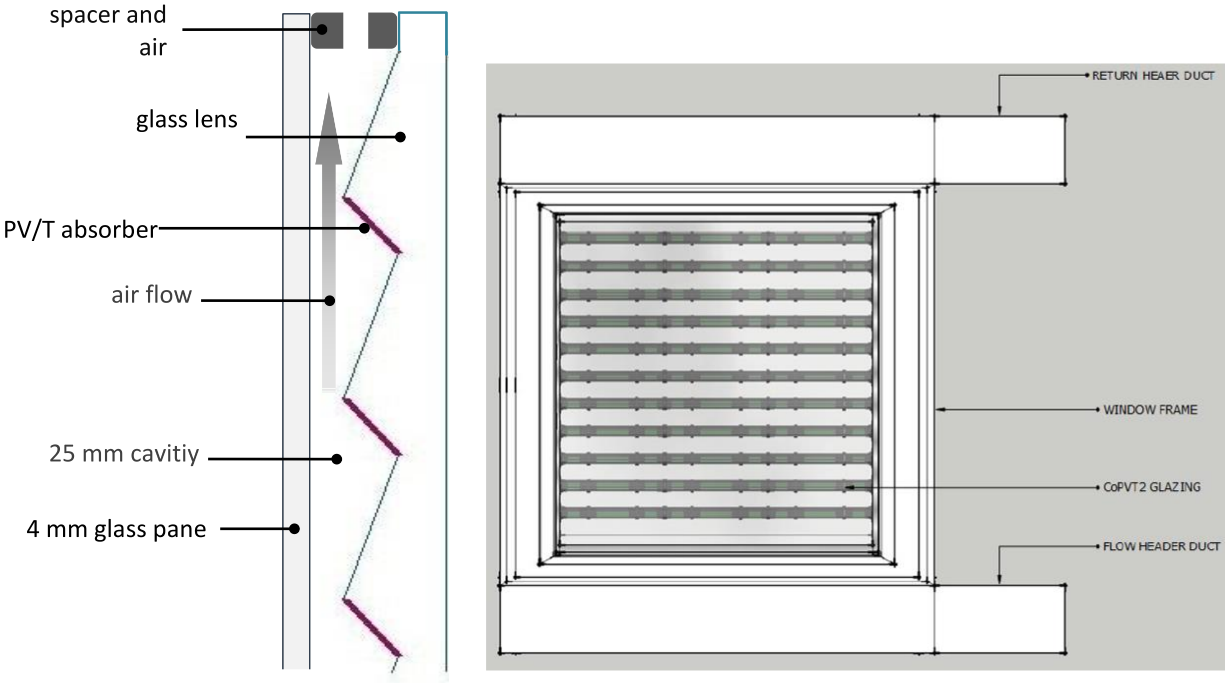

Figure 4.3.3. a) Cross section of the fabricated CoPVTG prototype and b) schematic of the prototype unit inserted into a PVC window frame (right).

Both header and return flow ducts were covered with polystyrene insulation to minimise heat loss. A DC fan was used to produce and control an air flow through the CoPVTG glazing cavity using a power supply.

4.3.3.2 Engineering drawings

Concentrating lens

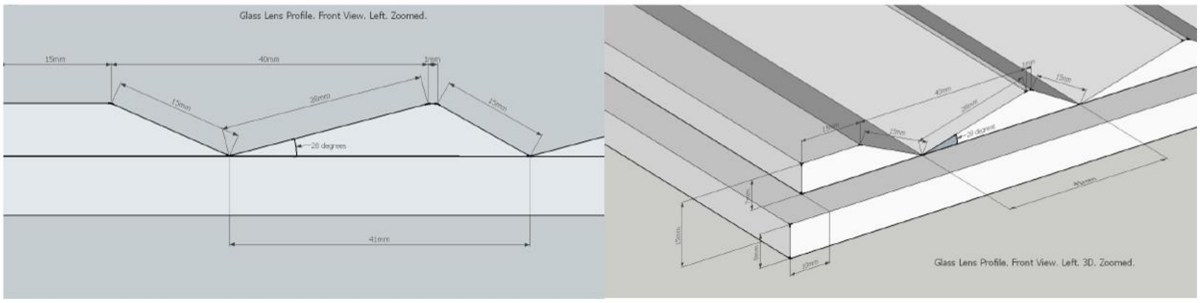

PVT absorbers

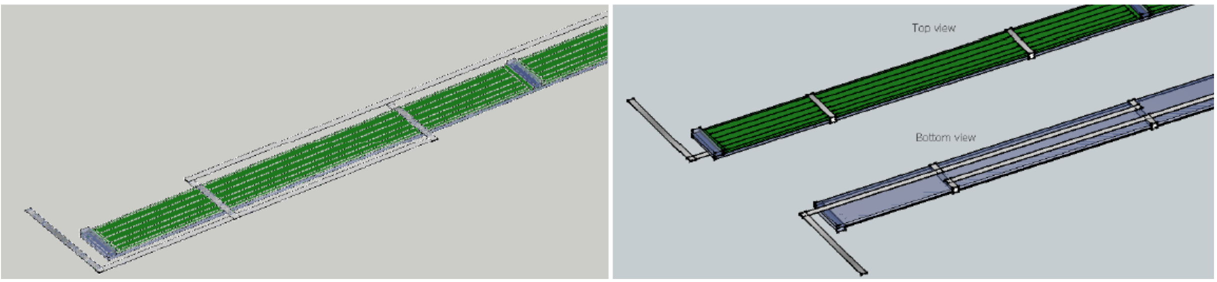

Concentrating glass

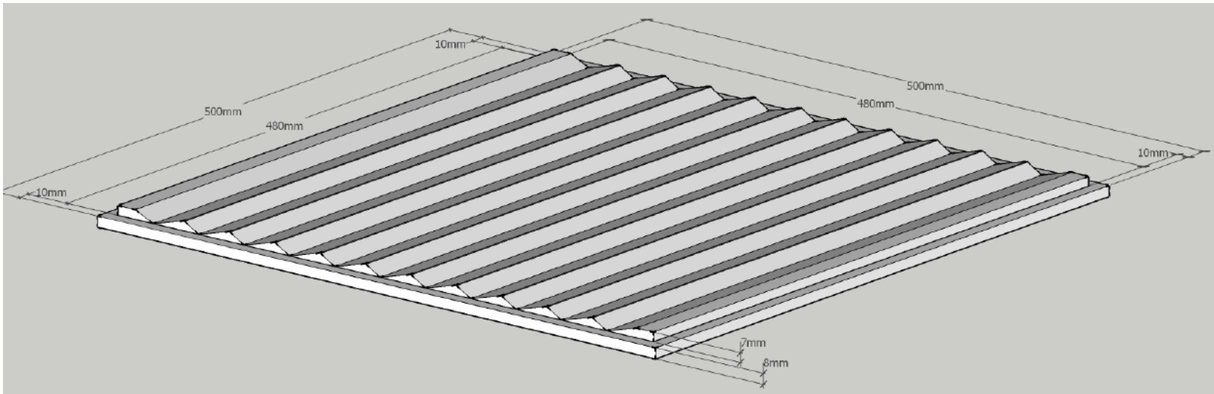

CoPVTG integrated with inlet and outlet ducts

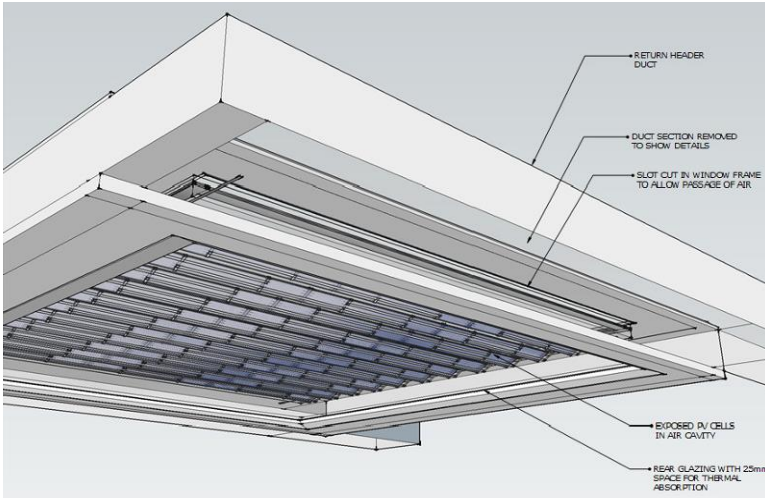

4.3.3.3 Materials

The full size prototype unit fabricated, assembled and tested at Ulster University is still in its infancy in terms of product design. A number of design enhancements and developments are ongoing. The prototype unit consists of the following material components:

Concentrating PVT glazing unit

- Opti-white glass pane 1 x 500 mm x 500 mm x 15 mm (concentrating glass lens pane)
- Opti-white glass pane 1 x 500 mm x 500 mm x 4 mm (flat pane)
- Poly-Si solar cells 33 x 0.2 mm x 156 mm x 15 mm
- Connecting ribbon for solar cells 1 mm x 2.5 mm x 6100 mm
- Opti-white glass strips 12 x15 mm x 48 mm
- Opti-white glass spacers 60 x 15 mmx 1 mmx 2 mm
- Opti-clear, UV stable silicon 85ml (bonding solar cells onto glass)

Window frame and inlet-outlet air ducts

- Conventional UPVC window frame to accommodate 500 mm x 500 mm double glazing unit
- 25 mm spacer for double glazing
- UPVC ducting 1400 mm x 50 mm x 100 mm
- DC air fan
- Polystyrene insulation

4.3.4 Fabrication and assembly process

The concentrating glass lens unit was fabricated by CNC machining using cutting tools, specifically fabricated for the given The PV cells were connected in series forming 11 rows of 3 cells each. To prevent damaging the cells during the fabrication of the prototype each row of 3 cells was mounted onto the opti-white glass strips. The 11 rows of cells were then bonded onto the corresponding focal planes of the concentrating glass lens using opt-clear silicon.

A UPVC window frame would be utilised to mount the concentrating PV glass as double glazed unit. The window frame had a slot cut out along its top and bottom to allow air to flow through the unit (Figure 4.3.4). This would be supplied by the flow and return header ducts which have slots cut identical to that of the window frame allowing a clear passage of air flow.

Figure 4.3.4. The UPVC window frame used to mount the glazing. Slots on the upper and lower sections allow for the air to flow through the glazing cavity.

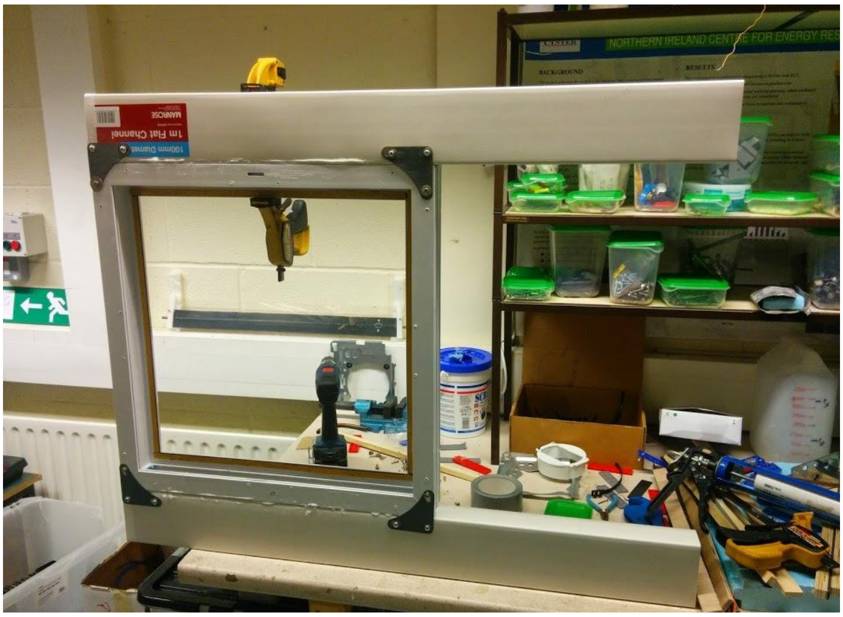

Figure 4.3.5. The inlet and outlet header air ducts attached on the UPVC window frame.

Header ducts for the flow and return were made up, using 100mm x 50mm uPVC ducting. The slots were cut on the 50mm side of the ducting to be identical to the slots cut in the window frame. Brackets were then attached to the header ducts so that they could be securely fitted to the window.

The ducts were attached using metal brackets, these screwed into the duct and into the window frame making for a very sturdy attachment. To ensure air tightness so as to not affect the results, silicone sealant was applied to the window and the duct before they were attached together (Figure 4.3.5).

A fan was needed that would be easily controllable; a DC fan was sourced from an old PC that was no longer in use. This can be easily controlled and would be able to be set for the flow rates needed. An adapter was made so that the fan would fit onto the ducting.

The header ducts were covered with insulation which was securely taped to the window frame ensuring a good tight fit. The concentrating PVT glass was placed into the window frame (Figure 4.3.6) and the second, flat glass pane placed behind using the double glazing spacer to create a 25 mm wide cavity between the two glass panes. The full prototype is presented in Figure 4.3.7.

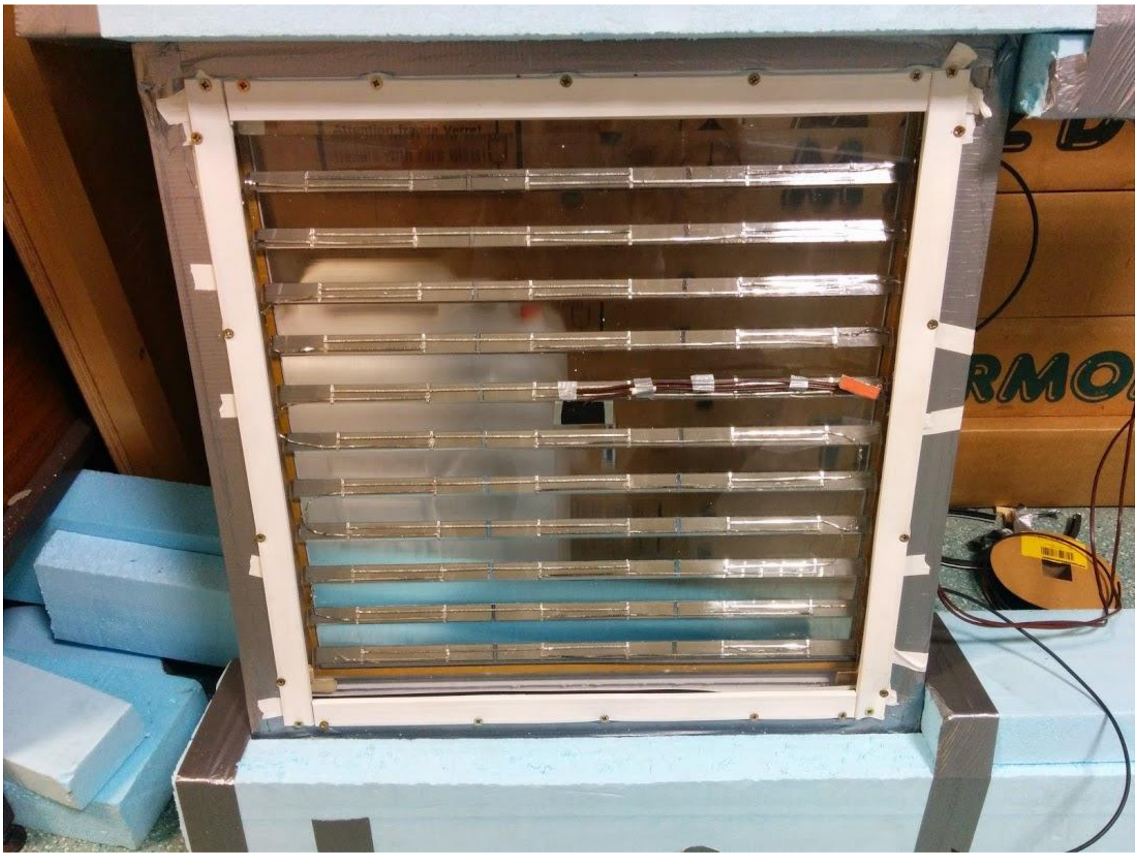

Figure 4.3.6. The concentrating PVT glass fitted into the UPVC window frame with integrated air ducts.

Figure 4.3.7. The full CoPVTG prototype.

4.3.5 Modular configuration

4.3.5.1 Units weight and dimensions

The complete prototype unit (excluding ducting) has dimensions of 600 mm x 600mm x50 mm. The weight of the unit is approximately 10.5 kg.

4.3.5.2 Modularisation and upscaling

The CoPVTG technology is both modular and scalable in the same way as double glazing. The size of a single unit can be several m^2 and is limited only by the structural strength of the building frame supporting the glazing. A number of units can be connected in series or parallel (both electrically and thermally) to allow maximum coverage of a given building façade. However, the requirement of air ducting could impose some restrictions as it will make necessary the use of air handling units. The CoPVTG can potentially be operated in conjunction with a heat pump was also considered whereupon collected/stored heat quality could be improved via the use of the heat pump powered by the PV array.

4.3.5.3 Product development

The CoPVTG has been proved as a concept. The focus now is on determining the best method for manufacturing it in large volumes. The formation of the concentrating PVT lens either by cutting them from glass (e.g. CNC machining) or using acrylics or other synthetic materials need to be investigated. A third option may be casting. The bonding of the PV cells onto the focal planes of the prisms is also an important area of investigation as the opti-clear silicon used for the prototype is both time consuming and expensive. The use of cells which are the by-product of the manufacturing process of PV panels can offer a saving compared to using PV strips cut from full size cells.

4.3.6 Physical mounting/installation

4.3.6.1 Structural integration

The system's building integration is done by the accession of the system on the building shell in the same way that a conventional window is built. The only difference, as shown in Figure 4.3.9, is that the lintel of the window is divided into two parts in order to accommodate the air duct system.

4.3.6.2 Section Detailing

The system is placed within the building's masonry in such a manner that it becomes a part of it like a conventional window, as shown in Figures 4.3.8 and 4.3.9. The construction is such that it can accommodate a conventional opening (e.g. window), in the position of which, the system's module is placed. Inside the masonry, at the top and bottom of the system, a special, insulated space is created, which accommodates the required air ducts of the system. In selected internal locations, control points are placed. The edge of the wall is cut diagonally, in order not to prevent the sunlight to pass.

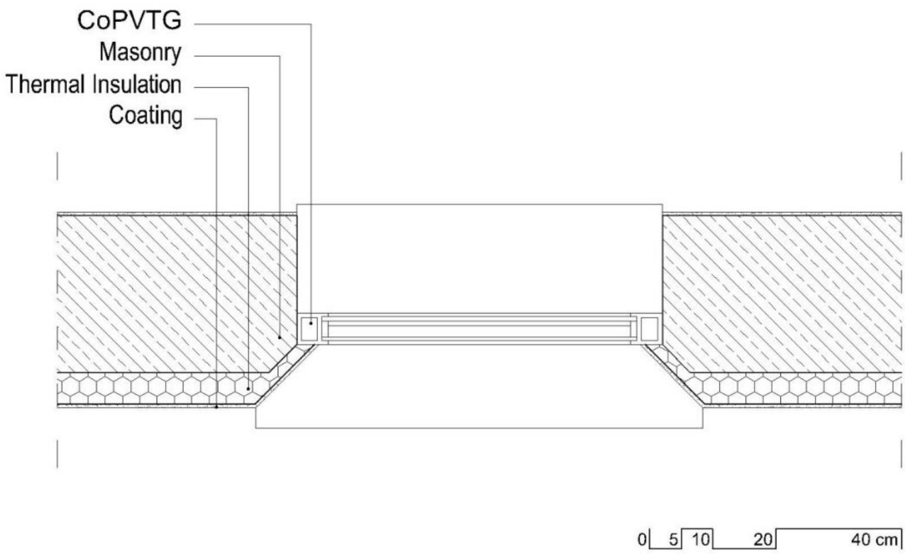

Figure 4.3.8. Horizontal Section.

4.3.6.3 Weather proofing and specific conditions influence

The installation of the system is in such a way that the external thermal insulation and contingent waterproofing covers at least 1-2 cm of the perimeter of it, ensuring its adequacy on the weather conditions (Figure 4.3.8). At the same time, this overlap provides maximum insulation because the combination of the system's double glazing with the insulation of the shell reduces to a minimum the thermal bridges. The sealed installation of the system as a conventional window, ensures the continuity of the shell thus providing the necessary fire safety. Furthermore, the continuity of the shell provides the necessary soundproofing.

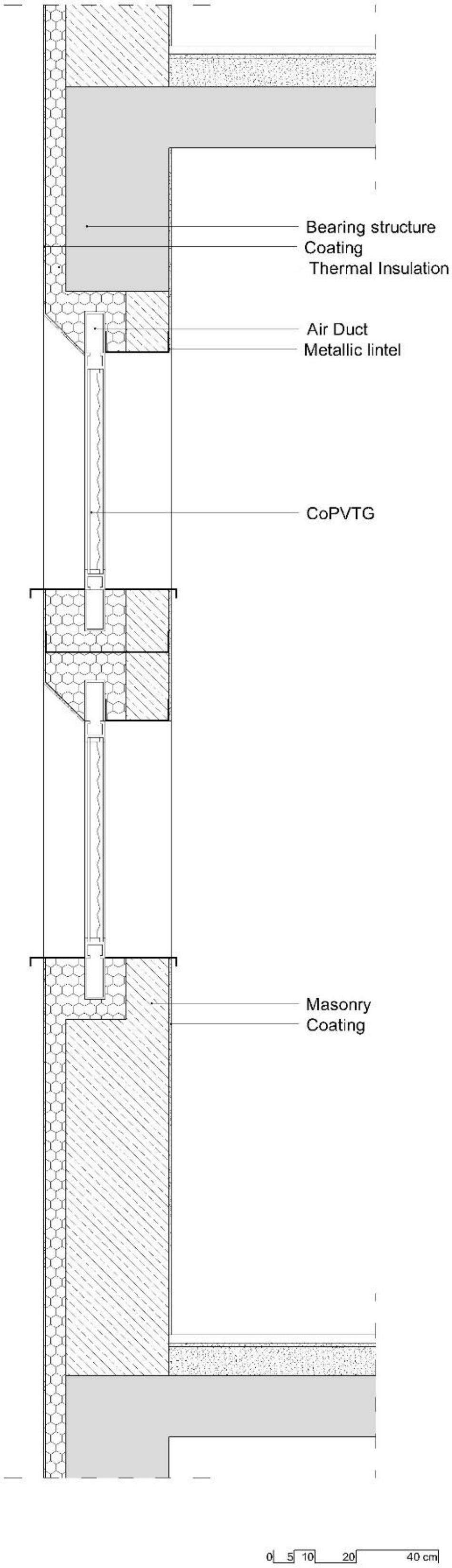

Figure 4.3.9. Vertical Section.

4.3.6.4 Services interconnection

Regarding to the services interconnection, they consist only of air ducts, which will reach the system at the top and bottom of the system as shown in Figures 4.3.9. In relation to the air ducts that pass through the masonry, they will be built, pass in the conventional way (by opening channels through the walls).

4.3.6.5 Relevant regulations

The full integration of the system in the building is as a conventional window, along with the fact that its construction and building integration takes into account all of the above, it makes its use viable without violating any potential regulations.

4.3.7 In situ artist impression

4.3.7.1 Images and perspectives

Figure 4.3.10 shows how the system could be integrated in a small ground floor building layout.

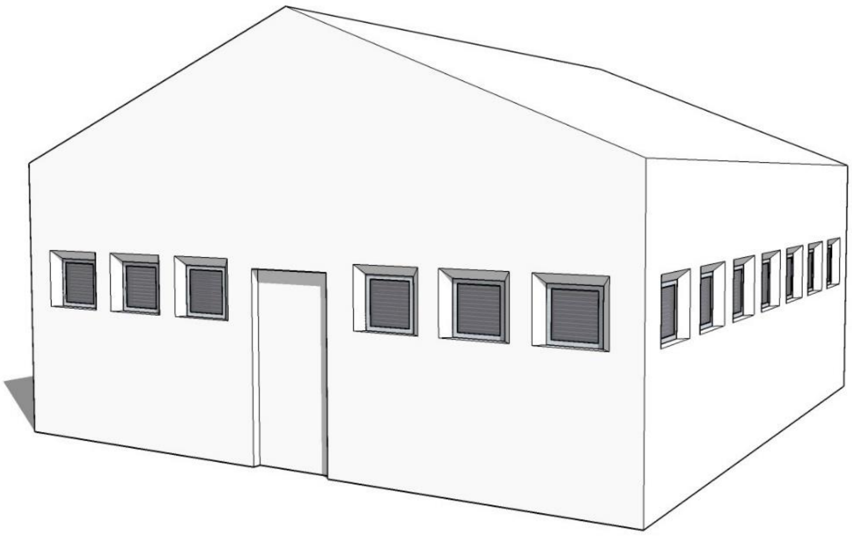

Figure 4.3.10. Integration on small building.

Figures 4.3.11 and 4.3.12 show possible building integrations of the system in multi-storey buildings, where there are several solutions.

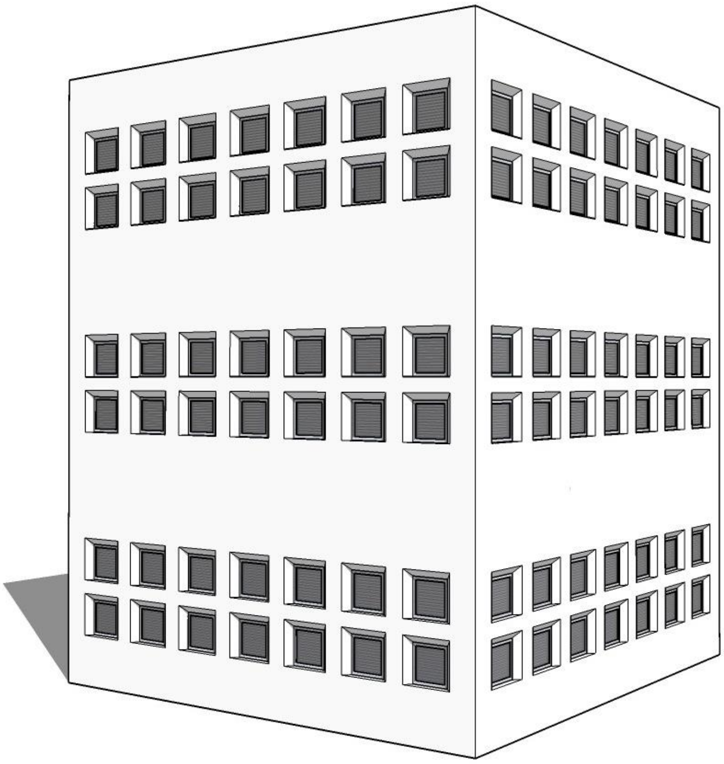

Figure 4.3.11. Integration on a multi-storey building.

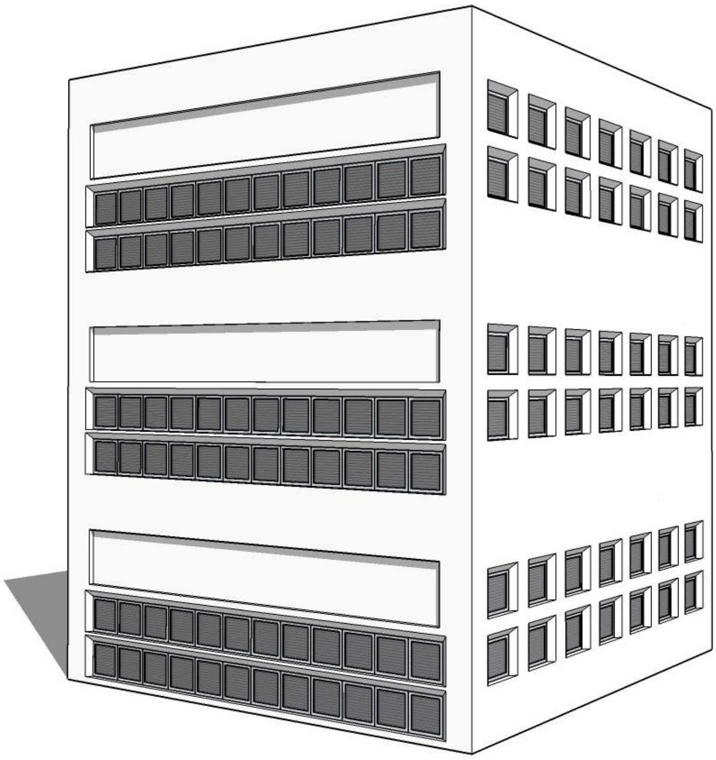

Figure 4.3.12. Integration on a multi-storey building.

4.3.7.2 Influence on aesthetics, appearance, empathy

The building integration (as shown in Figures 4.3.10, 4.3.11, 4.3.12, 4.3.13) of this system can follow the basic design principles of the building in which it is integrated. Its square shape helps it to replace openings while the creation of multiple-module sequences can be placed in horizontal or vertical arrays which can be easily integrated into a building's design principles.

Figure 4.3.13. Realistic visualization of the system integrated on a multi-storey building.

4.4 BUILDING INTEGRATED TRANSPIRED AIR HEATER

Brian Norton, Mick McKeever, David Kennedy, Andreas Savvides[5], Constantinos Vassiliades[5]

4.4.1 Concept

The "solar plenum" is an air heating solar collector which integrates an asymmetric compound parabolic concentrator with a tertiary reflector sector that reflects solar radiation into a downward facing absorber surface. Being downward-facing, convection heat loss from the absorber surface is inhibited. The concentration of insolation to an absorber leads to it being at a much higher temperature than ambient. Air enters the solar plenum via a grille beneath its glazed aperture. That glazed aperture prevents external wind perturbing the convection suppression at the absorber. Air is conveyed through the solar plenum by a fan. Heat is removed by the air passing through pin holes in the transpired absorber. The flow rate is maintained at a rate that allows air plumes to pass through the thermally stratified air layers beneath the absorber without significantly diminishing the thermal insulation of the absorber provided by the stratification.

This product involves the design and development of a Concentrating Transpired Air Heating (CTAH) unit. This air heating solar collector comprises of an inverted perforated absorber and an asymmetric compound parabolic concentrator (see Figure 4.4.1) that increases the intensity of solar radiation incident on the perforated absorber. The development included optimum system components considering efficiency, compatibility, cost, weight and scaling. The average thermal efficiency was found to be approximately 55%-65% with average radiation above 400 W/m^2 for flow rates in the range of 0.03 kg/s/m^2 to 0.09 kg/s/m^2. Experimental results at air flow rates of 0.03 kg/s/m^2 and 0.09 kg/s/m^2 showed a temperature rise of 38^{o}C and 19.6^{o}C respectively at a solar radiation intensity of 1,000 W/m^2. As the pressure drop in the system was found to be 10 Pa for an air flow rate of 0.1 kg/s/m^2 between the inlet and the outlet, the required fan power consumption was very small in comparison to the recovered energy. Thermal efficiency remained high at higher air flow rates.

4.4.2 Applications

Solar Air Heating Collectors have applications in space heating and space ventilation, timber seasoning, curing of industrial products and drying.

At present, two main types of Solar Air Heating Collectors exist commercially: Unglazed Solar Air Heating Collector (USAHC) and Glazed Solar Air Heating Collector (GSAHC). The basic difference between two main types of solar air heating collectors is presence of glazing cover and design of absorber surface. The device can also be used for cooling building at night time, removing heat from the various rooms in an efficient and low cost method.

4.4.3 Design and construction of the concentrator system

The design consists of the integration of a Transpired Air-heating Collector (TAC) and an Asymmetric Compound Parabolic Concentrator (ACPC).

[5] Contributed only to the architectural integration demonstrations

4.4.3.1 Construction of the concentrator system

A diagram of the CTAH system is presented in Figure 4.4.1. A perforated absorber has been incorporated in the design which faces downward to reduce radiation loss. The perforated surface allows air to flow through the absorber which enhances heat transfer between the absorber and the flowing air. Solar air heaters are generally constructed using metal plates as the absorber of the incident solar radiation which introduces conduction losses. Instead of a heavy metal absorber, a nonconventional low conductive light weight carbon fibre absorber has been used. A fan is placed at the end of the air duct to extract air through the perforated absorber. This heated air can be transported to the required environment or supplied through a simple flexible hose to another unit for accumulating more heat. The input of the system is insolation at the aperture. The available insolation varies for local climate and orientation of the aperture. The concentrator of the system works as an amplifier which increases the amount of solar radiation on a decreased absorber area. The heat from one absorber can be transferred to a number of other absorbers, placed adjacent to the first one, in order to accumulate the solar energy to produce a clean, high temperature air for use in a building.

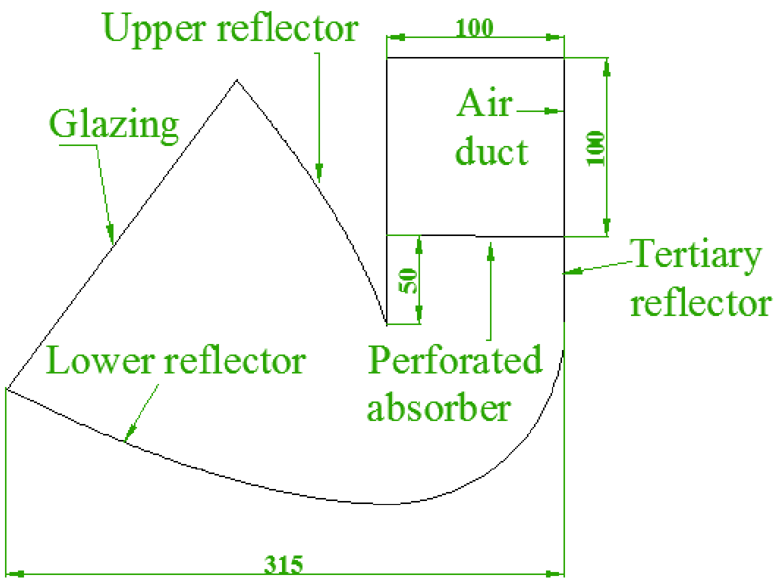

Figure 4.4.1. Schematic of the Collector.

The upper reflector is a combination of primary parabolic and straight tertiary reflectors. The lower reflector is a combination of parabolic primary, circular secondary and straight tertiary reflectors. The secondary circular part of the concentrator concentrates all incident radiation on the inverted absorber. A parallel reflector section just below the inverted absorber helps to improve the stratified thermal layer below the absorber which enhances the heat transfer mechanism. Concentration of solar radiation becomes necessary when higher temperatures are desired. Heat losses from the collector are proportional to the absorber area. A glazing cover has been introduced which works as the heat trap for the emitted radiation from the absorber surface. A high transmittance glazing material (Low e) reduces the optical loss. The glazing surface is also necessary to provide protection from dust deposition, rain, wind and wildlife.

4.4.4 Materials (quantity and quality), durability, duration

The concentrating reflector, transpired absorber and the glazing cover are the main components of the system. The unit is built from thin gauge sheet material, shaped and cut to the specified dimensions. The physical length of the unit can be cut to suit the mounting wall dimensions. Reflector material (95% total light reflection) from Alanod® company in Germany called Miro-sun®. The main properties of this material is shown in Table 4.4.1.

Table 4.4.1. Properties of Miro-sun® reflector material.

Properties	Parameters	Values
Mechanical	Tensile strength (Mpa)	160-200
	Yield strength (Mpa)	140-180
	Elongation a 50%	≥ 2
	Bending radius	$\leq$1.5 fold of thickness
Optical	Total solar reflectance %	95%
	Front side	PVD-improved
	Reverse side	Anodised
Physical	Density (g/cm^2)	2.7
	Heat resistance (1000h)	1500C
Dimension	Max. Width (mm)	1250
	Thickness (mm)	0.5
Warranty	Years	10

The glazing material cover of the unit is a sheet of 6 mm thick low iron glass. The glazing surface protects the reflecting and absorbing surfaces and reduces thermal losses from the absorber. It has a maximum transmittance of 96% and a refractive index of 1.526.

4.4.5 Physical fabrication

4.4.5.1 Fabrication process

The unit can be produced as a flat-pack and is modular in design and construction. The sections are formed from flat sheet, laser cut or profile cut, assembled and folded together on-site and of light weight to be erected by a 2-person team. The length of the unit can be produced to suit the building width or to customer requirements. The units can be used individually or are stackable to enhance energy accumulation.

4.4.6 Modular configuration

4.4.6.1 Units size and dimensions

The end plate dimensions are shown in Figure 4.4.2.

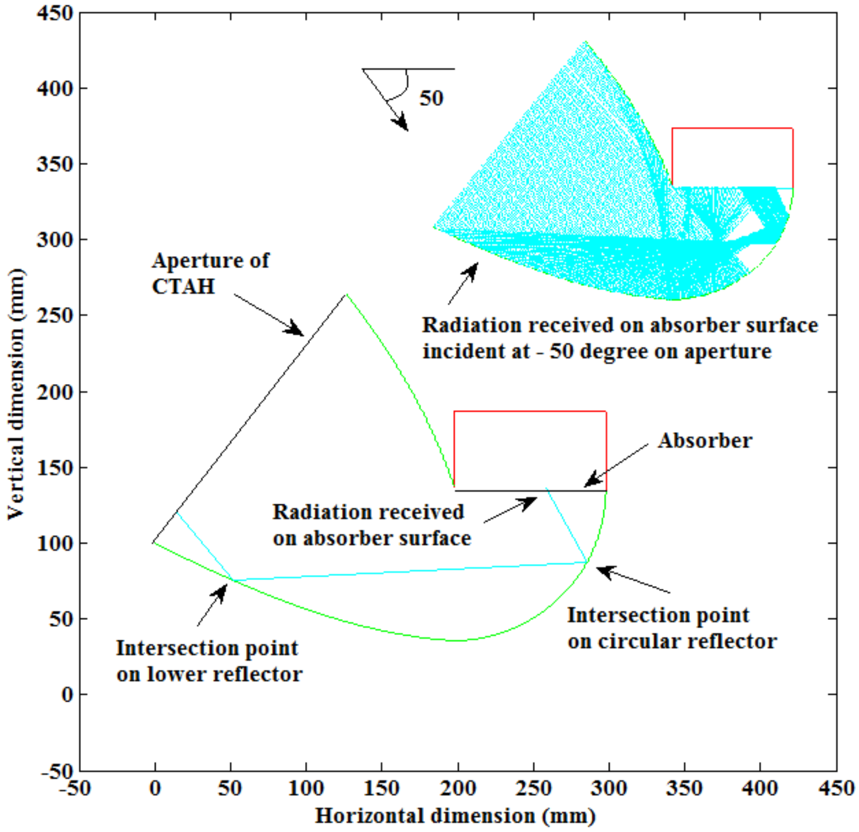

Figure 4.4.2. End plate dimensions.

4.4.6.2 In situ artist impression

Artist's impressions of the Solar plenum are shown in Figures 4.4.3(a) and 4.4.3(b).

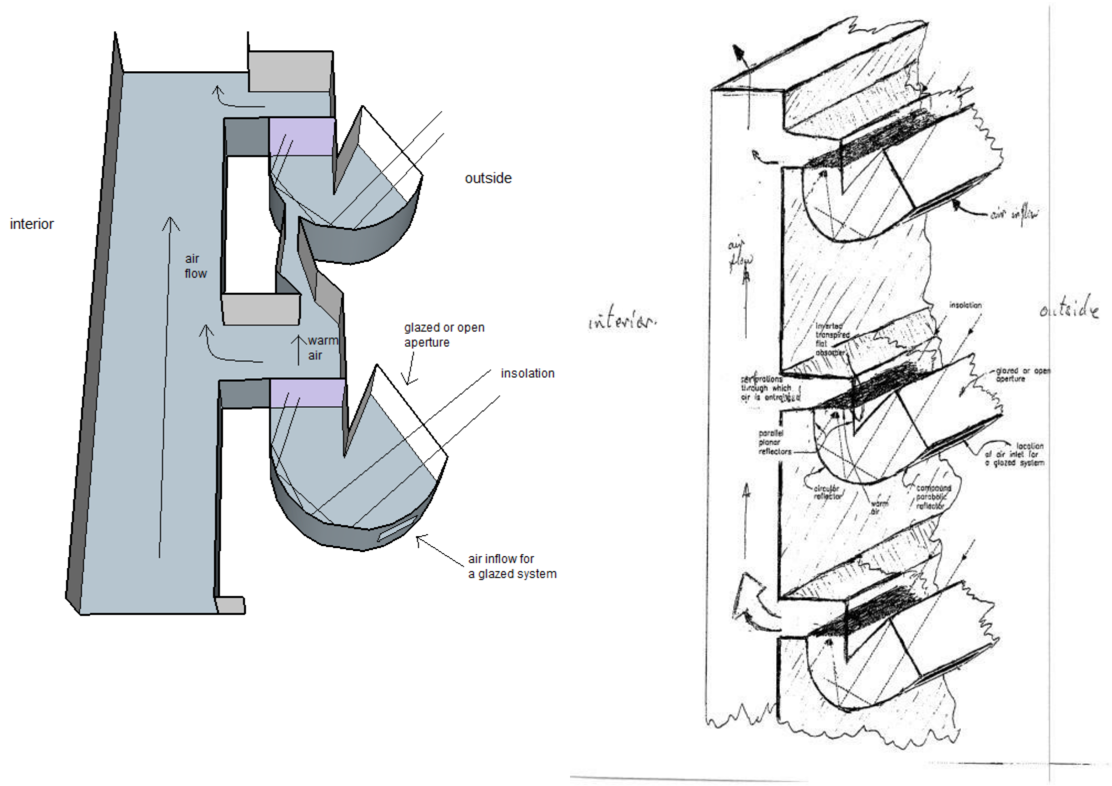

(a) (b)

Figure 4.4.3. (a) and 4.4.3 (b). Artistic impression of Solar Plenum.

4.4.7 Physical mounting/installation

4.4.7.1 Structural integration

The system's building integration is done by the accession of it on the lintel of a building's window (Figure 4.4.4 – Solution 1). When the system is placed on a linear array, the array is anchored on the masonry's base and on the beam (Figure 4.4.4 – Solution 2). These frameworks provide the structural efficiency of the wall on which the system belongs.

4.4.7.2 Section Detailing

The system is placed within the building's masonry in such a manner that it becomes a part of it, as shown in Figure 4.4.4. In Figure 4.4.4 "Solution 1" configuration, the construction is such that it can accommodate a conventional opening (e.g. window), on the top of which, the system's modules are placed. In Figure 4.4.4 "Solution 2" configuration, the construction is such that it can accommodate a conventional opening (e.g. window), in the position of which the system's module vertical array is placed, covering the opening. In selected internal locations, control points are placed.

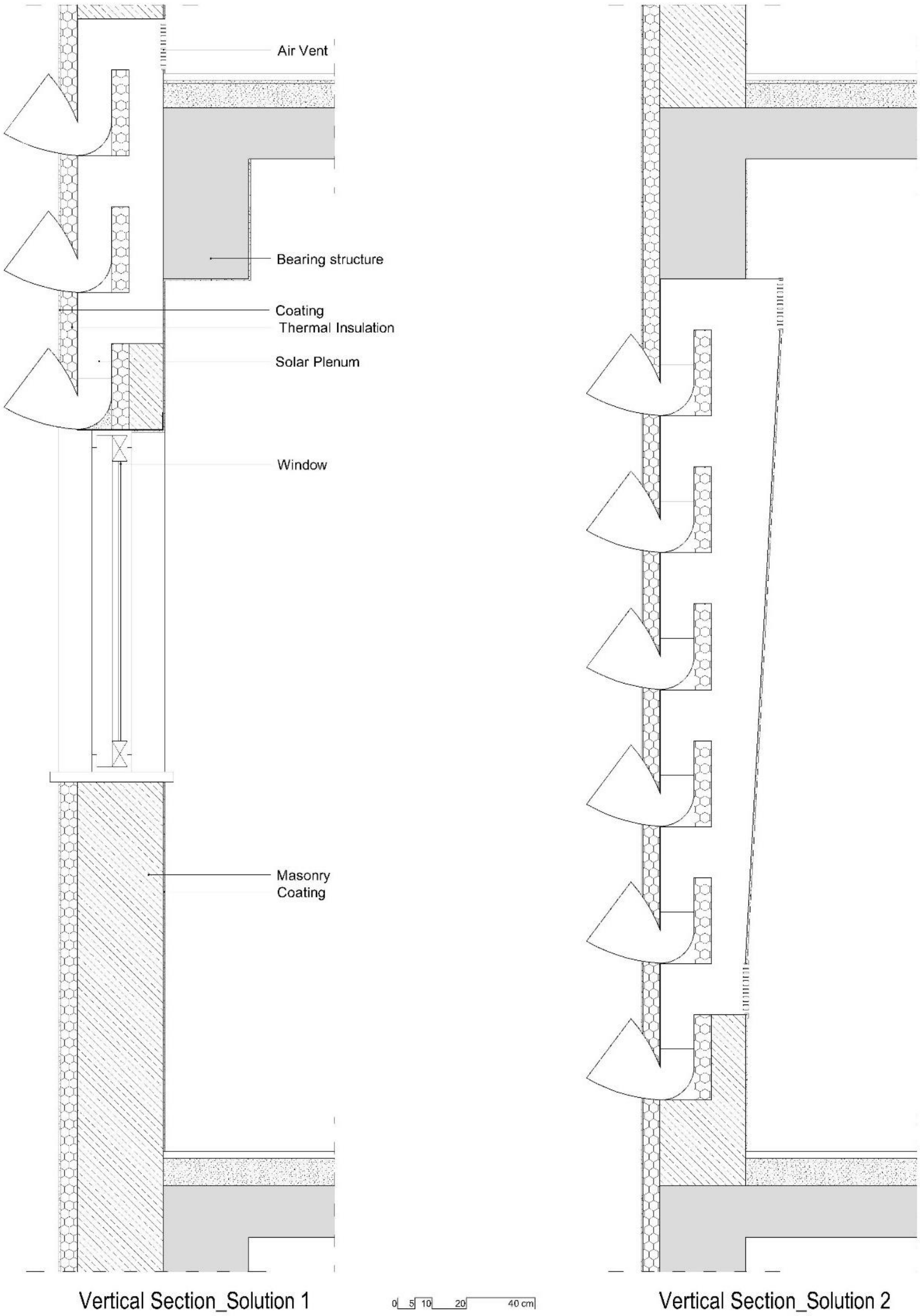

Figure 4.4.4. Vertical Sections.

4.4.7.3 Weather proofing and specific conditions influence

The installation of the system is in such a way that the external thermal insulation and contingent waterproofing comes into the system's geometry, ensures its adequacy for weather conditions. At the same time, this overlap provides adequate insulation because the combination of the system's internal thermal insulation with the insulation of the shell reduces the potential geometrical thermal bridges. The positioning of a second wall behind the system (Figure 4.4.4 – Solution 1) and the placement of plasterboard behind the module's vertical array (Figure 4.4.4 – Solution 2), ensures the continuity of the shell thus providing the necessary fire safety. Furthermore, the continuity of the shell provides the necessary soundproofing.

4.4.7.4 Services interconnection

Regarding services interconnection between two modules that are placed within a distance and in relation to the pipes that will start from the system to go to the machinery space, they will pass in the conventional way (through the walls) as with any other building piping.

4.4.7.5 Relevant regulations

The full integration of the system in the building walls and its interconnection with the conventional systems and piping, along with the fact that its construction and building integration takes into account all the above, it makes its use viable without violating any potential regulations.

4.4.8 In situ artist impression

4.4.8.1 Images and perspectives

Figure 4.4.5 shows how the system could be integrated in a small ground floor building layout.

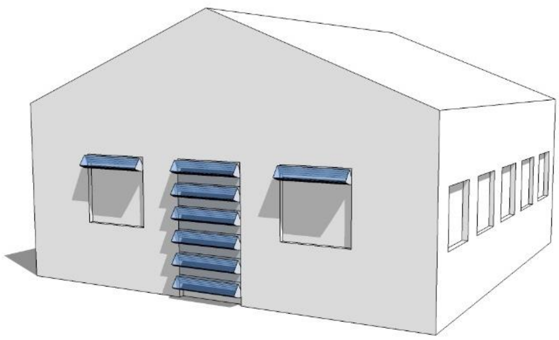

Figure 4.4.5. Integration on small building.

Figures 4.4.6 and 4.4.7 show possible building integrations of the system in multi-storey buildings, where there are several solutions.

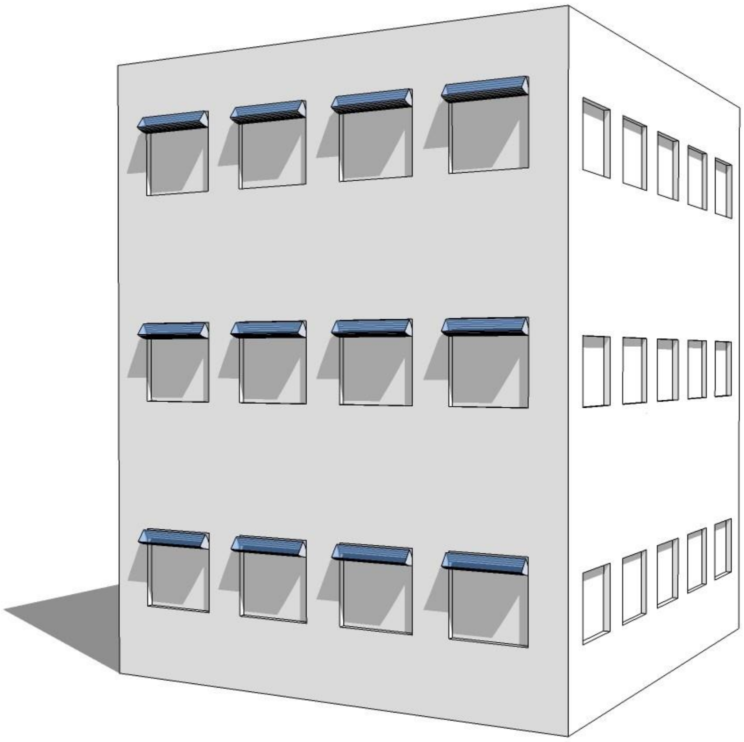

Figure 4.4.6. Integration on a multi-storey building.

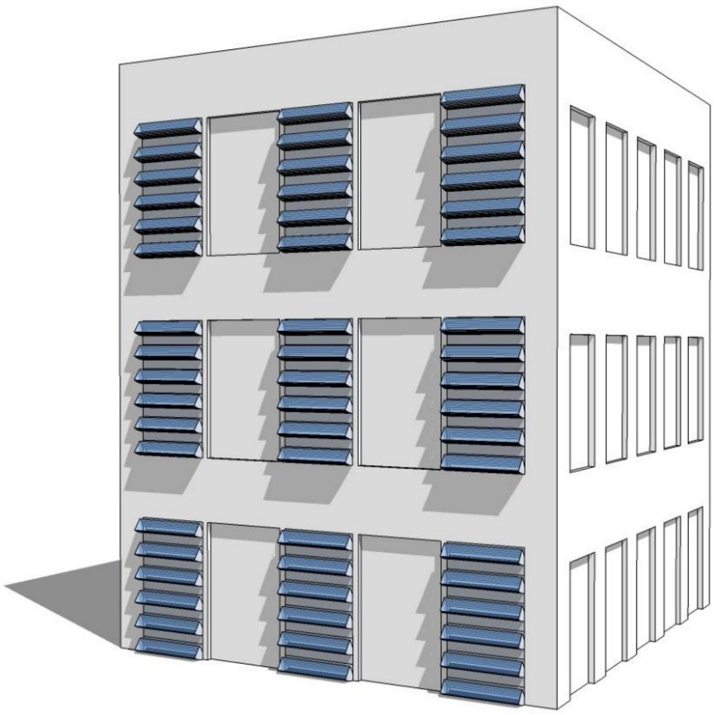

Figure 4.4.7. Integration on a multi-storey building.

4.4.8.2 Influence on aesthetics, appearance, empathy

The building integration (as shown in Figures 4.4.5, 4.4.6, 4.4.7, 4.4.8) of this system can follow the basic design principles of the building in which it is integrated. Its shape is indicated for it to be used as a horizontal louver for the south facing windows (Figure 4.4.5 and 4.4.6). When the system is consisted of multiple-module sequences, it can be alternated with orthogonal windows (Figure 4.4.7), which can be easily integrated into a building's design principles.

Figure 4.4.8. Realistic visualization of the system integrated on a multi-storey building.

4.5 NOVEL SOLAR-THERMAL COLLECTORS/ARRAY WITH INCREASED ARCHITECTURAL ACCEPTANCE FOR BUILDING INTEGRATION

Ion Vișa, Mihai Comsit[6], Anca Duță[6], Mircea Neagoe[6], Macedon Moldovan[6], Bogdan Burduhos[6], Dana Perniu[6], Alexandru Enesca[6], Luminita Isac[7], Mihaela Cosnita[7], Ioan Totu[7], Andreas Savvides[8], Constantinos Vassiliades[8]

4.5.1 Concept

The need to get power or heat from renewable energy sources is now well recognised at European and national level, due to the active measures taken in the past years for complying with the 20-20-20 EU Directive (2009/28/CE). Additionally, the development of the sustainable built environment (e.g. Nearly Zero Energy Buildings) is now subject of regulation at EU level and asks for implementing renewables on or near the buildings to meet a large share of the energy demand. Thus, implementing solar-thermal systems (STS) in the built environment is part of an ongoing effort and many barriers have to be lifted; thus, new solutions has to be found for thermal energy production, storage and management, as recognized also by the H2020 priorities. One main challenge is represented by the urban integration of the STS, which is a well addressed, yet unsolved problem. The best suited convertors for building integration are the flat-plate solar thermal collectors (FPSTC) which are mostly black or blue coloured, for obvious efficiency reasons but that have very low architectural acceptance. For façade and balconies integration there already were developed demonstrative projects, some involving coloured (others than black or dark blue) FPSTC but the solutions did not largely penetrate the market. Additionally, facades and urban structures may have very different geometries, not always suited to the rather large, state of the art FPSTC.

Following the analysis of the state of the art, a R&D project was developed aiming to develop flat-plate solar thermal collector arrays with various geometries, based on efficient solar thermal collectors adapted for urban integration, supporting the international effort towards sustainable communities. The project with the acronym EST IN URBA was granted in 2012, financed by the Romanian Agency for Research (ANCS-UEFISCDI), under the contract no. 28/2012. The project will be finalized in December 2016.

The project is divided in yearly work packages: Conceptual design (2012); Components design and development (2013); Components integration in the new FPSTC demonstrator, indoor testing and constructive optimization (2014); Functional optimization, prototyping and standardization (2015); Implementation of the FPSTC in facades and outdoor testing (2016).

The project proposes a “lego-type” interconnection of FPSTC with non-traditional shapes and colours allowing to build up facades with different geometries. To meet this prerequisite, average sized FPSTC are targeted (aperture area of 0.5…1,5 m^2), with the shape and colour following aesthetical constraints, as for example with trapezium shape and red colour.

[6] Non-COST Action member but member of COST BIST Romania Network.

[7] Non-COST Action member.

[8] Contributed only to the architectural integration demonstrations

The project is developed under the coordination of Prof. dr. eng. Ion Visa, in the research Center Renewable Energy Systems and Recycling (RESREC), part of the R&D Institute of the Transilvania University of Brasov, Romania. It is a cooperation project also involving two other universities: Politechnica University of Bucharest (Team leader: Prof. dr. Aurelia Meghea) and the University of Civil Engineering in Bucharest (Team leader: Prof. dr. eng. Florin Iordache), along with a company, The Center for Technology, Innovation and Business, in Brasov, (team leader: Eng. Ioan Totu).

The RESREC team has interdisciplinary competences: Prof. dr. eng. Ion Visa (mechanical engineering, solar energy conversion systems), Prof. dr. eng. Mircea Neagoe (industrial engineering, STS tracking systems), Assoc. prof. dr. eng. Mihai Comsit (design), Lect. dr. eng. Moldovan Macedon (installations and mechanical engineering - STS modelling and implementation), Lect dr. eng. Bogdan Burduhos (electronics – solar radiation modelling and integrated BEMS); the team is completed by the group developing materials: Prof. dr. eng. Anca Duta (solar energy materials), Prof. dr. Dana Perniu (thin films deposition techniques for absorber coatings), Prof. dr. Luminita Isac (advanced characterisation) and Assoc. prof. dr. Alexandru Enesca (self-cleaning glazings). The project involved young Ph.D. students (4) and research assistants (2).

4.5.2 Application

Typical applications of the project are the visible parts of the buildings, as facades or tilted roofs. The initial design pre-requisites of the lego-type solar-thermal arrays are:

- To be able to cover various wall and roof configurations;
- Flexible design, of lego type, matching collectors with different shapes and/or colours;
- Implementable on new or retrofitted buildings;
- Fixed ST arrays or with limited tracking;
- Mounting should allow equilibrated hydraulic pressure;
- Urban/architectural acceptance.
- To be able to significantly contribute in meeting the thermal energy demand in buildings located in temperate continental climates.

Thus the lego-type array concept can apply in various configurations, as presented in Figure 4.5.1.

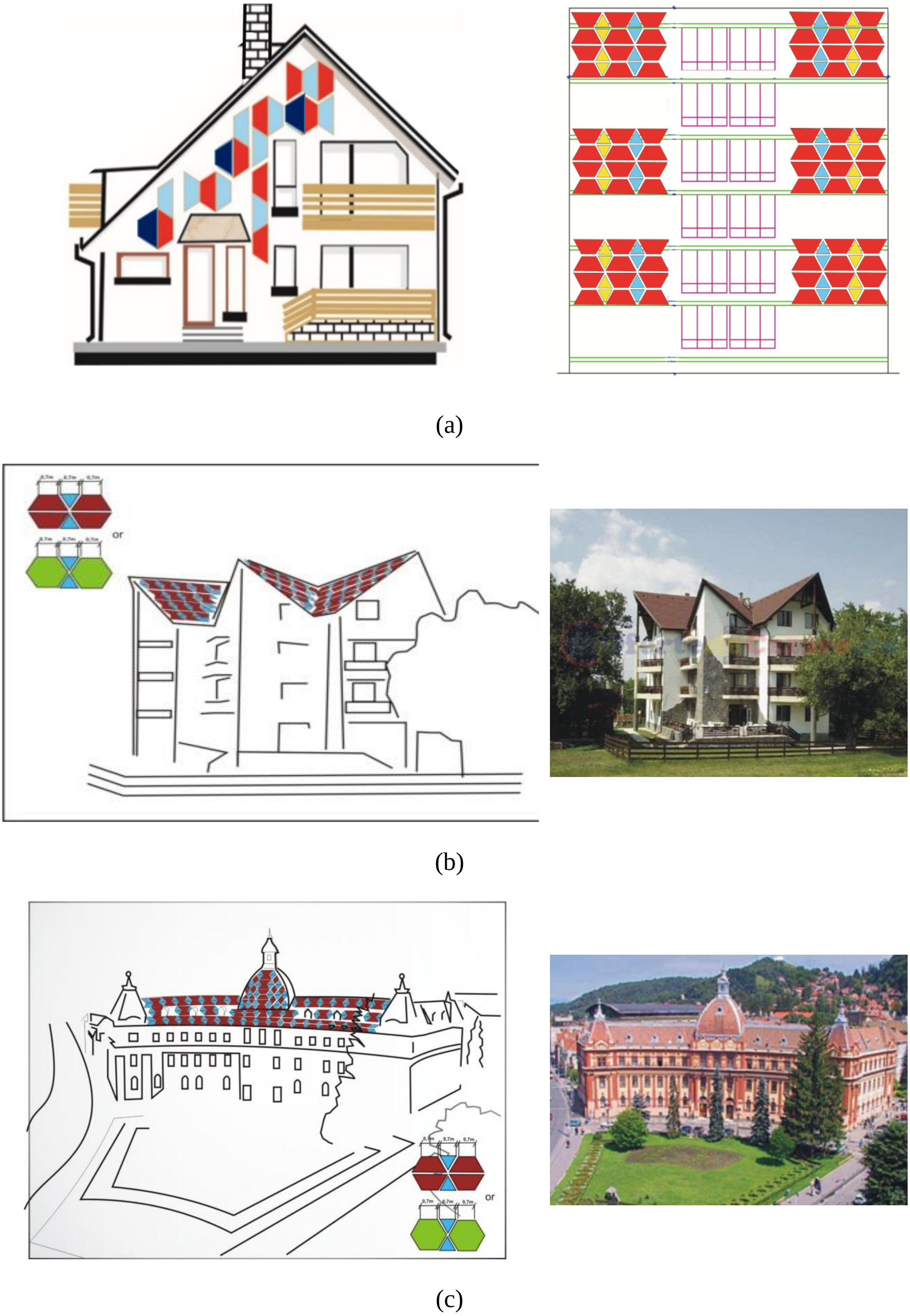

Figure 4.5.1. Concept of lego-type arrays implemented in: (a) facades of single-family houses or multi-family blocks of flats; (b) visible parts of the rooftops suitably exposed to solar radiation; (c) historical buildings.

Implementation can be done on multi-family buildings facades, Figure 4.5.1a; this allows fulfilling the obvious functionality (thermal energy production) and can increase the urban acceptance of the rather monotone city districts, mainly consisting of blocks of flats built in the previous century. In this case, the shape and the colour of the building blocks (trapeze FPSTC) and of the entire array are important mainly for aesthetical purposes. However, the arrays can be implemented on roofs with unusual shapes (Figure 4.5.1b) when the aesthetical features are complementary to the main function, of thermal energy production. A similar case is valid for historical buildings, where plenty of challenges have to be faced for preserving the "spirit of the city" while increasing the buildings' sustainability, Figure 4.5.1c.

4.5.3 Physical Description

4.5.3.1 Physical description and detailing

The new trapeze solar-thermal collector

The building block in the lego-type solar-thermal arrays with increased architectural and urban acceptance is the trapeze FPSTC. The main new/innovative features embedded in this collector are presented in Figure 4.5.2.

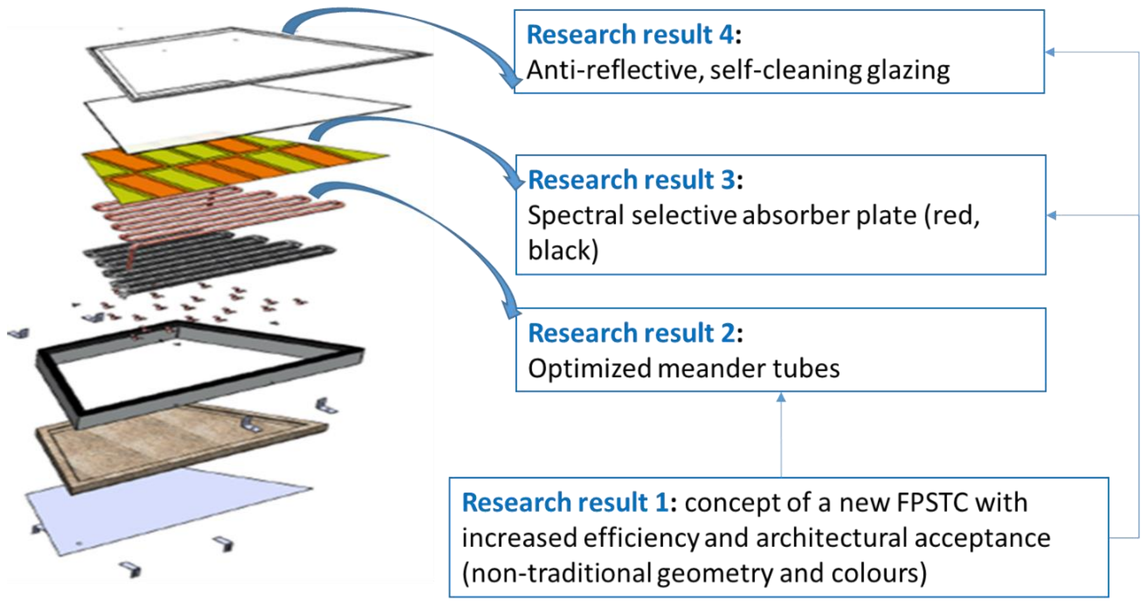

Figure 4.5.2. New/innovative features in the trapeze solar thermal collector.

Following the design and modelling step (TRL 2), a demonstrator was stepwise optimised (TRL3) as already published (Visa I., et al., Applied Thermal Engineering, 90, 2015, pp. 432–443). The main components subject of optimisation were: the absorber substrate (optimised choice: copper), the meander tube register (length, tube diameter, distance between meanders), the insulation (material, thickness and position inside the collector), the glazing (with special anti-reflecting and self-cleaning coating); the contact tubes – absorber was found – as expected - to have a significant influence on the overall performance of the collector. In the demonstrator, intermediate contact through copper clamps was used.

Starting from this demonstrator, in a second step, the prototype was developed (TRL4), considering manufacturing and scaling up issues.

The re-design mainly considered

- The components: the casing and the insulation,
- The assembly process: the solution for connecting the meander tubes with the absorber plate.
- The overall sustainability of the product: the absorber coating was re-optimized: starting from the initial rather energy intensive deposition process (spray pyrolysis deposition) and ending up with a much less energy intensive process, cold spraying of inks prepared through a green chemistry rout, sol-gel.

The solar-thermal array

Linking the trapeze solar-thermal collectors in arrays considered serial and parallel connections. These were modelled considering the thermal transfer.

In concrete terms, important is the inlet/outlet connections and, so far, these are positioned on the parallel edges of the trapeze, Figure 4.5.3a.

Central inlet/outlet positions can be considered, although these raises significant hydraulic challenges. These central connection, Figure 4.5.3b, can be well applied for roofs mounting as presented for a model considering triangle collectors:

(a)

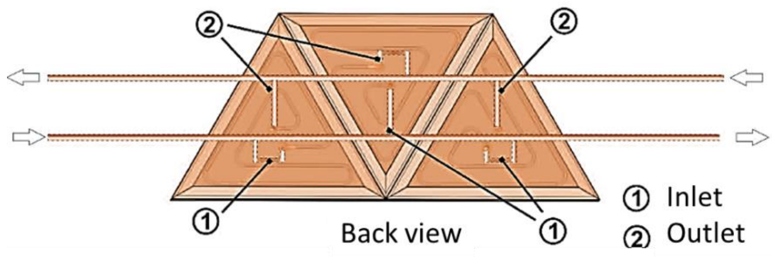

(b)

Figure 4.5.3. Inlet/outlet options of the FPSTC for arrays development: (a) for vertical facades of trapeze FPSTCs; (b) for flexible geometry of roof-mounted arrays.

4.5.4 Engineering drawings

Following the design pre-requisites, the trapeze FPSTC has an overall area of 0,67 m^2. The detailed design of the meander tubes is presented in Figure 4.5.4 while the detailed design of the entire collector is given in Figure 4.5.5.

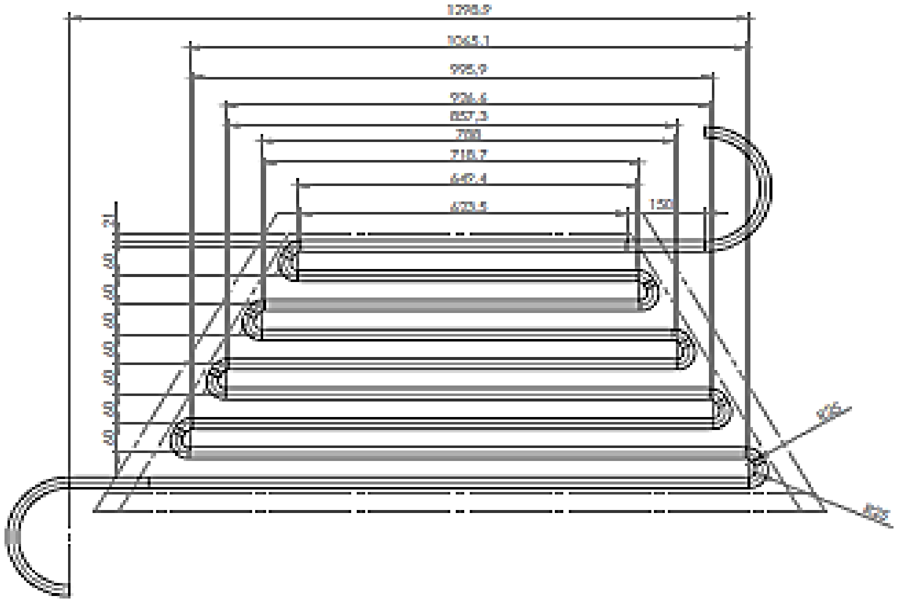

Figure 4.5.4. Detailed design of the meander tubes.

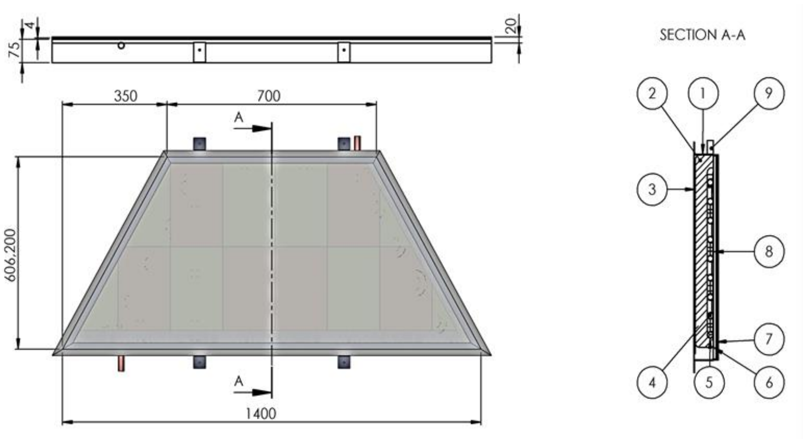

(1) metal casing with rectangular profile (surface zinc thermal treatment);

(2) mineral wool insulation;

(3) aluminium back plate (0.7mm);

(4) copper tubes;

(5) spectral selective absorber plate on aluminium substrate;

(6) copper elements for mounting the absorber plate

(7) glazing with anti-reflective and self-cleaning coating;

(8) PVC profile;

(9) fittings for the hydraulic elements

Figure 4.5.5. Detailed design of the trapeze collector.

4.5.4.1 Materials (quantity and quality), durability, duration

A synthetic presentation of the materials embedded in the prototype is given in Table 4.5.1.

Table 4.5.1. Materials in the main components of the trapeze FPSTC.

Component	**Material**	**Amount of material to develop one collector**
Casing	Steel plate with zinc surface thermal treatment	4 m
Back plate	Steel plate with zinc surface thermal treatment	0.7x700x1500mm
Insulation	Mineral wool	50 mm thickness
Meander tubes	Copper tubes (Ø22mm)	10 m
Absorber plate – substrate	Aluminium plate	0.7x700x1500mm
Absorber plate – red coating	Iron oxide(s) nano-sized pigment	93.6 g
Absorber plate – black coating	Nickel sulphide nano-sized pigment	162 g
Glazing	Polymeric glass	Glass sheet: 4x700x1500mm Plastic fixing: 2m bar
Anti-reflective and self-cleaning coating	Silica/Titania/Au nano-sized coating (insuring the solar radiation transmittance: T > 80%)	1.05

4.5.5 Physical fabrication

4.5.5.1 Fabrication process (stages, steps, effort, images, techniques, specialisms)

The general flow for developing the trapeze FPSTC prototype is presented in Figure 4.5.6, while in Figure 4.5.7 several images during the prototype development are included.

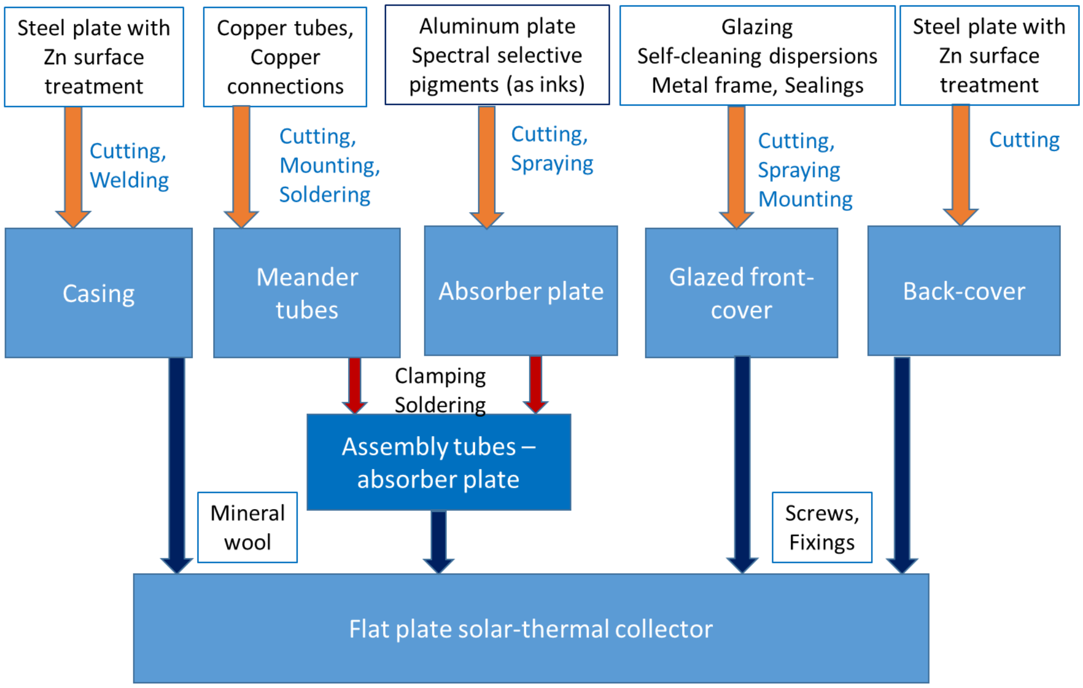

Figure 4.5.6 General flow for manufacturing the prototype of the trapeze flat plate solar thermal collector.

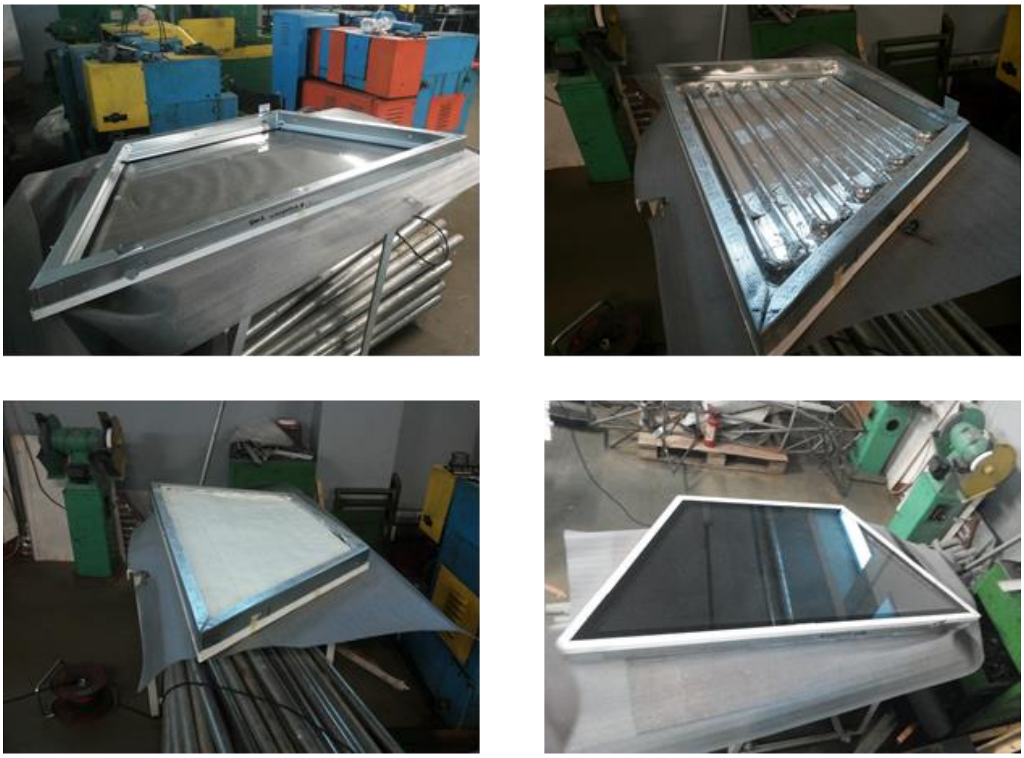

Figure 4.5.7. Steps in developing the prototype.

The red spectral selective absorber plate was obtained in black and in red colours, starting from an aluminium plate (99.7% Al), subjected to cleansing (nitric acid), controlled roughing (acid/alkaline successive treatment), rinsing; this substrate was infiltrated with iron oxides particles, as Figure 4.5.8 shows. The oxide particles were obtained through a room temperature technique (sol-gel synthesis) and were deposited through spraying (industrial technology), at 100^{o}C.

(a) (b) (c)

Figure 4.5.8. Steps in manufacturing the absorber plate: (a) aluminium substrate; (b) roughened aluminium substrate; (c) red spectral selective coating ($Al/Al_2O_3/FeO_x$).

The anti-reflective and self-cleaning glazing was obtained starting from the polymeric glass, successively cleaned with water and alcohol. The anti-reflective coating was obtained from dispersions/inks containing silica and titania nano-particles deposited in a layer – by layer spraying process. Standard “heavy duty” photocatalytic tests (using methylene blue as pollutant/dirt simulator) showed a self-cleaning capacity of about 40% after 4 hours under solar simulated radiation.

4.5.5.2 Assembly process (stages, steps, effort, images, techniques, specialisms)

To develop the façade, the trapeze FPSTCs have to be assembled, following serial or parallel connections. However, in meeting a certain energy demand, the facades design has to use infield data (energy output and solar to thermal conversion efficiency). To collect these data, the FPSTC was vertically installed on the façade of the solar-thermal laboratory, in the R&D Institute of the Transilvania University. The experimental set-up includes one commercial FPSTC and one evacuated tube collector, installed on the same façade, along with similar commercial collectors installed on the laboratory flat roof, tilted at the optimal angle of 35^{o}. The experimental set-up is presented in Figure 4.5.9.

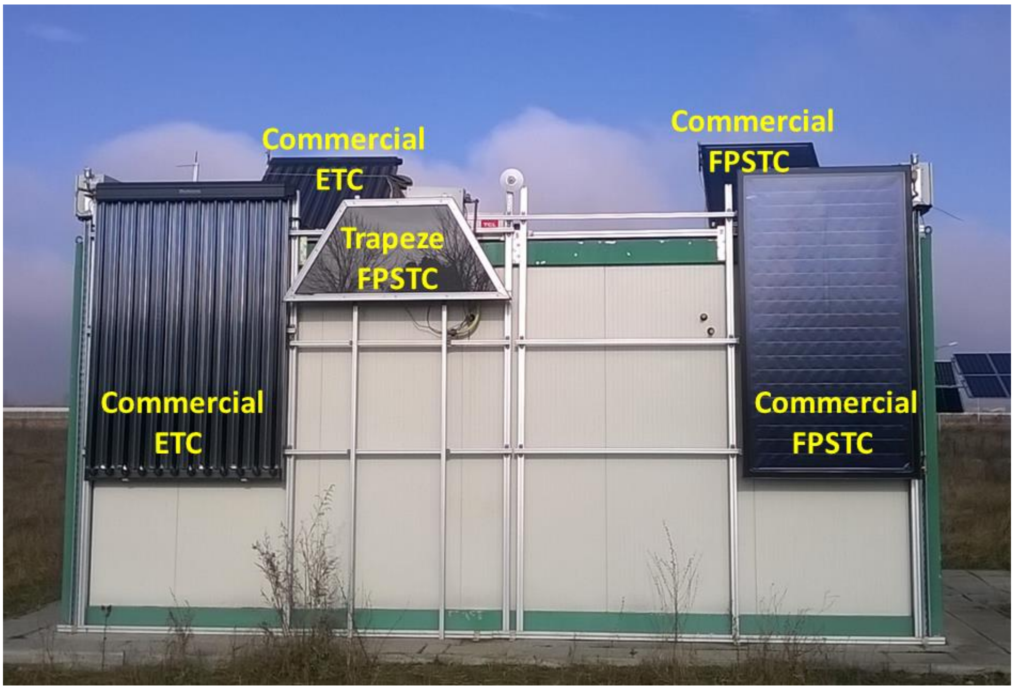

(a)

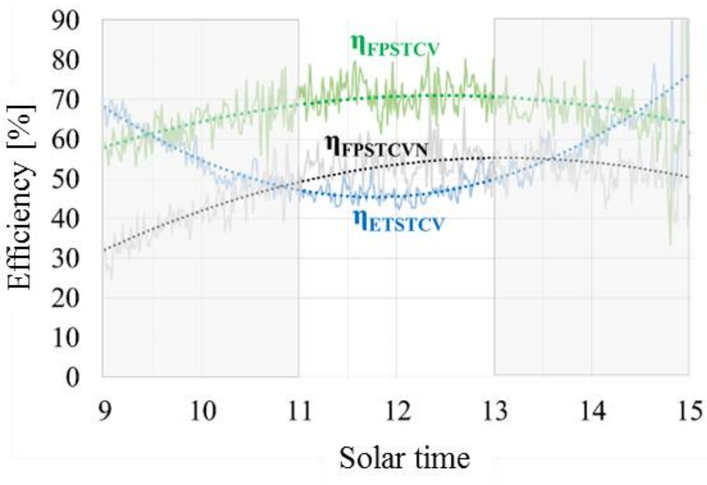

(b)

Figure 4.5.9. (a) Outdoor set-up for comparative outdoor testing the trapeze flat plate solar-thermal collector and commercial collectors of flat plate (FPSTC) and evacuated tubes (ETC) types; (b) efficiency variation of the vertically mounted trapeze collector (FPSTCVN), of the commercial flat plate collector (FPSTCV) and of the commercial evacuated tube collector (ETSTCV), during June 23, 2015.

For the vertically mounted collectors, the efficiencies were calculated and one example for a day close to the summer solstice is given in Figure 4.5.9b.

4.5.6 Modular configuration

4.5.6.1 Units size and dimensions

The building block of the new solar-thermal facades has the dimensions as described in Figure 4.5.5.

4.5.6.2 Modularisation and upscaling

The isosceles trapeze geometry of the unit flat plate solar-thermal collector allows developing modular structures. The limit in assembling the collectors into arrays is given by the connection geometry (parallel or serial); while for parallel connections the hydraulics is the main optimisation feature, for serial connection, the output temperature of the last collector in the series will govern the number of units in a row. Preliminary modelling shows that optimally no more than four collectors are recommended to be serially connected. Further on, modelling showed that the trapeze collector can be linearly up-scaled at dimensions as presented in Figure 4.5.10. For these collectors, modularisation can be translated to the manufacturer, by delivering assemblies of two collectors.

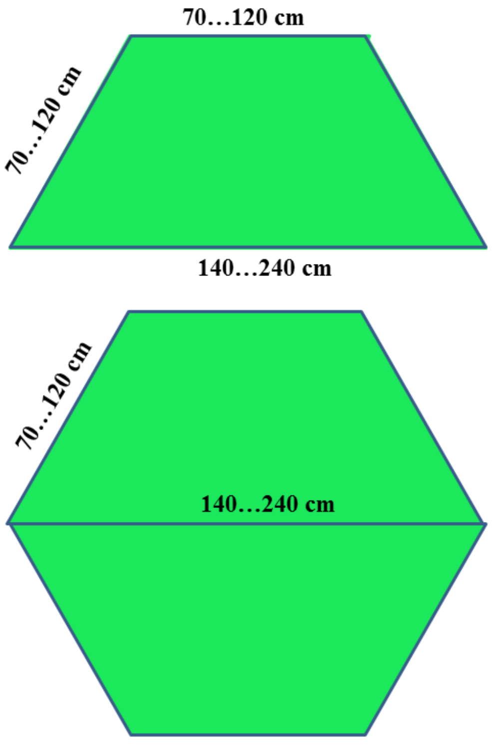

Figure 4.5.10. Modular units of two trapeze FPSTC possible to be delivered by the manufacturer.

Considering the building of the RESREC R&D Centre, building integration was developed at conceptual level, as presented in Figure 4.5.11.

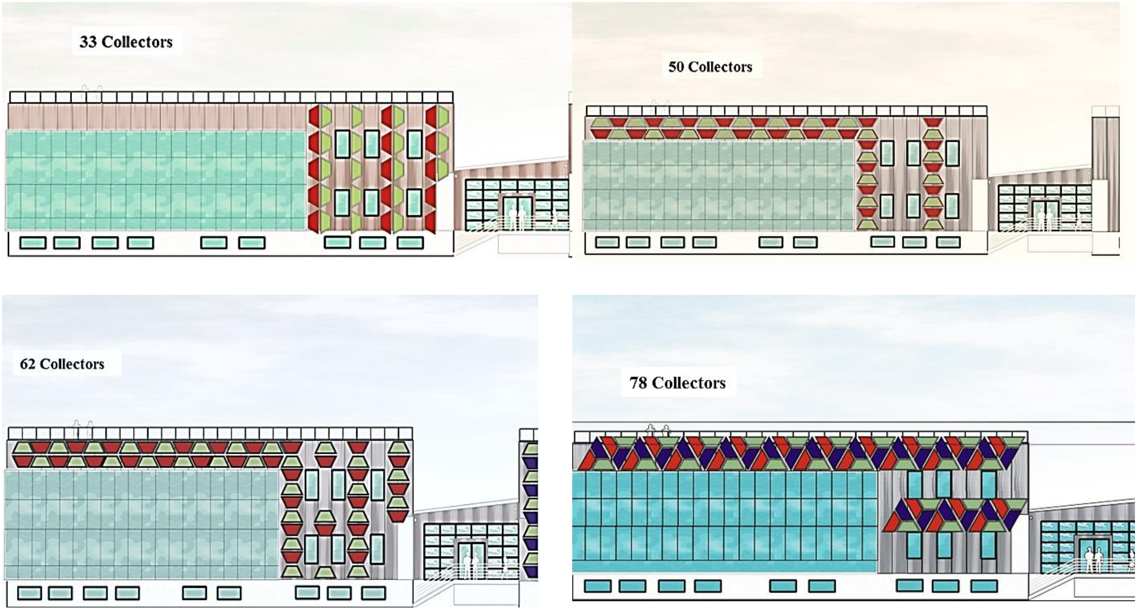

Figure 4.5.11. Solar-thermal arrays integrate on the facades.

The development and testing of the solar-thermal facade is ongoing and the results will be comparatively analysed at the end of 2016.

4.5.6.3 Product development (potential for commercialisation, mass manufacturing, DfM)

The EST in URBA project has as final outcome a prototype façade. A pre-feasibility study developed by the industry partner considered, for market implementation, only existent technologies. The feasible alternative is to develop an integrated approach for the design, development and implementation of customised projects, for urban integration, thus embedding products and knowledge for tailored finite products adapted to the end-users (building owners). It was estimated that for a 10 m^2 array system with variable geometry, the number of implemented arrays/year (after finalizing the project) will be: year I: 4; year II: 6; year III: 10; year IV: 12.

A cost – benefit analysis on the project’s implementation shows that the financial investment of the industry partner will be recovered in: 4.21 years. The solely risk presumed to have success with this project is associated to the political and financial instruments supporting the implementation of solar-thermal systems in the built environment.

During the project development, two patent applications were submitted and are under evaluation:

1. Visa I., Duta A., Neagoe M., Comsit M., Moldovan M., Burduhos B., System of flat polygonal solar panels modular built for being integrated into the facades, RO128860(A0)

2. Vișa I., Comsit M., Duță A., Neagoe M., Saulescu R., Ciobanu D., Moldovan M., Burduhos B., Perniu D., Enesca A., Isac L., Mihoreanu C., Ienei E., Totu I., Modular solar collector to optimize the conversion efficiency and increase the architectural acceptance, RO130275 (A0)/29.05.2015

4.5.7 Physical mounting/installation

4.5.7.1 Structural integration

The system's building integration is done by the accession of the system on the shell of and the static body of the building. At some points, a metal frame is placed behind the system (by replacing the external insulation of the building), which accommodates the system's piping and at the same time reinforces the structural efficiency of the system (Figures 4.5.12 and 4.5.13).

4.5.7.2 Section Detailing

The system is placed on the building's masonry in such a manner that it becomes a layer of it, as shown in Figures 4.5.12 and 4.5.13. The construction is such that the system becomes the external layer of the building's shell, which covers the thermal insulation of it. At the points where the system is used as a horizontal shading louver, a metallic beam is used in order to ensure its structural integrity and accommodate the necessary pipes. In selected external locations, control points are placed.

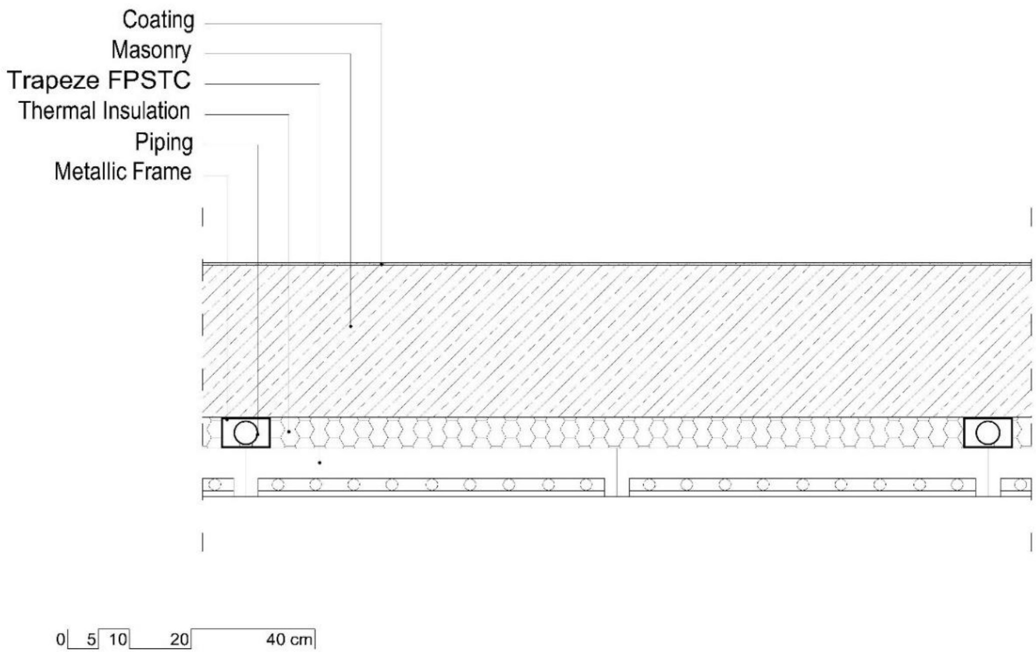

Figure 4.5.12. Horizontal Section.

4.5.7.3 Weather proofing and specific conditions influence

The installation of the system is in such a way that provides an extra layer of protection on the external thermal insulation and contingent waterproofing, ensures the shell's adequacy on weather conditions. At the same time, this extra layer provides maximum insulation because the combination of the system's internal insulation with the insulation of the shell reduces the possibility of thermal bridges and at the same time increases the overall thermal insulation. The positioning of the system as an independent layer, provides the necessary continuity of the shell thus providing an indicative fire safety. Furthermore, this continuity of the shell provides the necessary soundproofing.

4.5.7.4 Services interconnection

Regarding services interconnection, they will connect to the system through the metal frame which also acts as a structural reinforcement of the system (Figures 4.5.12 and 4.5.13).

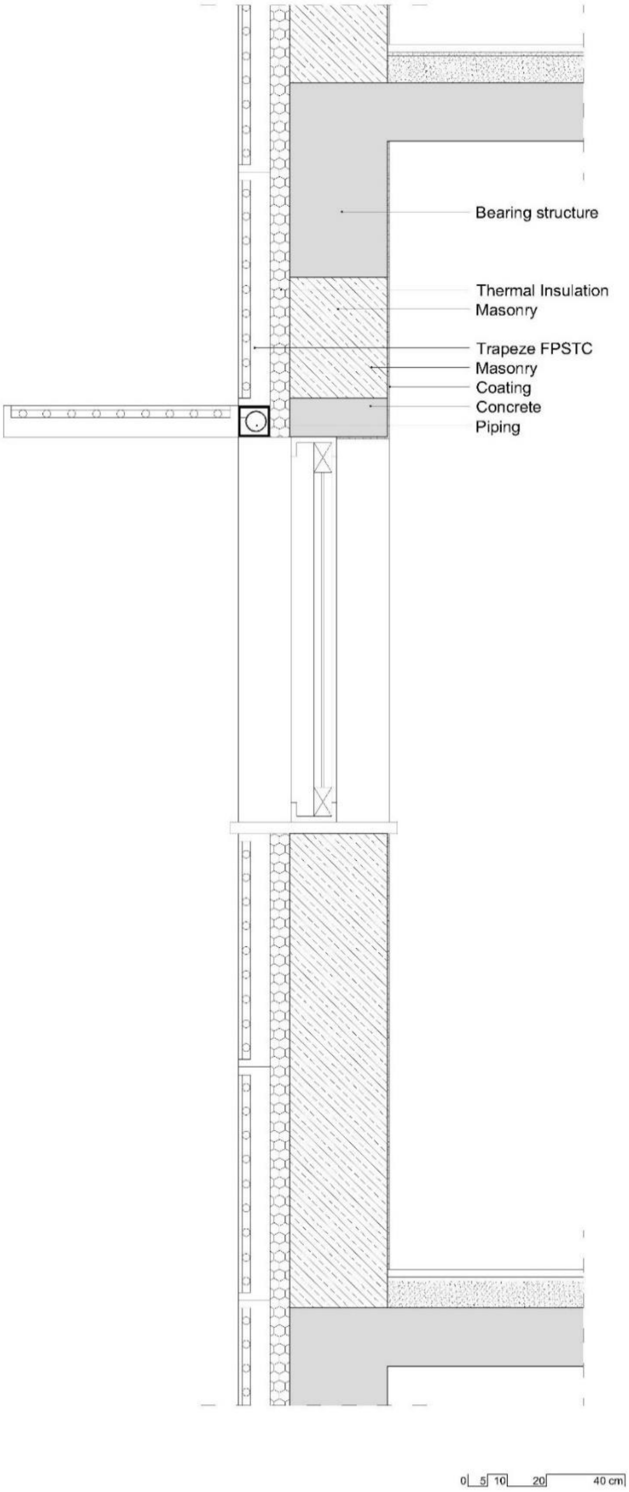

Figure 4.5.13. Vertical Section (corresponding to Figure 4.5.16).

In relation to the piping between two modules that are placed within a distance and in relation to the pipes that will start from the system to go to the machinery space, they will pass in the conventional way (through the walls) as the rest of the building's piping.

4.5.7.5 Relevant regulations

The full integration of the system in the building walls and its interconnection with the conventional systems and piping, along with the fact that its construction and building integration takes into account all the above, it makes its use viable without violating any potential regulations.

4.5.8 In situ artist impression

4.5.8.1 Images and perspectives

The collectors developed within the EST IN URBA project have several distinct features: non-traditional shape (trapeze) and rather small conversion area; additionally, they have colours that support architectural acceptance: red, green. These features show that the collectors are not aiming at replacing the commercial FPSTC for traditional implementation areas on the buildings (e.g. on the roofs or top terraces). The novel type of collectors is therefore designated for implementation areas on the buildings which are not commonly considered as suitable.

Therefore, besides the distinct features supporting architectural integration, the design of the arrays or single collectors as part of the buildings represents an important support in the market and social acceptance. Additionally, multi-functionality can enlarge the applications, as e.g. the shading role of the collectors, mounted on the facades.

These were the concepts that further allowed formulating several implementation solutions; some of these are further on detailed, at conceptual design phase, along with several constraints imposed by functionality.

Figure 4.5.14 shows how the system could be integrated in a small ground floor building layout. The design in Figure 4.5.14a and b uses the building units in Figure 4.5.14c.

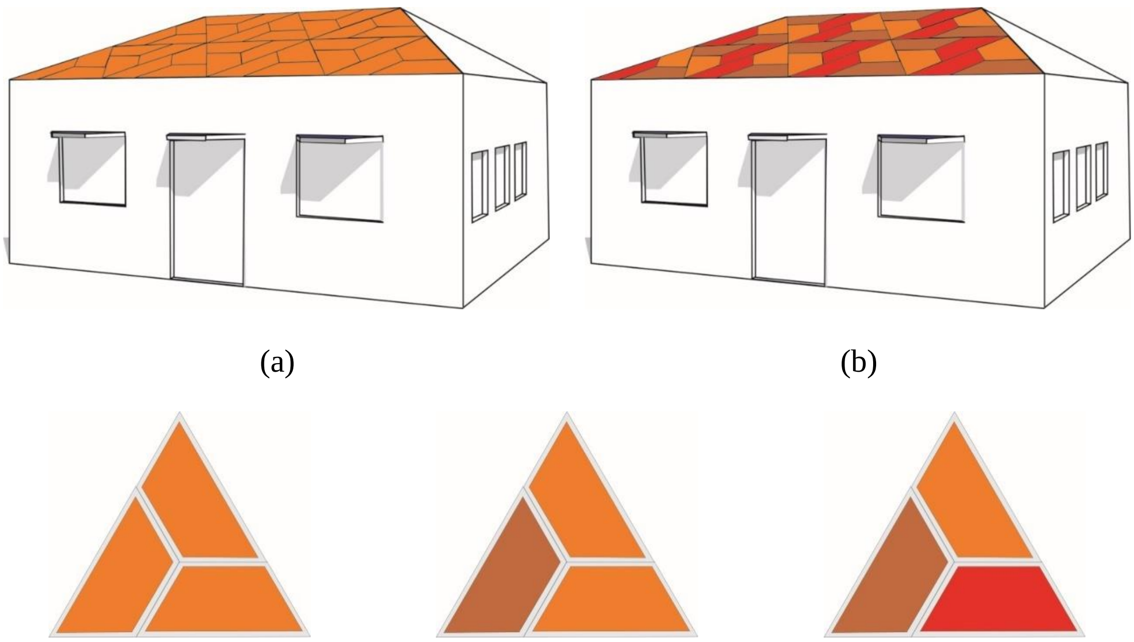

(a) (b)

(c)

Figure 4.5.14. Integration on small building: (a) mono-chromatic and (b) multi-coloured roofs using (c) one typical building unit of three trapeze collectors.

Figures 4.5.15 and 4.5.16 show possible building integrations of the system in multi-storey buildings, where there are several solutions.

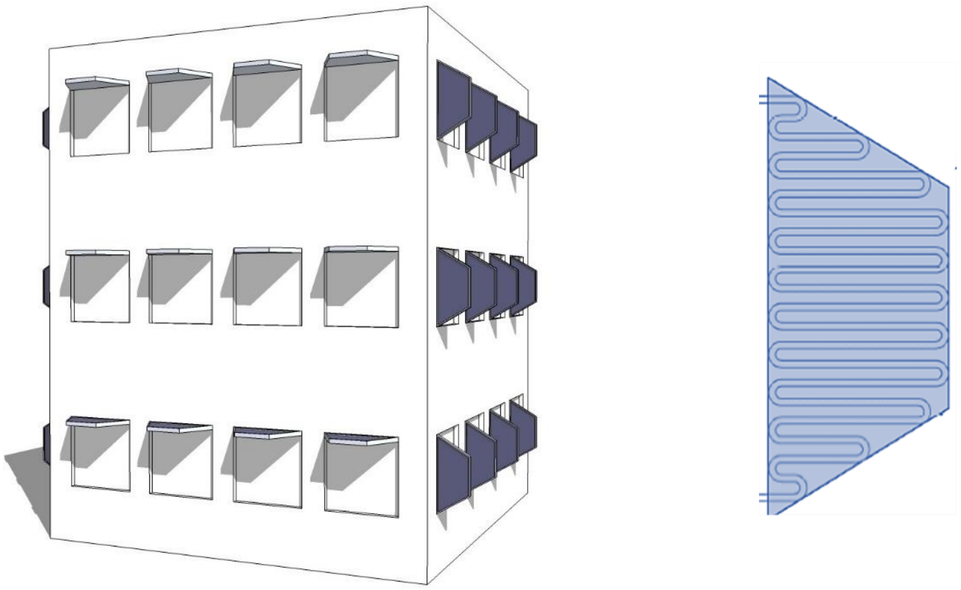

(a) (b)

Figure 4.5.15. (a) Integration on a multi-storey building; (b) typical tubing for a collector used as vertical louvre.

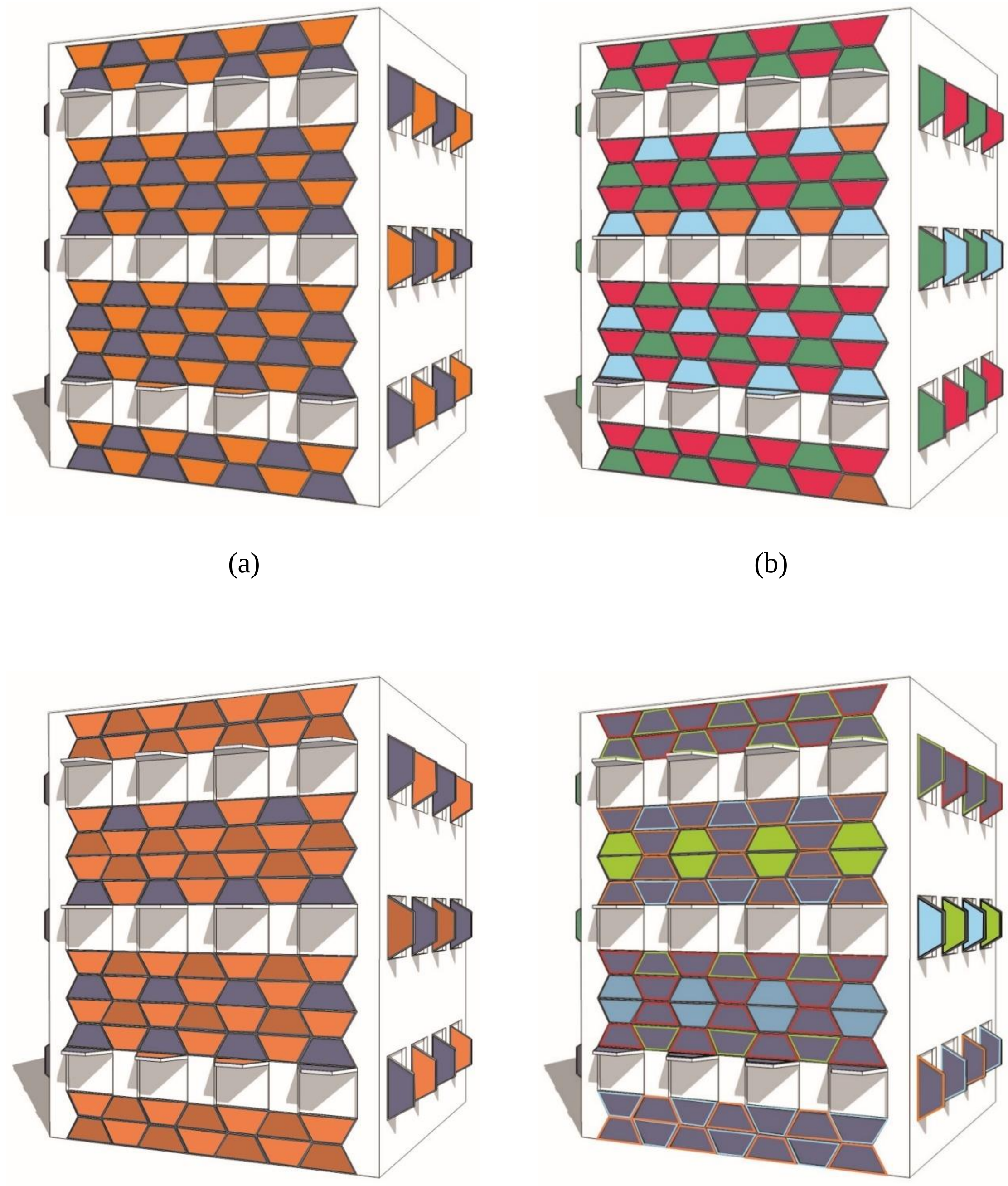

(a) (b)

(c) (d)

Figure 4.5.16. Integration on a multi-storey building of arrays consisting of multi-coloured trapeze collectors (a…d), with mono-chromatic (a…c) or variously coloured (d) frames.

4.5.8.2 Influence on aesthetics, appearance, empathy

The building integration (as shown in Figures 4.5.14, 4.5.15, 4.5.16) of this system can follow the basic design principles of the building in which it is integrated. Its planar shape is indicated for it to be used as a horizontal louver for the south facing windows (Figures 4.5.14, 4.5.15, 4.5.16).

The horizontal mounting can be subject of improvement by accepting a tilt angle that allows water-flow (e.g. rain water cleaning the surface) and can limit snow retention if the collectors are installed in regions where winter brings low temperatures and significant precipitations. The tilt angle should offer a compromise between these functional pre-requisites, the shading effect, the light penetration in the building, and the solar-thermal conversion efficiency, thus it can vary from 5^o up to the optimal tilt angle in the implementation location. In a further approach, this tilt angle can be set variable (at least seasonally).

Additionally, the horizontal/tilted mounting asks for re-designing the piping outside the collector. This issues have to be solved by a smart design of the mounting frame.

The collectors can be mounted also as a vertical louver for the east and west facing windows (Figures 4.5.15, 4.5.16). This will add the shading functionality but asks for constructive changes, as the tubes serpentine has to be differently mounted, Figure 4.5.15b.

At the same time the system can easily be used as a wall and/or a roof covering layer (Figures 4.5.14, 4.5.16), which provides a lot of advantages, such as the limitation of the building's cost (no need for wall paint or roof tiles) or the reduction of the building's energy needs (it could provide an extra layer of insulation). When the system is consisted of multiple-module sequences, it can be placed in horizontal arrays which can be easily integrated into a building's design principles (Figure 4.5.17).

Figure 4.5.17. Realistic visualization of the system integrated on a multi-storey building.

4.6 PORTER BUILDING, TEL AVIV, ISRAEL

Yasha Grobman, Nir Chen[9], Joseph Cory[9], Sandra M. Silva, Ricardo Mateus, Manuela G. Almeida

4.6.1 Introduction

The Porter School of Environmental studies (PSES), Tel-Aviv, Israel, building was designed as a "green building". The building design utilized environmental parameters (such as solar radiation, wind, acoustics and more) in determining the form that the building would take and its position on the site. The building makes use of passive and active technologies for production of energy, energy conservation and recycling of waste and water.

4.6.2 Description of the building

This chapter presents the new building of the Porter School of Environmental Studies (PSES), located on Tel-Aviv University campus. It incorporates classrooms, graduate student rooms, offices, an atrium, a cafeteria, an auditorium and a green roof. It also provides various internal spaces for informal activities such as meeting places for students and researchers, as well as government officials, industry representatives, and members of environmental organizations, involved in the school's activities.

4.6.3 Design concept and building features

The Porter School was designed on a site that served as a Parking lot and was previously the dumpsite for building debris of the Tel Aviv University. It is located on one of the highest hills in Tel Aviv overlooking the Cities of Tel-Aviv and Ramat Gan and the Yarkon metropolitan park. The site is exposed to the harsh condition of the Israeli southern sun radiation and to the acoustic pollution from the automobile and rail transport rising for Israel’s busiest highway (Figure 4.6.1).

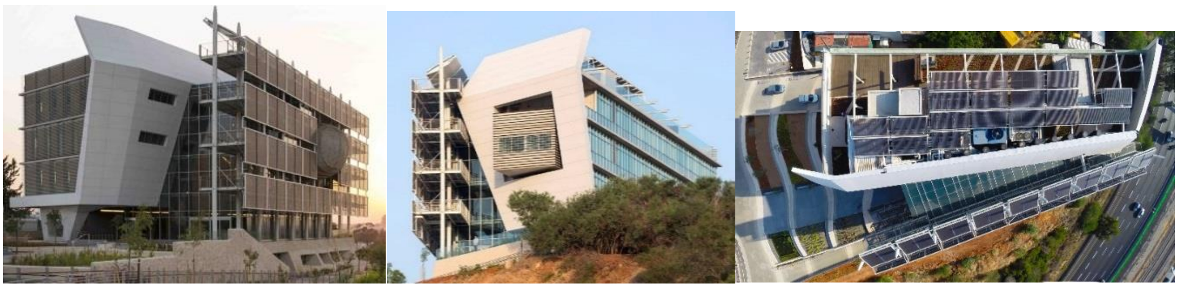

Figure 4.6.1. General views of Porter Building (west, south, east and north façade and roof).

The building form is a rectangle stretched out along an east-west axis. The south facing area is due to the public and the main offices and other functions are located on the northern façade area. An atrium connects these two areas housing the public activities and the main

[9] Non-COST Action member.

building circulation paths. The main materials of the building are exposed concrete, Euro panel cladding tiles, wood (mainly bamboo) and metal. The colour scheme of the building is mainly white grey and natural wood.

The auditorium, which is the largest function of the building, is located in the basement, with an independent entrance (designed using ideas from vernacular traditional terraces design) for external events. The main conference room of the building is “the capsule” (Figure 4.6.2). “The capsule” creates a balance in the composition of the south façade and serves as a screen on which the building’s energy savings and regional air pollution can be publically projected.

Figure 4.6.2. “The capsule” view from outside and inside.

Shading of the main building is accomplished with an "Eco-wall", an area with one row of indoor / outdoor occupied spaces, used as open laboratories or closed plug-in rooms for visiting researchers, situated along the South side of the building. These spaces are minimally conditioned and act as a buffer to control the solar radiation incident upon the building.

The form of the main mass of the building and the angle between the “Eco-wall” and the main mass of the building were defined to integrate natural light conditions and natural ventilation. It creates a Venturi effect that enhances airflow for natural ventilation and a wind turbine. The inclined walls of the main building mass were created and optimized to contain future photovoltaic cells.

The south facade of the “Eco-wall” is covered with an array of solar thermal tubes which produce hot water and shade the “Eco-wall” spaces. The hot water also serves to heat the building during the winter and power an absorption cycle chiller to cool the building in summer.

A four-storey atrium is the center of the buildings mixed-mode ventilation strategy. Equipped with solar chimneys at the roof level (Figure 4.6.3), the stack effect generated helps to provide ventilation to most of the building when conditions permit (Figure 4.6.4). Supplementary ventilation as well as air conditioning is provided by a rooftop makeup air unit equipped with energy recovery. At the zone level, spaces are conditioned by fan coil units, 4-pipe active chilled beams, and radiant floor. Occupancy and photo-sensors throughout the building tune the lighting system to the precise level required as dictated by space use and available daylight.

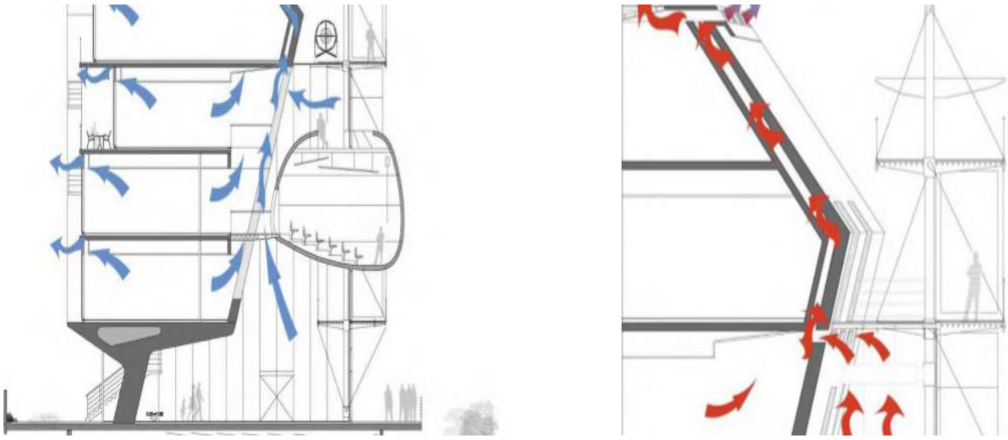

Figure 4.6.3. Passive ventilation scheme (left) and hot air chimney - hot air discharges through special chimneys in the building envelope (right).

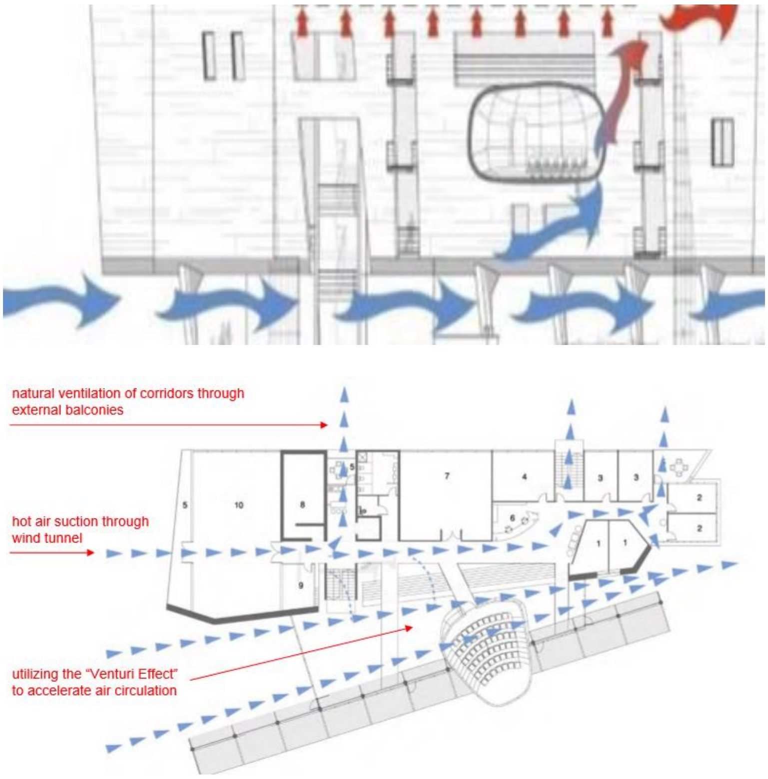

Figure 4.6.4. Passive ventilation through Main Atrium.

The building incorporates the following technologies:

- A thermo solar air-condition system running on energy created via a system of vacuum tubes on the building facades and roof (Figure 4.6.5). This system (the air condition system or the vacuum tubes system) transfers energy surplus generated in the building to adjoining buildings in the campus;

- Chilled beam system for air condition – an air condition diffuser that works about 20% more efficiently than normal systems (works on higher temperatures and does not need strong electric fans to distribute the cool air);

- A computer controlled natural ventilation system that allows natural ventilation and night cooling in predefined conditions;
- A computer control system for artificial illumination and shading curtains;
- A green roof;
- A grey water system that reuses water from the showers, kitchenette and air-condition to irrigate the green roof and the landscape;
- Floor heating and cooling.

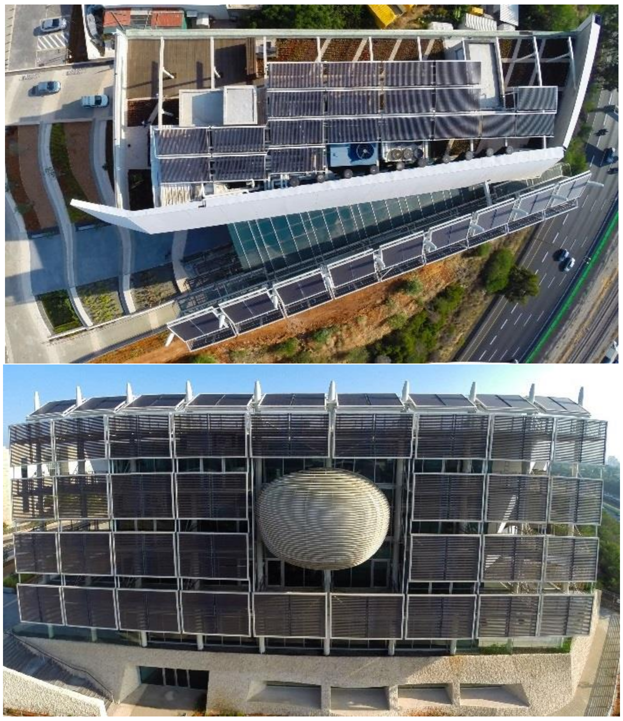

Figure 4.6.5. General view of the vacuum tubes installed on the building roof and façade.

4.6.4 Building Controls

The building operates with a Building Automation System scheduled on between 05h and 21h.

4.6.5 Cooling / Heating Plant Systems

4.6.5.1 Hot Water Loops

A 5000 litre hot water storage/transfer tank exchanges energy between hot water loops. A coil within the tank transfers energy to the medium hot water loop (50ºC). Boiler water is circulated on an open loop with the tank, and solar thermal water circulates on an open loop between the tank and the HX-1.

Three separate arrays of evacuated tube solar-thermal collectors provide hot water to the building. One array is mounted vertically on the façade of the "Eco-Wall". The second is mounted at an angle on the "EyeBrow" above the EcoWall. The third is mounted horizontally and shades mechanical equipment on the roof. 24 m^3/hr of water is circulated through the three arrays by P-1 at a common supply and return header. Design temperatures produced by the loop are 98ºC supply and 83ºC return. Heat is transferred via HX-1 to a loop, pumped by P-2 serving the hot water tank which has a separate gas boiler as backup heat source. 24 m^3/hr at 95/80ºC.

P-5 sends 24m^3/hr of hot water at 95ºC directly from the water tank to the absorption chiller, which operates on 10ºC ΔT. A heat exchanger within the hot water tank is pumped by two secondary loops (P-7 and P-8) which respectively serve the radiant floor slab circuit (in Winter) and air-side coils (FCUs, AHUs, IUs) with 50ºC supply / 40ºC return water.

4.6.5.2 Chilled Water Loops

The chilled water loop is designed in primary / secondary configuration. Then entire system is capable of producing 66 m^3/hr of chilled water at 7ºC. The absorption chiller produces 36 m^3/hr chilled water at a nominal 7ºC in optimal conditions. When the auditorium unit is running, or when the total building load on the chilled water loop exceeds the 60-ton capacity of the absorption chiller, a second air-cooled chiller rated at 70 tons capacity and connected to the primary loop is activated. Pump P-9 circulates primary chilled water of the absorption chiller to and from CHS/R primary headers. The air-cooled chiller has dual integral pumps which circulate CHW to the primary loop. Both chillers are connected to a common header.

The supply side header is connected to three secondary loops served by pumps P-10, P-11 and P-12. The first (P-10) is delivers chilled water at 7ºC to Fan coil units on each floor, as well as the basement Auditorium Air Handling unit. The second (P-11) is connected via a 3-way mixing valve to the tertiary loop which delivers water at 14ºC to the induction units at each floor. In summer, this loop also serves the radiant floor slab loops. Return water from this system is partially recirculated through Pump P-11, which is boosting the primary flow of 15 m^3/hr of 7ºC water to 26m^3/hr of mixed water at 14ºC.

The third (P-12) delivers up to 36m^3/hr of chilled water to a heat exchanger (HX-4). This connects to a cooling system serving data centre located in an adjacent building. In this way, the solar thermal collectors and the constant operation of the absorption chiller are taken full advantage of by essentially exporting renewable energy produced on the site of Porter.

4.6.5.3 Absorption Chiller

The 60-ton capacity absorption cycle chiller is energized by a heat medium (hot water) above 85ºC heated by a solar energy heat source and its condenser is cooled by a cooling tower. The absorption chiller uses a solution of lithium bromide and water, under a vacuum, as the working fluid. Water is the refrigerant and lithium bromide, a nontoxic salt, is the absorbent. Refrigerant, liberated by heat from the solution, produces a refrigerating effect in the evaporator when cooling water is circulated through the condenser and absorber. In the cooling cycle there are four dominant stages: generator, condenser, evaporator, and absorber. The energy consuming compressor stage of a conventional refrigeration cycle is obsolete in the absorption cycle.

The absorption chiller runs whenever solar hot water is available. When solar-thermal water is available and there is little or no cooling load in the building, the chiller runs at maximum capacity and sends any excess chilled water to another (existing) building on campus which always has cooling needs due to the presence of a data center. The capacity of the chiller exceeds the maximum production rate of the solar thermal arrays – solar thermal energy is never dumped or wasted.

4.6.6 Cooling tower

An open circuit cooling tower (Figure 4.6.6) is used to reject heat emitted on the condenser side of the absorption chiller unit. A variable speed fan regulates the cooling tower airflow so that leaving condenser water is at or below 30ºC going back to the chiller. Constant volume pump P-3 (84 m^3/hr) serves this loop.

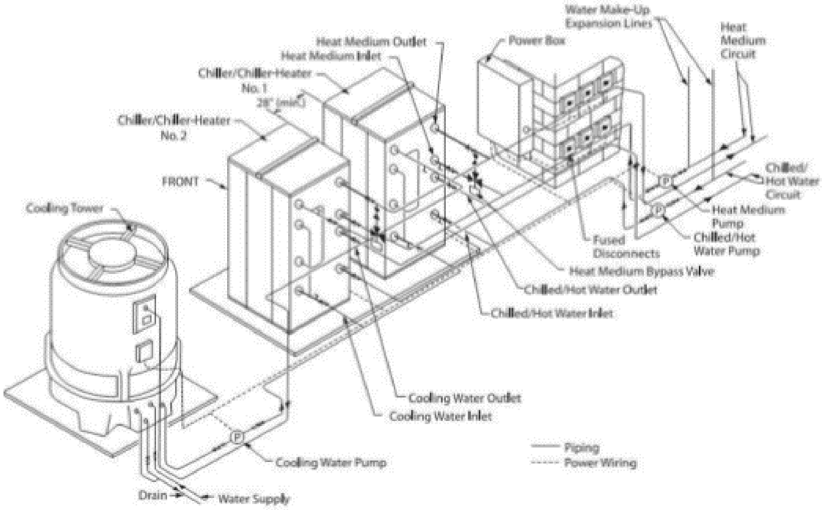

Figure 4.6.6. Cooling tower.

4.6.6.1 Air-Cooled Chiller

A 70-ton capacity High-Efficiency Trane air-cooled chiller with scroll compressors provides 70 tons capacity of chilled water to the main chilled water header. It uses refrigerant R-410a. This chiller is only in operation after the load of the building exceeds the capacity of the absorption chiller (e.g., during periods when there is insufficient solar insolation to produce 85ºC water, etc. or building loads are greater than 60 tons.). Minimum load is 30%. At design conditions, this chiller operates at 3.18 EER and at 4.64 EER under Eurovent Testing conditions. Twin pumps integral to the chiller provide CHW circulation.

4.6.6.2 Solar Thermal Evacuated Tubes

A total of 705.4 m^2 of U-Pipe evacuated solar thermal collector tubes are integrated into the façade of the “Eco-Wall” (422 m^2), above the “Eco-Wall” (108 m^2) and on the roof (175 m^2) as shading elements which produce most of the heating and cooling energy for the building. The array is connected via Pump P-1 (24 m^3/hr, VSD) and HX-1 to the Hot Water Storage Tank. The solar collectors are allowed to operate on a schedule of 6 am to 8pm in summer and 7am to 5pm in winter. Control valves keep the output temperature of the array between

75ºC and 120ºC. Variable speed pump P-2 operates the HW loop side of the HX-1 and modulates between 0 and 100% flow as the fluid temperature is between 30 and 100 ºC.

4.6.6.3 Boilers

A natural gas boiler with capacity of 116 kW provides hot water flow, via Pump P-14 at 8.4 m^3/hr to a heat exchanger within the 5000 litre Hot Water Storage tank.

4.6.7 Space Heating / Cooling systems

4.6.7.1 Fan Coil Units

Spaces located in the "Eco-Wall" as well as the conference room, auditorium tech booth, and basement mechanical areas are conditioned with two-pipe fan coil units. Each FCU receives hot water from the solar thermal system and chilled water at 7ºC from the chilled water loop. Under design conditions, the water is returned to the CHW loop at 12ºC. Occupancy sensors tied to control valves on the IUs allow for space temperature set points to be reset to unoccupied values.

4.6.7.2 Active Chilled Beams

4- pipe Active Chilled Beams (Induction Units) condition the majority of the building. Each IU receives hot water from the solar thermal system at 50ºC and chilled water at 14ºC. One coil is dedicated to cooling, while another coil is dedicated to heating. Air temperature is maintained by coils via control valve. Occupancy sensors tied to control valves on the IUs allow for space temperature set points to be reset to unoccupied values.

4.6.7.3 Thermo-Active Slab

A radiant slab conditions the Lobby in both heating and cooling modes. The circuit consists of 12 sub loops connected to a common header. The slab is controlled to be in winter or summer mode with two-way control valves which determine which loop (heating or cooling) serves the radiant floor. Depending on mode, it will receive either 14ºC cold water or 35ºC hot water. In summer mode, Pump- P-7 which delivers warm water to the slab, is shut off. A space humidity sensor monitoring indoor relative humidity will shut off the radiant slab in cooling mode if space dew-point temperatures rise above slab surface temperature.

4.6.7.4 Offices and Classrooms Air Handling Unit

AHU-1-05 delivers pre-conditioned 100% OA ratio ventilation air to the entire building. Air is filtered with MERV-13 equivalent filters: a pre-filter at 30% effectiveness and final filter at 85% effectiveness. AHU-1-05, located on the roof operates an energy recovery wheel to reduce peaks loads. Effectiveness is 53% humidity and 56% temperature. In summer, this provides a 62 kW reduction in cooling load at peak design, while in winter is provides a 106 kW reduction in heating load. AHU-1 has a hot water coil as primary heating/reheat, and a chilled water coil as cooling and dehumidification. In cooling mode, air is cooled to between 10 and 14ºC and is then reheated by the solar hot water to 14ºC to avoid condensation at induction units. In heating mode, air is preconditioned to leave the unit at 22ºC. In unoccupied modes, the air handler is capable of recirculating return air via a bypass damper in front of the energy recovery wheel.

4.6.7.5 Lobby Air Handling Unit

This unit this unit conditions and re-circulates return air within the lobby/atrium space. AHU-2-L1, located in the basement level. It serves the lobby, including the conference room pod. AHU-2-L1 has a hot water coil (47,817) as primary heating and a chilled water coil (85,566 BTUH) as cooling. In cooling mode, air is cooled to 14ºC. In heating mode, air is heated to 21ºC.

4.6.7.6 Auditorium Air Handling Unit

This unit this unit conditions and re-circulates return air. AHU-1-L1, located in the basement level. It serves the large auditorium located in the basement. AHU-1-L1 has a hot water coil as primary heating (94,500 BTUH) and a chilled water coil (224,000 BTUH) as cooling. In cooling mode, air is cooled to 14ºC. In heating mode, air is heated to 21ºC. When operational, the building load is often above 60 tons – necessitating the operation of CH-2.

4.6.8 HVAC Ventilation

4.6.8.1 Air Handling Units

AHU-1-05 provides constant volume preconditioned supply / ventilation air to occupied spaces throughout the building. During unoccupied times, a bypass damper allows return air to bypass the energy recovery wheel to provide mixed return and makeup air to the building.

4.6.8.2 Natural and Mixed Mode Ventilation

The natural ventilation system consists of operable windows for perimeter spaces and the stack effect created by the four-story atrium equipped with 8 solar chimneys. The chimneys are capped vanned ventilators which act to further boost airflow induced via thermal stack effect. Two spaces located within the “Eco-Wall” are ventilated solely by operable windows.

During times when specific close temperature, and humidity control is not required, a natural ventilation can be used in entrance Atrium, office room and classrooms. During occupied hours, the natural ventilation system is activated when the outdoor air temperature is between 12ºC and 18ºC and/or when the outdoor enthalpy value is below 25. Chimney dampers open and mechanized actuators open low-level windows. Classroom and office windows opening to the atrium may be opened to provide outside airflow through these spaces. The Air Handling unit system serving the lobby as well as the radiant floor remain off during this time.

The climate in Tel Aviv will permit acceptable thermal conditions to be achieved for up to 35% of the year using a natural ventilation system. User involvement is a key determinant in the success of this mixed mode natural ventilation system.

4.7 MODELLING NOVEL SOLAR THERMAL COLLECTORS SUITABLE FOR BUILDING INTEGRATION

Buonomano Annamaria, Forzano Cesare[10], Adolfo Palombo

4.7.1 Introduction

The major goal of solar collectors is to produce as much thermal energy as possible at the minimum total cost. To this aim, particular attention is paid to the design of novel concepts which may increase the collection of solar energy and boost the building integration. Among the available typologies of solar collectors, stationary flat plate collectors, FPC, is one of the most inexpensive typology to be manufactured and installed. Through flat plate solar collectors, a large amount of solar energy transmitted through the cover and absorbed by the absorber surface (with a high absorptivity) is transferred to the transport medium, then stored or used. The typical design of flat plate solar thermal collector can be header and risers (only for water collector) or serpentine (for water and air collectors), as shown in Figure 4.7.1. Evidently, the interior geometry of a collector substantially varies according to the working medium (Kalogirou 2014). In order to reduce conduction thermal losses, the absorber plate and the frame of the collector are well insulated, and the use of transparent glass cover is often adopted to reduce convective losses. The heat transferred between the absorber and the fluid is enhanced by a suitable absorber plate.

In the recent years, with the manifold aim to reduce heat losses, increase the effective life of the collectors while reducing their costs, a particular research effort has been paid on the development of innovative absorber plates (e.g. with selective coatings) and glazing materials (e.g. with high temperature resistant transparent insulation), and on the implementation of vacuum techniques. To this aim, within the COST Action, several solar collector prototypes were developed. Specifically, for these prototypes, novel construction techniques and absorber configurations are developed and proposed with the aim to increase the system benefits vs. costs and boost the market uptake of building integrated solar thermal collectors.

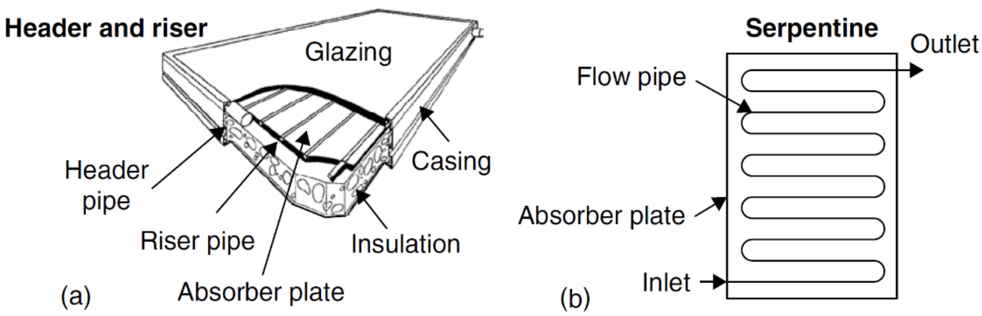

Figure 4.7.1. Typical flat plat collector - header and riser/serpentine (Kalogirou 2014).

In this section, the mathematical model, developed to simulate and predict the thermal performance of the solar collector prototypes of Project #1 and Project #5 are described and

[10] Non-COST Action member.

discussed. Such collectors, suitable for the building integration and the vertical installation, are: an air and a water rectangular shape - Project #1, and one water isosceles trapeze shape collector - Project #5. The prototypes description, the analytical algorithms included in the mathematical models and their validation procedures are also described. Finally, the analysis of active and passive effects due to the building integration of conventional FPC is also carried out.

4.7.2 Project #1 – Prototypes description (see Chapter 4.1)

The stationary flat-plate solar collectors of Project #1 are an air and a water prototype (serpentine and header and risers types). These collectors are designed and developed in order to obtain low cost devices also capable to provide good performance. All prototypes were designed and constructed at the Mechanical Engineering Department of Cyprus University of Technology, under the supervision of Professor S. Kalogirou.

The air collector purpose is to supply heated or pre-heated air in order to cover part of the building heating load, whereas the water collector produces hot water, or preheat it, for sanitary use (SHW). The air and water collector prototypes belong to the serpentine and header and risers configurations, respectively. Both the air and water prototypes (i.e. serpentine and header and risers types) are described in the following.

4.7.2.1 Water collector prototype

The water collector prototype, shown in Figure 4.7.2, consists of: i) a single layer of low iron glass; ii) a header and risers copper pipe line; iii) a selective surface (TiNox) absorber plate; iv) an insulation layer of glass fibre; v) a case made of galvanised sheet metal. The main geometrical features of the collector are reported in Table 4.7.1. The developed collector is expected to have a cost lower than the one showed by existing commercial collectors. Nevertheless, the obtained thermal efficiency of the prototype is similar to the efficiency usually found in commercial systems.

Figure 4.7.2. Water collector prototype.

Table 4.7.1. Solar Collector Prototype for Water Heating constructive parameters.

Parameter	Value	Parameter	Value
Collector length [mm]	1600	Glass transmittance [-]	0.93
Collector width [mm]	900	Insulation conductivity [W/m K]	0.041
Insulation thickness [mm]	25	Absorber plate emissivity [-]	0.95
Pipe diameter [mm]	22 (header), 8 (risers)	Absorber plate emissivity [-]	0.04
Pipe thickness [mm]	1	Number of risers [-]	7

4.7.2.2 Air collector prototype

The air prototype is designed with the aim to boost the heat exchange, through a multi-pass serpentine configuration, as shown in Figure 4.7.3a. This novel configuration aims at counteracting and overcoming the intrinsic drawback of air collectors, such as the low heat transfer coefficient between air and the absorber plate, resulting in a lower efficiency than the one showed by water collectors. Specifically, as shown in Figure 4.7.3a, the prototype ducts geometry is characterized by the implementation of serpentine flaps positioned between the absorber and the back plates, creating a particular flow path.

Figure 4.7.3. Air collector prototype; (a) internal configuration and (b) exterior design.

The collector dimensions depend upon the use, as cover, of a low-iron glass, provided by the Archimedes Solar Energy Laboratory (ASEL) and added to reduce the convective thermal losses. In addition, glasses with low iron content show a high solar radiation transmittance and an almost zero transmittance for longwave thermal radiations (5.0–50 □m), emitted by sun-heated surfaces. In order to obtain a lightweight prototype, the eight channels are designed by using several metal flaps. Such flaps and the back plate are made of aluminium, selected in order to obtain a low weight and low cost solar collector with a good efficiency. The absorber plate is made by a very thin iron plate (0.6 mm thickness), painted with black varnish with high absorptivity. The collector frame is made of wood, a cheap material capable to guarantee a good insulation. With the aim to reduce the conduction heat losses, the internal side of the wooden frame is insulated by means of stone wool. The assembly of the aluminium profiles to the absorber and back plate, as well as the assembly of the various components is made by using screws and a fireplace sealant, which resist to high temperatures and allow obtaining a good thermal bond. Table 4.7.2 summarizes the main collectors design features. Finally, Figure 4.7.3b shows the assembled prototype, mounted on a vertical surface (facing South) on the roof of the ASEL at the Department of Mechanical Engineering of Cyprus University of Technology, Limassol - Cyprus.

Table 4.7.2. Solar collector prototype for air heating constructive parameters.

Parameter	**Value**	**Parameter**	**Value**
Collector length [mm]	1631	Glass emissivity [-]	0.95
Collector width [mm]	846	Insulation conductivity [W/m K]	0.030
Glass cover to absorber plate distance [mm]	50	Edge conductivity [W/m K]	0.120
Insulation thickness [mm]	50	Absorber plate emissivity [-]	0.90
Duct width [mm]	105	$(\tau\alpha)$ [-]	0.85
Duct high [mm]	75	Back plate emissivity [-]	0.90
Flap thickness [mm]	0.8	Brick wall thickness [mm]	250
Number of duct [-]	8	Brick wall conductivity [W/m K]	0.360
Absorber plate thickness [mm]	0.6	Edge thickness [mm]	100

4.7.3 Project #5 - Novel trapeze solar-thermal flat plate collector (see chapter 4.5)

The project #5 water prototype consists of a novel solar-thermal collector with isosceles trapeze shape, developed, prototyped, modelled and step-wise optimised at the Transilvania University of Brasov (Romania), under the supervision of Prof. Ion Visa. The collector is designed mainly for developing arrays implemented in facades with increased architectural acceptance. Therefore, colours like red, green, blue are targeted for the absorber plate, along with the conventional black, as shown in the schematic description of the collector reported in Figure 4.7.4. The isosceles trapeze shape collector is used to heat or pre-heat water for building heating and domestic hot water purposes.

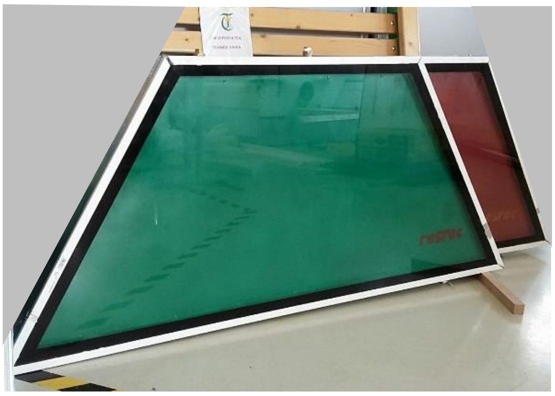

Figure 4.7.4. Different colors of the absorber plate.

The collector has an active area of 0.67m^2 and consists of a cover, an absorber, meander tubes, and insulation at the backend and edges of the collector. The cover glass with high optical absorptance is used for reducing both radiation and convection loss from the collector.

The absorber plate is designed with an aluminium substrate with a spectral selective black non-reflective coating. The fluid, heated by the absorber, is circulated in the meander tubes, bonded to the absorber plate by copper clamps. Conduction losses from the backend and edges of the collector are reduced by insulation: a layer of mineral wool is placed on the back plate, while a layer of polyurethane is placed around the frame. The main prototype design features are summarized in Table 4.7.3.

Table 4.7.3. Isosceles trapeze shape solar collector prototype - constructive parameters.

Parameter	**Value**	**Parameter**	**Value**
Glass cover optical absorptance [-]	0.89	Absorber plate conductivity [W/m K]	205
Glass cover emittance [-]	0.88	Absorber plate emissivity [-]	0.11
Glass cover thickness [mm]	4	Absorber plate absorptance [-]	0.887
Wool insulation thickness [mm]	45	Air gap thickness [mm]	20
Wool insulation conductivity [W/mK]	0.045	Tubes diameter [mm]	22.7 10.7
Polyurethane insulation thickness [mm]	20	Number of tubes [-]	9

4.7.4 Mathematical models

For the assessment of the thermal performance of the above described prototypes, suitable mathematical models, implemented in computer simulation codes, are developed. For such models, derived by those proposed by (Duffie and Beckman 2013) and (Kalogirou 2014), thermodynamic equilibrium, steady state regime, one dimensional heat transfer, kinetic and gravitational terms negligible in the energy balances are assumed. In addition, in order to simplify the mathematical formulation, the additional main adopted assumptions are:

- one dimensional flow through the back cover;
- neglected temperature gradients around the ducts or pipes;
- homogeneous, isotropic and time independent properties of materials;
- radiation uniformly concentrated along the absorber area;
- no solar energy absorbed by the glass cover, which is opaque to infrared radiation;
- negligible temperature drop through the cover;
- negligible dust effects on the cover;
- front and back of the collector face the same boundary ambient temperature;
- no shadings on the absorber plate.

By following the above mentioned assumptions, the general formulation for the calculation of the solar thermal collector efficiency can be obtained from the Hottel-Whillier equation, based on the assessment of the energy losses and of the useful energy (Duffie and Beckman

2013). It is worth noting that the thermal losses calculation procedure is the same for all of the collectors, whereas the useful energy calculation depends on the prototypes geometry and typology.

4.7.4.1 Energy losses

In a solar collector, the heat losses substantially reduce the amount of produced useful energy. In the case of flat plate collectors, two types of losses, optical and thermal, occur. While optical losses are assessed through the glass cover transmittance-absorbance $(\tau\alpha)$, after discussed, thermal losses can be divided into three heat parts: heat loss from the top, the back and the edge of the collector. Such losses act in parallel in the form of convection, conduction and radiation, as reported in thermal network schematic of Figure 4.7.5 (Kalogirou 2014).

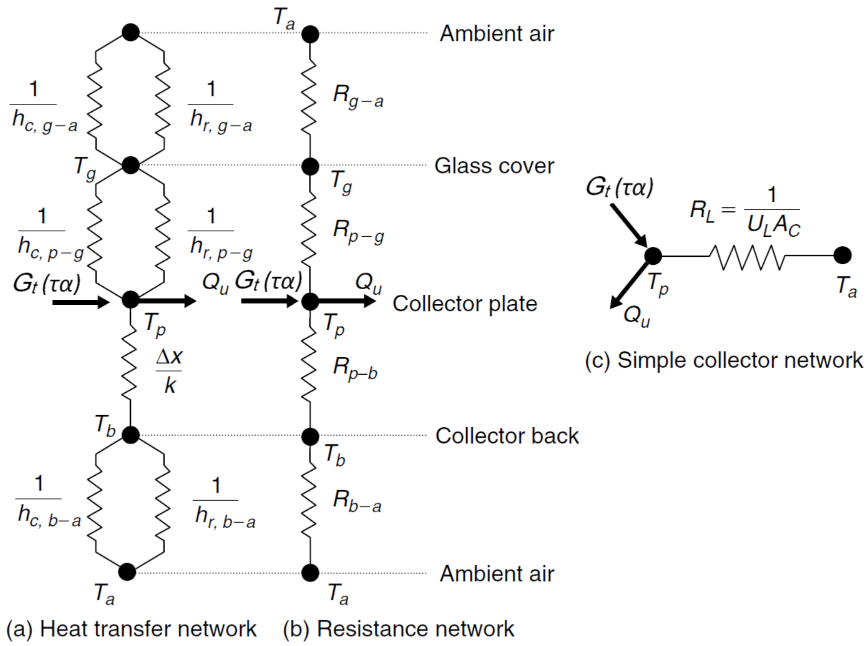

Figure 4.7.5. Energy losses thermal network (Kalogirou 2014).

Here, by considering T_p as the absorbing plate temperature [K], T_a as the ambient air temperature, also known as sink temperature [K], T_g as the estimated temperature of the cover (glazing) [K], R_L as the simple combined thermal resistance [m^2 K/W], and U_L the overall heat loss coefficient [W/m^2K] based on collector aperture area A_C [m^2], the energy losses can be estimated by:

$$Q_{loss} = \frac{T_p - T_a}{R_L} = U_L A_C \left(T_p - T_a\right) \tag{4.7.1}$$

The overall heat loss coefficient term U_L is the sum of top loss coefficient, U_t, the bottom loss coefficient, U_b, and the edges loss coefficient, U_e, [W/m^2K], as:

$$U_L = U_t + U_b + U_e \tag{4.7.2}$$

The bottom and edge loss coefficients are known since they depend on collector geometry and materials. Both the coefficients are calculated by i) the conductance of the materials constituting the external structure of the collector, ii) the convective heat exchange with the ambient air, and iii) the infrared radiation to the sky. The radiation term is considered as negligible (due to low temperature of the back cover) in the case of project #1 prototypes, whereas the convective heat exchange is neglected for the prototype of project #5.

By taking into account the above mentioned assumptions, the back energy losses are given by:

$$U_b = \frac{1}{\frac{L_b}{k_b} + \frac{1}{h_{c,b\text{-}a}}} \tag{4.7.3}$$

where L_b is the back insulation thickness [m], k_b is back insulation conductivity [W/mK], and $h_{c,b\text{-}a}$ is the convection heat loss coefficient from back to ambient [W/m^{2}K].

Similarly, heat losses from the edge of the collector can be obtained as:

$$U_e = \frac{1}{\frac{L_e}{k_e} + \frac{1}{h_{c,e-a}}} \tag{4.7.4}$$

where L_e is the edge insulation thickness [m], k_e is the edge insulation conductivity [W/mK] and $h_{c,e\text{-}a}$ is the convection heat loss coefficient from edge to ambient [W/m^{2}K].

Note that the edge loss coefficient, U_e, becomes significant (representing up to 10% of the total losses) especially for small area collectors, like the trapeze solar-thermal flat plate collector of project# 5. For this reason, to estimate U_e, the Tabor model (1958), based on the edge loss coefficient – collector area product $(UA)_{edge}$, is taken into account, calculated as:

$$U_e = \frac{(UA)_{edge}}{A_C} = \frac{\left(\frac{k_e}{L_e} A\right)_{edge}}{A_C} \tag{4.7.5}$$

where U_e is the conductive loss coefficient of the edges, A is the overall area [m^2] subjected of losses through edges, calculated as the product of the collector perimeter and thickness.

In a well-insulated collector, the largest heat losses are expected to be those through the top of the device. The estimation of the top loss heat coefficient, U_t, requires a more complicated procedure since it depends on conduction, convection and irradiation phenomena acting in parallel. In addition, as for all the modelled prototypes, in the case of a single glass cover necessary to reduce the heat losses, it is necessary to split the heat loss from the front of the collector in two different parts: i) the heat lost from the absorber plate toward the glass cover and ii) the heat lost from the glass cover toward the ambient air.

The heat lost from the absorber plate toward the glass cover can be calculated as:

$$Q_{t,a-g} = A_C h_{c,p-g}\left(T_p - T_g\right) + \frac{A_C \sigma\left(T_p^4 - T_g^4\right)}{\frac{1}{\varepsilon_p} + \frac{1}{\varepsilon_g} - 1} \tag{4.7.6}$$

where hc,p-g is the convection heat transfer coefficient between the absorber plate and glass cover [W/m^{2}K]; σ is the Stefan-Boltzmann constant (5.67.10-8 W/m^{2}K^4), ε_p is the absorber plate emissivity and ε_g is the glass cover emissivity.

In order to assess the convection heat transfer coefficient between the absorber plate and the glass cover, $h_{c,p-g}$ can be calculated by means of the Nusselt number, Nu, relationship:

$$h_{c,p-g} = Nu\frac{k}{L} \tag{4.7.7}$$

where k is the thermal conductivity of the air [W/mK] and L the characteristic distance (plate-to-cover spacing) [m].

The Nusselt number can be calculated by means of different correlations, based on the Rayleigh number, Ra, and on additional parameters. In particular, for the modelled prototypes, the selected Nusselt correlation for vertical plates is:

- given by Shewen et al. (Shewen, Holiands et al. 1996) for the prototypes of project #1:

$$Nu = \left[1 + \left(\frac{0.0665 Ra^{0.333}}{1 + \left(9600 / Ra\right)^{0.25}}\right)^2\right]^{0.5} \tag{4.7.8}$$

- given by Holland et al. (Hollands, Unny et al. 1976) for the prototype of project #5:

$$Nu = 1 + 1.44\left[1 - \frac{1708\left(\sin 1.8\beta\right)^{1.6}}{Ra\ \cos\beta}\right]\left[1 - \frac{1708}{Ra\ \cos\beta}\right]^{+} + \left[\left(\frac{Ra\ \cos\beta}{5830}\right)^{1/3} - 1\right]^{+} \tag{4.7.9}$$

where β is the tilt angle (with values between 0…75^o) and the exponent + means that only positive terms in the brackets are considered.

The Rayleigh number, Ra, can be calculated by:

$$Ra = \frac{g\beta/Pr}{k}\left(T_p - T_g\right)L^3 \tag{4.7.10}$$

where L is the characteristic distance (plate spacing), g is the gravitational constant [m^2/s], β' is the volumetric coefficient of expansion (air was considered an ideal gas, thus β' = 1/T) [1/K], ΔT is the temperature difference between the absorber plate and the glass cover [K], ν is the kinematic viscosity [m^2/s] and Pr is the Prandtl number (Incropera and Dewitt 2011). It worth noting that all the fluid properties are estimated at the average temperature (Tp+Tg)/2.

With the aim to linearize the radiative terms Eq. (4.7.6), an equivalent radiative heat transfer coefficient, $h_{r,p\text{-}g}$, from plate to cover, is defined as it follows:

$$h_{r,p\text{-}g} = \frac{\sigma\left(T_p^2 + T_g^2\right)\left(T_p + T_g\right)}{\frac{1}{\varepsilon_p} + \frac{1}{\varepsilon_g} - 1} \tag{4.7.11}$$

As a result, Eq. (4.7.6) can be rewritten as:

$$Q_{t,a-g} = A_C\left(h_{c,p-g} + h_{r,p-g}\right)\left(T_p - T_g\right) = \frac{\left(T_p - T_g\right)}{R_{p-g}} \tag{4.7.12}$$

with $R_{p-g} = \left[A_C\left(h_{c,p-g} + h_{r,p-g}\right)\right]^{-1}$.

Similarly, the heat loss from the glass to the ambient air can be calculated as:

$$Q_{t,g-a} = A_C\left(h_{c,g-a} + h_{r,g-a}\right)\left(T_g - T_a\right) = \frac{\left(T_g - T_a\right)}{R_{g-a}} \tag{4.7.13}$$

with $R_{g-a} = \left[A_C\left(h_{c,g-a} + h_{r,g-a}\right)\right]^{-1}$, where $h_{c,g\text{-}a}$ is the convective heat coefficient between the glass and the air [W /m^{2}K], $h_{r,g\text{-}a}$ is the radiative heat coefficient between the glass and the air [W/m^2 K].

The radiation coefficient from the cover to the air outside the collector, $h_{r,g\text{-}a}$ was calculated by:

$$h_{r,g-a} = \varepsilon_g\sigma\left(T_g^2 + T_a^2\right)\left(T_g + T_a\right) \tag{4.7.14}$$

It is worth noting that T_a is used for convenience instead of T_{sky}, that does not affect the results (Kalogirou 2014).

Finally, the energy losses from the top of the solar collector to the ambient air are calculated as:

$$Q_t = \frac{\left(T_p - T_a\right)}{R_t} = U_t A_C\left(T_p - T_a\right) \tag{4.7.15}$$

where R_t is the overall top resistance, calculated as:

$$R_t = R_{p-g} + R_{g-a} = \left(U_t A_C\right)^{-1} \tag{4.7.16}$$

The estimation of the overall heat loss coefficient U_L requires the knowledge of the above discussed unknown variables. Therefore, an iterative method was implemented. Specifically, at the time step t, the calculation procedure starts with the assessment of the cover glazing temperature T_g, as first attempt value. The iterative procedure continues until it is reached an acceptable minimum difference between the estimated value of T_g and the one calculated as:

$$T_g = T_p - \frac{U_t\left(T_p - T_a\right)}{h_{g,p-g} + h_{r,p-g}} \tag{4.7.17}$$

4.7.4.2 Useful energy

Under steady-state conditions the rate of useful heat delivered by a solar collector to the thermal medium is equal to the rate of energy absorbed by the heat transfer fluid minus the heat losses from the surface to the surroundings, as it follows:

$$Q_u = A_C\left[G_t\left(\tau\alpha\right) - U_L\left(T_p - T_a\right)\right] = \dot{m}c_p\left(T_o - T_i\right) \tag{4.7.18}$$

where G_t is the incident total solar radiation [W/m^2], $(\tau\alpha)$ is the product between the solar transmittance of the glass cover and the absorbance of the absorber plate, $\dot{m}$ is the fluid mass flow rate [kg/s], T_o and T_i are the water outlet and inlet temperatures [K]. It is worth noting that the term $(\tau\alpha)$ - product of the glass transmittance and the absorber plate absorptivity - takes into account the multiple reflections of the solar radiation within the air gap between the absorber plate and the glass cover, as shown in Figure 4.7.6, and it is considered that $\left(\tau\alpha\right) \cong 1.01\ \tau\alpha$ (Duffie and Beckman 2013).

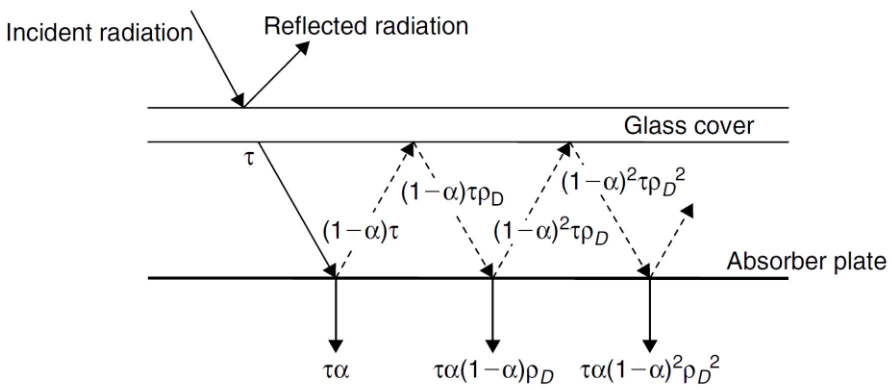

Figure 4.7.6. Radiation transfer between the glass cover and absorber plate (Kalogirou 2014).

A general formulation for the calculation of the solar thermal collector efficiency can be obtained from the Hottel-Whillier equation (Duffie and Beckman 2013). Here, in order to calculate the fluid outlet temperature, T_o, an iterative procedure is necessary. In order to simplify the procedure, it is possible to consider the useful heat as a function of the inlet temperature, T_i, by taking into account the so-called heat removal factor, F_R. As a result, the useful energy can be calculated as:

$$Q_u = A_C F_R\left[G_t\left(\tau\alpha\right) - U_L\left(T_i - T_a\right)\right] \tag{4.7.19}$$

where F_R represents the ratio of the actual energy gain to the useful energy gain of a collector, calculated as if the whole collector absorbing surface were at the fluid inlet temperature, such as:

$$F_R = \frac{\dot{m}c_p\left(T_o - T_i\right)}{A_C\left[G_t\left(\tau\alpha\right) - U_L\left(T_i - T_a\right)\right]} \tag{4.7.20}$$

The heat removal factor, F_R, depends on the geometry of the collector and on its flow rate. Therefore, different formulations of F_R must be taken into account as a function of the absorber configuration (i.e. serpentine and header and risers collector typologies) and the thermal medium. In steady state conditions and assuming constant heat transfer and specific heat coefficients, F_R can be written also as (Kalogirou 2014):

$$F_R = \frac{\dot{m}c_p}{A_C U_L}\left[1 - \exp\left(-\frac{A_C U_L F'}{\dot{m}c_p}\right)\right] \tag{4.7.21}$$

where F' is the collector efficiency factor, defined as the ratio of the actual useful energy gain to the useful energy gain that would result if the collector absorbing surface were at the local fluid temperature.

Finally, once the heat removal factor F_R is calculated, the solar collector efficiency, η, equal to:

$$\eta = \frac{Q_u}{A_C G_t} \tag{4.7.22}$$

can be rewritten as:

$$\eta = \mathrm{F_R}\left[\left(\tau\alpha\right) - \frac{U_L\left(T_i - T_a\right)}{G_t}\right] \tag{4.7.23}$$

In the following sections the assessment of F_R for the water serpentine pipe and header and risers pipe configurations of project #1 and #5, as well as for the air prototype of project #1, are presented.

***F_R* calculation for water collectors of project #1 and #5**

Different procedures for the calculation of F_R must be selected as a function of the geometry of the water collector. In particular:

- the sheet-tube configuration, shown in Figure 4.7.7, can be taken into account for the fin and tube assembly in a riser header configuration (e.g. water collector project #1) and for the serpentine configuration where the pipes are fixed to separate fins (e.g. water collector project #5) (Duffie and Beckman 2013; Kalogirou 2014);

- the serpentine configuration, shown in Figure 4.7.1b, can be used for a tube arrangement obtained by a continuous absorber plate (Duffie and Beckman 2013; Kalogirou 2014).

Sheet-tube configuration procedure

In the case of sheet-tube configuration, the collector efficiency can be calculated by considering the temperature distribution between two pipes of the collector absorber and by assuming that, due to good conductors used as sheet materials, the temperature gradient in the flow direction is negligible (Duffie and Beckman 2013; Kalogirou 2014). As a result, the region between the centre line separating the tubes and the tube base can be considered as a classical fin problem (the pipes are fixed to separate fins) (Duffie and Beckman 2013).

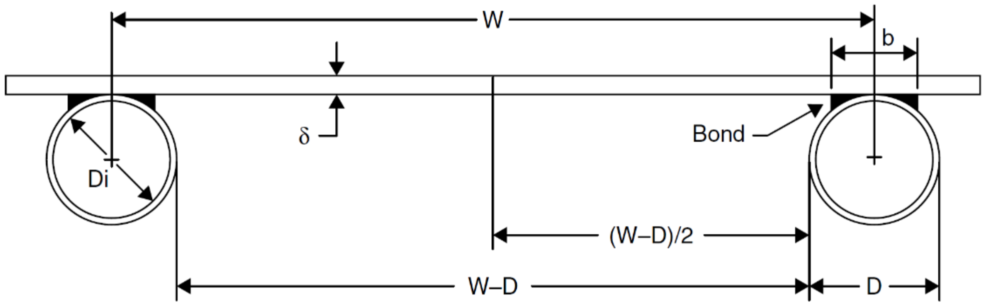

Figure 4.7.7. Flat plate sheet and tube configuration (Kalogirou 2014).

The collector efficiency factor F' is can be calculated as:

$$F' = \frac{1/U_L}{W\left\{\frac{1}{U_L\left[D+(W-D)F\right]}+\frac{1}{C_b}+\frac{1}{\pi D_i h_{fi}}\right\}} \qquad (4.7.24)$$

where W is the distance between two consecutive pipes axis [m], D is the exterior diameter of the pipes [m] and D_i is the pipe interior diameter [m]. F is the standard fin efficiency factor, which depends on geometrical configuration of the absorber plate and the pipeline, and it is expressed as:

$$F = \frac{\tanh\left[\frac{m(W-D)}{2}\right]}{\frac{m(W-D)}{2}} \qquad (4.7.25)$$

being m a characteristic of the plate absorber given by:

$$m = \sqrt{\frac{U_L}{k_p \delta}} \qquad (4.7.26)$$

where k_p is the absorber plate thermal conductivity [Wm/K], δ is the absorber thickness [m] and C_b is the conductance of the bond between the absorber plate and the pipes [Wm/K], calculated as:

$$C_b = \frac{k_b b}{\gamma} \qquad (4.7.27)$$

being k_b the bond thermal conductivity [Wm/K], b the bond width [m], γ the bond thickness [m], and h_{fi} the heat transfer coefficient [W/m^{2}K] between the fluid and the pipe wall, depending on the geometry of the pipeline and on the flux condition of the thermal medium, calculated as:

$$h_{fi} = \frac{Nu\ k_f}{D} \tag{4.7.28}$$

where k_f is the fluid thermal conductivity [W/mK] and Nu is the Nusselt number, calculated based on the Prandtl, Pr, and Reynolds, Re, numbers. Different correlations are used as a function of the prototype geometry, such as:

- for the header and risers collector of project #1, if Re < 2300 (laminar flow), Nu is considered equal to 3.66 (Incropera and Dewitt 2011), conversely, it is calculated by means of the Dittus and Boelter equation (Winterton 1998), such as:

$$Nu = 0.023\left(Re^{0.8}Pr^{0.4}\right) \tag{4.7.29}$$

- for the serpentine collector of project #5, Nu is calculated as:

$$Nu = Nu_\infty + \frac{a\left(Re\ Pr\ D_i/L_p\right)^m}{1+b\left(Re\ Pr\ D_i/L_p\right)^n} \tag{4.7.30}$$

being L_p the length of the pipes [m] and the selected valued of the constants Nu_∞, a, b, m and n are those used for circular tubes with constant heat rates, as reported in Table 4.7.4.

Table 4.7.4. Coefficients necessary for calculating Nu for circular pipes with constant heat rate (Duffie and Beckman 2013).

Pr	**a**	**b**	**m**	**n**	**Nu_∞**
0.7	0.00398	0.0114		1.12	
10	0.00236	0.0086	1.66	1.13	4.4
∞	0.00172	0.0028		1.29	

Note that all the geometrical parameters, within the above equations, and related to Figure 4.7.7.

Serpentine configuration procedure

In the case of the serpentine tube arrangement, the pipes are not fixed to separate fins and a continuous absorber plate is used. For the serpentine configuration, discussed for the sake of completeness, a different approach, based on the Zhang and Lavan (Zhang and Lavan 1985), study is taken into account. By this procedure, valid for the serpentine configuration of any number of bends, the heat removal factor F_R is suitably calculated as:

$$F_R = F_1 F_3 \left[1 + \frac{2F_4 F_5}{F_6 \exp\left(\frac{-\sqrt{1-F_2^{\ 2}}}{F_3} \right) + F_4} - \frac{1}{F_2} - F_5 \right] \tag{4.7.31}$$

with

$$F_1 = \frac{KNL}{U_L A_C} \frac{KR(1+\gamma)^2 - 1 - \gamma - KR}{\left[KR(1+\gamma) - 1\right]^2 - (KR)^2} \tag{4.7.32}$$

$$F_2 = \frac{1}{KR(1+\gamma)^2 - 1 - \gamma - KR} \tag{4.7.33}$$

$$F_3 = \frac{\dot{m}c_p}{F_1 U_L A_C} \tag{4.7.34}$$

$$F_4 = \frac{1}{F_2} + F_5 - 1 \tag{4.7.35}$$

$$F_5 = \sqrt{\frac{1-F_2^{\ 2}}{F_2^{\ 2}}} \tag{4.7.36}$$

$$F_6 = 1 - \frac{1}{F_2} + F_5 \tag{4.7.37}$$

$$K = \frac{k\delta n}{(W-D)\sinh n} \tag{4.7.38}$$

$$n = (W-D)m \tag{4.7.39}$$

$$\gamma = -2\cosh n - \frac{DU_L}{K} \tag{4.7.40}$$

$$R = \frac{1}{C_b} + \frac{1}{\pi D_i h_{fi}} \tag{4.7.41}$$

where N is the number of the pipe bends.

Note that, by recognizing that A_C is equal to NWL, F_1 can be rewritten as:

$$F_1 = \frac{K}{U_L} \frac{KR(1+\gamma)^2 - 1 - \gamma - KR}{\left[KR(1+\gamma) - 1\right]^2 - (KR)^2} \tag{4.7.42}$$

and by taking into account the formulations of m, Eq. (4.7.26), and n, Eq. (4.7.39), Eq. (4.7.38) can be rewritten as:

$$K = \frac{\sqrt{k\delta n}}{\sinh n} \tag{4.7.43}$$

As a result, for the serpentine collector type, a more simplified form of Eq. (4.7.31) can be obtained:

$$F_R = F_1 F_3 F_4 \left[\frac{2F_5}{F_6 \exp\left(\frac{-\sqrt{1-F_2^{\ 2}}}{F_3} \right) + F_4} - 1_5 \right] \tag{4.7.44}$$

Note that in order to calculate F_R and to assess the collector efficiency, η, it is necessary to calculate h_{fi} and T_p by means of an iterative procedure.

F_R calculation for air collectors of project #1

In the case of air collectors, as the one of project #1, the heat removal factor F_R is assessed starting by the knowledge of the collector efficiency factor F', calculated as:

$$F' = \frac{h}{h+U_L} = \frac{1/U_L}{1/U_L + 1/h} \tag{4.7.45}$$

where h is calculated as:

$$h = h_{c,p-a} + \frac{1}{\frac{1}{h_{c,b-a}} + \frac{1}{h_{r,p-b}}} \tag{4.7.46}$$

where $h_{c,p-a}$ and $h_{c,b-a}$ are respectively the convective heat transfer coefficient between the absorber plate and flowing air, and between the back cover and flowing air [W/m^{2}K]; $h_{r,p-b}$ is the radiative heat transfer coefficient between absorber plate and back cover [W/m^{2}K].

In order to assess the heat transfer coefficients, $h_{c,p-a}$ and $h_{c,b-a}$, the Dittus - Boelter correlation (Winterton 1998) for the Nusselt number calculation, reported in Eq. (4.7.29), is taken into account. Note that for fully developed laminar flow, Nu is calculated as a function of the cross section only (Incropera and Dewitt 2011). For the calculation of Re and Pr, the hydraulic diameter, for not circular cross sections (as those of the air collector), is calculated as (Incropera and Dewitt 2011):

$$D_h = \frac{4A_{CS}}{P} \tag{4.747}$$

where A_{CS} and P are the flow cross-sectional area [m^2] and the wetted perimeter [m], respectively.

The radiative heat transfer coefficient is calculated as:

$$h_{r,p-b} = \frac{\sigma\left(T_p + T_b\right)\left(T_p^2 + T_b^2\right)}{\dfrac{1}{\varepsilon_p} + \dfrac{1}{\varepsilon_b} - 1} \qquad (4.7.48)$$

where ε_b is the back collector emissivity and T_b is the back collector temperature [K].

Outlet air temperature calculation

Finally, note that the calculation of the useful energy delivered by the collector is carried out by assessing the outlet air temperature value T_o, as well as the temperature distribution among the absorber plate. To this aim, by considering the schematic diagram of an air heating collector, as the one reported in Figure 4.7.8, several energy balances must be written on generic control areas and volumes (Kalogirou 2014).

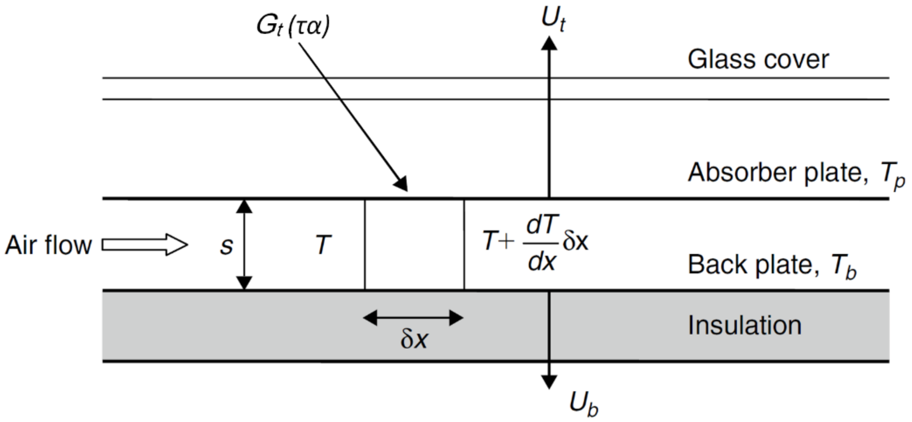

Figure 4.7.8. Schematic diagram of an air-heating collector (Kalogirou 2014).

The energy balance on the absorber plate of area (1 x δx) gives:

$$G_t\left(\tau\alpha\right)\left(\delta x\right) = U_t\left(\delta x\right)\left(T_p - T_a\right) + h_{c,p-a}\left(\delta x\right)\left(T_p - T\right) + h_{r,p-b}\left(\delta x\right)\left(T_p - T_b\right) \qquad (4.7.49)$$

The energy balance on the air stream volume (s x 1 x δx) gives:

$$\left(\frac{\dot{m}}{W}\right)c_p\left(\frac{dT}{dx}\delta x\right) = h_{c,p-a}\left(\delta x\right)\left(T_p - T\right) + h_{c,b-a}\left(\delta x\right)\left(T_b - T\right) \qquad (4.7.50)$$

The energy balance on the back plate of area (1 x δx) gives:

$$h_{r,p-b}\left(\delta x\right)\left(T_p - T_a\right) = h_{c,b-a}\left(\delta x\right)\left(T_b - T\right) + U_b\left(\delta x\right)\left(T_b - T_a\right) \qquad (4.7.51)$$

By considering that U_b is negligible, Eq. (4.7.51) can be solved for T_b obtaining:

$$T_b = \frac{h_{r,p-b} T_p - h_{c,b-a} T}{h_{r,p-b} - h_{c,b-a}} \tag{4.7.52}$$

T_b is then substituted in Eq. (4.7.49) and Eq. (4.7.50), which opportunely combined lead to:

$$\left(\frac{\dot{m}}{W}\right) c_p \frac{dT}{dx} = F' \left[G_t(\tau\alpha) - U_L (T - T_a) \right] \tag{4.7.53}$$

The air temperature distribution within the duct can be obtained by fixing the inlet condition T = T_i at x = 0 in Eq. (4.7.53), which becomes:

$$T = \left(\frac{G_t(\tau\alpha)}{U_L} + T_a \right) - \frac{1}{U_L} \left[G_t(\tau\alpha) - U_L (T_i - T_a) \right] \exp\left[1 - \frac{U_L F'}{(\dot{m}/W) c_p} x \right] \tag{4.7.54}$$

Finally, to obtain the outlet temperature T_o, by taking into account x = L and W L = A_C, (4.7.554) can be rewritten as:

$$T_o = T_i + \frac{1}{U_L} \left[G_t(\tau\alpha) - U_L (T_i - T_a) \right] \left[1 - \exp\left(- \frac{A_C U_L F'}{\dot{m} c_p} \right) \right] \tag{4.7.55}$$

4.7.5 Experimental characterization and validation procedures of prototypes

In order to prove the efficacy of the developed simulation models, validation procedures are performed by means of experimental analyses. Specifically, for the air and water collector of project #1 and project #5, the obtained simulation results are compared with the experimental ones. In addition, for the simulation model relative to the serpentine configuration, a comparison analysis with an existing commercial water collector is also developed. Such analysis is carried out with aim to assess the effects on the building energy consumptions due to the integration of solar collector into the building façade.

4.7.5.1 Air prototype - Project #1

The prototype model for the air collector was validated through the results obtained during an experimental campaign carried out at the Archimedes Solar Energy Laboratory (ASEL) at the Department of Mechanical Engineering of Cyprus University of Technology, Limassol (Cyprus).

The experimental analysis was performed during three during three sunny days, April 7th, 18th and 27th. The developed simulation model shows a good reliability, and the simulated results match very well with the collected experimental data.

During the tests, the collector was exposed to solar radiation and the measurements, recorded every 5 minutes, are related to the instantaneous values of:

- G_t, global radiation on the vertical surface;
- T_a, outdoor air temperature;
- W, wind velocity;
- $\dot{m}$, air mass flow rate;
- T_G, glass temperature;
- T_{P1}, absorber plate temperature at the inlet section;
- T_{P2}, absorber plate temperature at the outlet section;
- T_o, outlet air temperature.

The thermocouples (e.g. in Figure 4.7.3b) were connected to a digital thermometer, Tecpel DTM-318, Figure 4.7.9 left, for use with any Type K thermocouple as its sensor. Its temperature indication follows the National Bureau of Standards and IEC584 temperature/voltage table for Type K thermocouples. Some specifications are: measuring range -200 to 1370°C, resolution 0.1°C, accuracy 0.5% +1°C. The air mass flow rate was measured by means of a hot wire anemometer, Omega HHF2005HW, Figure 4.7.9 right, with a real time data logger, which has multiple features and an RS232 computer interface that make it suitable to use for environmental testing. The anemometer measures velocity, as well as air temperature, and has an input probe socket that accepts a Type J or K thermocouple, used as a highly accurate thermometer. Some specifications are: measuring range 0.2 to 20 m/s and 0 to 50 °C, resolution 0.1 m/s and 0.1 °C, full scale accuracy ±10 %+lsd and ±0.8 °C. Note that the air was circulated within the collector by means of a Soler & Palau TD 160/100 N silent fan. The solar radiation incident on the collector was measured and recorded through a pyranometer, Figure 4.7.10, mounted on the wooden frame (i.e. vertical surface) of the collector. For the calculation of the instantaneous value of the radiation, the pyranometer output, in mV, was measured by multimeter, a Mastech MS8209, Figure 4.7.10, with a light level sensor. Then, the measured voltage was converted into W/m^2 by considering the constant 9.1×10^{-6} V/m^2W. Some specifications of the multimeter: measuring range from 0 to 320 mV, resolution 0.1 mV, accuracy ±0.7%.

Figure 4.7.9. Digital thermometer (left) and hot wire anemometer (right).

Figure 4.7.10. Pyranometer (right) and multimeter (left).

In order to allow the simulation model to run, the measured data used as input were: G, T_a (i.e. equal to the inlet one), w, ṁ. For the validation procedure, measurements and simulation results of T_P, T_G, T_o and η (calculated as in Eq. (4.7.21)) were compared. Note that T_P, absorber plate temperature, is the arithmetic average of the two measured temperatures T_{P1} and T_{P2}.

Figure 4.7.11shows the trend of T_P, T_G, T_o and η related to the data simulation results and measurements recorded on April 18th from 10:00 until 17:00. During this day, the maximum measured value of G_t was 438 W/m^2. In the subplots of Figure 4.7.11, measurements and predictions show the same patterns, resulting in very low average percentage differences. A good agreement between the simulated results and the collected experimental data was also observed for the tests performed on April 7th and 28th. A relatively higher percentage difference (still acceptable) was observed between experimental and simulation results on April 27th, due to particular weather conditions. Specifically, during the test performed on April 27th, with respect to the previous days lower daily instantaneous solar radiations and stronger wind velocities were measured. Moreover, on the same day, the maximum recorded G_t value, equal to 405 W/m^2, was lower than the one observed on April 7th and on April 18th (i.e. 523 and 438 W/m^2, respectively).

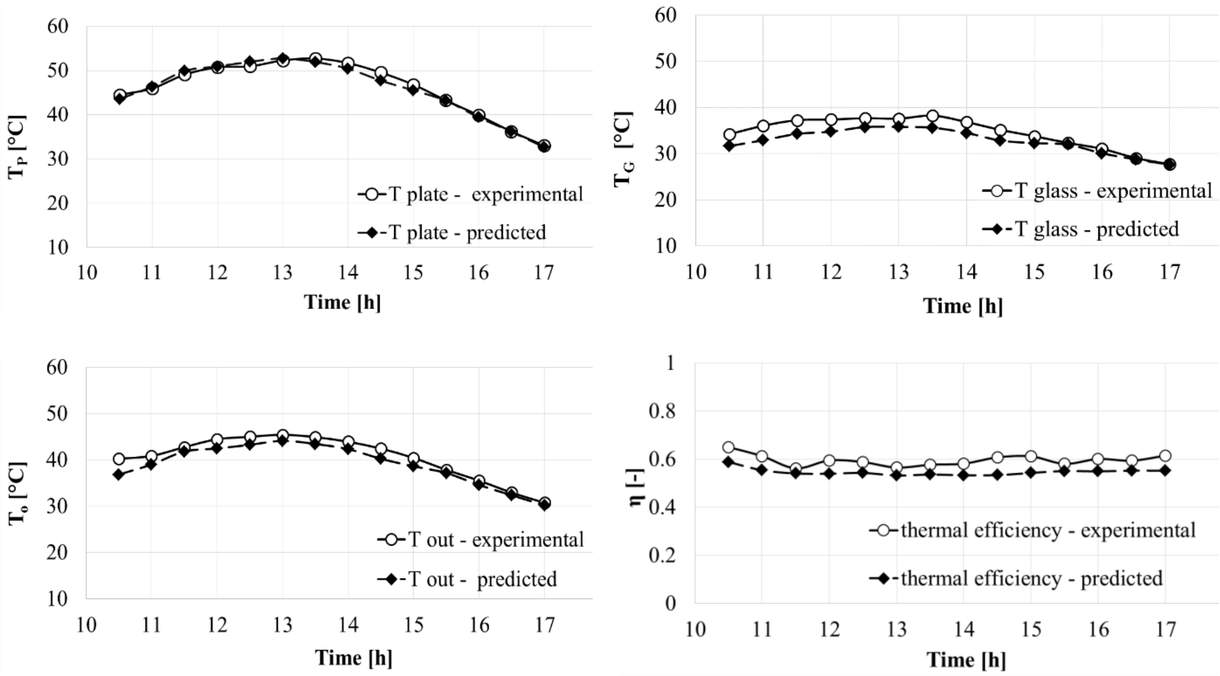

Figure 4.7.11. Experimental and simulated data of T_P, T_G, T_o and η –April 18th.

In general, during all three measurements days, the absolute percentage differences between predicted and measured values of T_o, T_P, T_G, and η were calculated. Their average percentage differences, $\Delta_{m\%}$, reported in Table 4.7.5, resulted to be acceptable, being always lower than 6.40% for T_o, T_P and T_G and lower than 13.4% for η. Finally, the obtained average efficiency of the solar collector is about 58 %, similar to the one showed by this typology of systems.

Table 4.7.5. Average percentage differences between simulated and experimental results.

Date:	**April 7th**				**April 18th**				**April 27th**			
Parameters	T_o	T_g	T_p	η	T_o	T_g	T_p	η	T_o	T_g	T_p	η
$\Delta_{m\%}$ [%]	6.39	1.68	2.08	13.4	3.65	5.06	1.53	8.24	2.99	3.47	4.95	8.87

Building integration - active effect

The developed model validation allows performing simulation and parametric analyses, useful to assess and optimize the thermal performance of the prototype. To this aim, a brief analysis on the prototype thermal energy production, Q_u, was carried out by taking into account different weather conditions. Specifically, the thermal behaviour of the prototype under different weather conditions was simulated. To this aim, six different European climates were considered through the use of weather data files (typical year – Meteonorm database). The selected weather zones are representative of different climate conditions, varying from cold to warm climates (such as Copenhagen, Freiburg, Dublin, Naples, Athens, Limassol). By performing yearly simulations, the obtained prototype total yearly energy productions, Q_u, are reported in Figure 4.7.12.

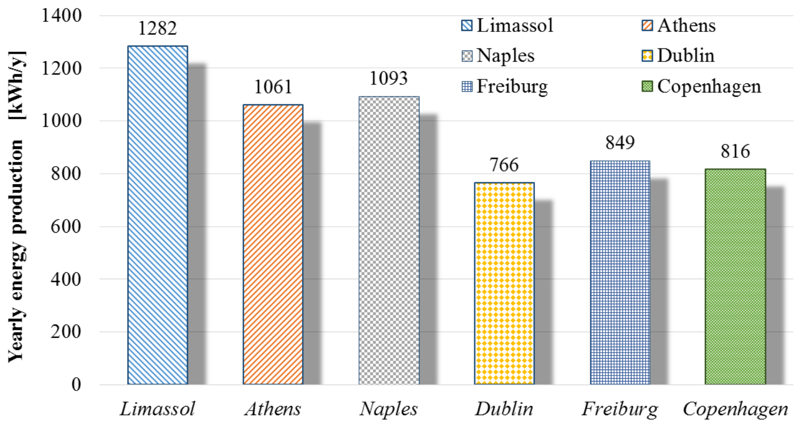

Figure 4.7.12. Simulated yearly thermal energy production in different European weather zones.

As expected, the higher energy production is achieved in the southern Europe zones, which are characterized by a higher value of the incident solar radiation (i.e. ranging from 2000, in Limassol, to 990, Copenhagen, kWh/m^{2}y). The prototype is competitive also in the northern Europe zones due to the vertical installation. In fact, the collector tilt angle β is closer to the optimal one observed in these zones (i.e. equal to the location latitude +10° for space heating applications (Kalogirou 2014)).

4.7.5.2 Water prototype (header and risers) - Project #1

The thermal performance of the water collector prototype was tested during an experimental campaign carried out at the ASEL at the Department of Mechanical Engineering of Cyprus University of Technology, Limassol (Cyprus). For measurements purposes, the same instrumentation used for the air collector tests was used.

Thermocouples were installed at different positions of the collector, specifically on the absorbing plate, T_P, on the cover glass, T_G, and at the back of the insulation T_B, with the aim to allow the calculation of the heat transfer toward the wall. Thermocouples were also installed at the inlet, T_i, and outlet, T_o, pipe of the collector, as shown in

Figure 4.7.13. The pyranomenter was used for the measurement of the solar radiation incident on the collector, G_t. Therefore, it was mounted on the vertical plane (on the right hand side) of the collector, as shown in Figure 4.7.14.

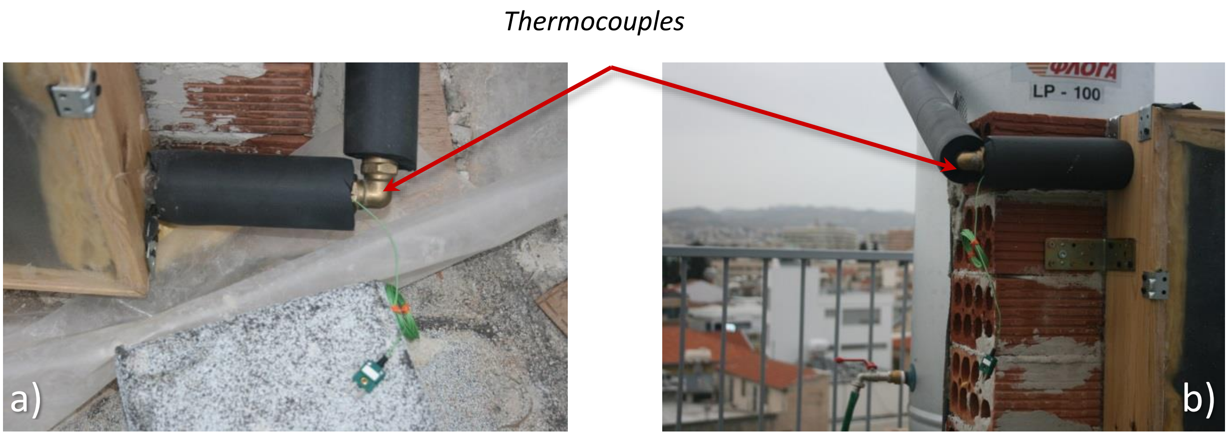

Figure 4.7.13. Installation of thermocouple at the inlet (a) and outlet (b) of the collector.

Figure 4.7.14. Installation of the pyranometer on a vertical plane.

For tests purposes, the collector was connected to a hot water tank and operated thermosiphonically. Measurements of the temperature and radiation were recorded every 30 minutes, from 8:30 until 16:00 during a clear-sky summer day with a constant ambient temperature at 21.5°C. Note that the same equipment shown in Figure 4.7.9 and Figure 4.7.10 was used. Table 4.7.6 shows the measured values of T_i, T_o, T_G, T_P, T_B and G_t.

Table 4.7.6. Experimental measurement of temperature and radiation.

Time [h]	T_i [°C]	T_o [°C]	T_G [°C]	T_P [°C]	T_B [°C]	G_t [W/m^2]
8:30	21.5	32.1	32.6	32.3	22.1	373.2
9:00	24.4	34.5	35.0	34.1	23.2	417.1
9:30	25.4	36.1	36.8	35.5	25.9	472.0
10:00	24.8	38.5	38.8	38.3	25.2	526.9
10:30	26.0	39.5	39.3	38.6	28.1	559.8
11:00	27.4	41.1	40.9	42.0	29.1	581.8
11:30	28.2	42.1	40.0	42.2	30.3	581.8
12:00	28.4	43.1	40.4	42.7	31.2	603.7
12:30	34.4	45.0	41.0	42.1	34.3	559.8
13:00	37.6	48.5	43.2	48.0	37.3	548.8
13:30	37.4	47.7	40.6	48.8	37.6	515.9
14:00	38.5	47.5	38.4	48.1	36.1	472.0
14:30	42.2	50.5	40.0	50.4	39.5	428.1
15:00	40.4	47.9	34.4	47.0	38.2	329.3
15:30	39.6	47.7	31.1	45.6	39.0	274.4
16:00	38.5	46.6	31.0	43.7	37.4	230.5

The thermal efficiency of the solar collector, η, was calculated as the ratio between the useful energy, Q_u, and the total solar energy incident on the collector, $G_t \cdot A_C$, as in Eq. (4.7.22). By the knowledge of the collector area, A_C, equal to 1.20 m^2, $G_t \cdot A_C$ is easily calculated by integrating the results of G_t, reported in Table 4.7.6. Q_u was instead obtained by discharging the storage tank and repeatedly measuring the temperature of a small quantity (i.e., 1 litre) of water coming out from the tank, until the temperature of the delivered water was equal to the inlet temperature (i.e. all thermal energy is discharged). This operation, completed late in the afternoon, allowed the assessment of the thermal efficiency of the prototype, which resulted to be about 55.7 %, very similar to that one usually found in commercial thermosiphonic systems.

The obtained experimental results were used to validate the developed simulation model for the water solar thermal prototype, by performing a comparison with those predicted by the simulation model. With the aim to simulate the thermosiphonic behaviour of the collector, the estimation of the water flow rate (in natural convection) was obtained by the experimental equation (Koffi, Andoh et al. 2008):

$$\left(1+\varphi\right)\frac{128\nu L_{cl}\dot{m}}{\pi N d^4} - g\rho\beta' \sin\theta \frac{L_{cl}}{2}\left(T_{fo}-T_{fi}\right)=0 \qquad (4.7.56)$$

where ν is the kinematic viscosity [m^2/s], L_{cl} is the collector height [m], N is the number of risers [-], d_{cl} is the internal diameter of the risers [m], ρ is the water density [Kg/m^3], θ is collector's slope [°], T_{fo} is the outlet water temperature [°C], T_{fi} is the inlet water temperature [°C]. The term φ characterizes the resistance to mass flow in the collector and the connection tubes, calculated as:

$$\varphi = N\frac{L_{cl}}{L_{ct}}\left(\frac{d_{cl}}{d_{ct}}\right)^2 \quad (4.7.57)$$

where L_{ct} is the length of connecting tubes [m] and d_{ct} is the diameter of connecting tubes [m].

The comparison between measured and predicted results of T_P and T_o is shown in Figure 4.7.15. Here, a good agreement between the hourly profiles of the plate and outlet water temperatures is observed. In particular, the differences between the simulated and experimental results, for both T_P and T_o, are averagely lower than 1°C (with the only exception of the initial and final data in the case of T_o and for the measurement of T_P at 12:30). It is worth remarking that the correct prediction of T_P and T_o is crucial in order to assess the active (i.e. thermal energy production) and passive effect (i.e. reduction and increase of space heating and cooling requirements) of the building integrated solar water thermal collector.

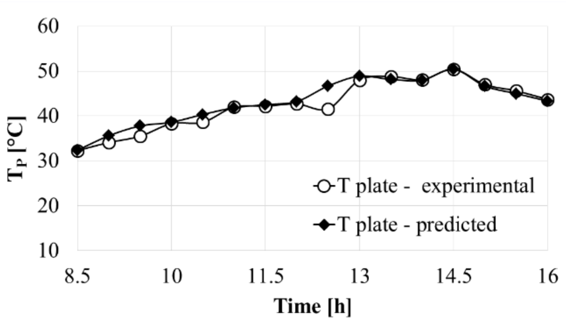

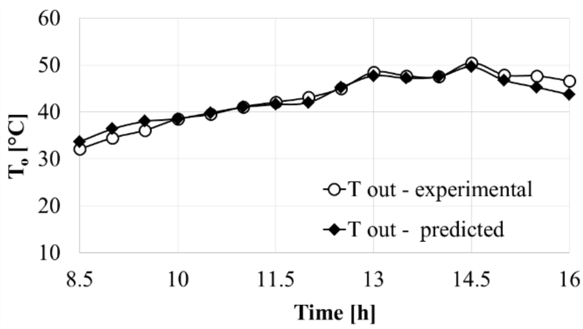

Figure 4.7.15. Experimental and simulated data of T_P and T_o.

4.7.5.3 Water prototype (serpentine configuration) - Project #1

In order to assess the passive and active effects due the building integration of existing water solar collectors on the energy performance (e.g. building thermal loads), the simulation model for the serpentine water collector was used. Such model was validated by means a comparative approach. Specifically, the simulation results relative to the collector thermal performance are compared to those obtained by a commercial water collector. Therefore, by taking into account the design and operating features of the collector, produced by Kloben - model KF25A, the efficiency curve, η, obtained by the developed simulation model was compared with the one provided by the manufacturer (i.e. data sheet). The collector is a typical flat plate solar thermal collector, with a serpentine configuration and a total surface of 2.4 m^2. All the geometrical data provided by the manufacturer are reported in Table 4.7.7. The validation is performed by considering all the possible working conditions. The comparison among the efficiency curves is shown in Figure 4.7.16. A good agreement is observed, in fact, the mean percentage variation between the manufacturer efficiency and the simulated one is averagely lower than 1%.

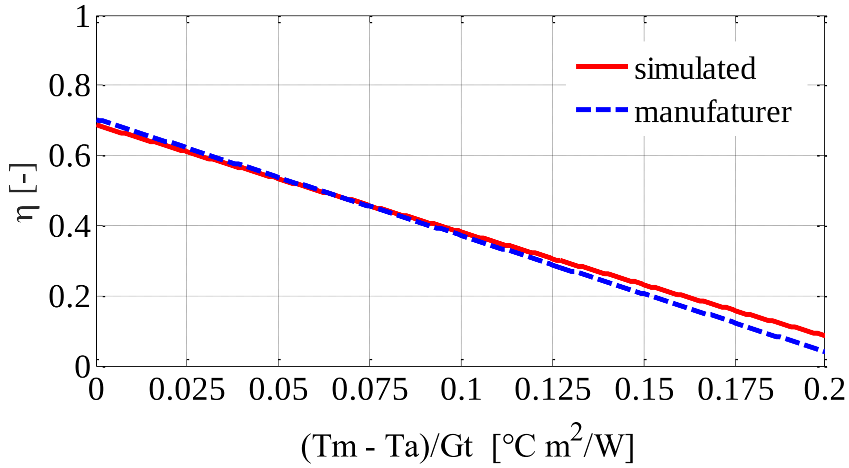

Figure 4.7.16. Comparison between Kloben® (real collector) and simulated efficiency (model).

Table 4.7.7. KF25A Kloben water solar collector - technical data.

Parameter	**Value**	**Unit**
Collector surface, A_C	2.4	m^2
Height, H	2	m
Width, W	1.2	m
Back/lateral thickness, s	40	mm
Back/lateral conductivity, k	0.03	W/m^2K
Number of curves, N	12	-
Water flow rate, ṁ	30	l/hm^2
Pipe pace, W	120	mm
Absorber plate emissivity, ε_p	0.1	-
Glass cover emissivity, ε_g	0.88	-
Pipe internal diameter, D_i	10	mm
Pipe thickness	5	mm
Absorbed radiation, τα	0.8	%

4.7.5.4 Water prototype (isosceles trapeze shape) - Project #5

The isosceles trapeze shape collector, project #5, was tested by following the standard indoor testing ISO 9806:2013 (Solar energy - Solar thermal collectors - Test methods standard). The obtained experimental results were exploited to assess the thermal efficiency of the prototype. The maximum collector nominal efficiency, measured on the indoor testing rig, is about 61.6%, as shown in Figure 4.7.17 (Visa, Duta et al. 2015). Experimental data were also used to validate the mathematical model, developed in order to: i) assess the specific constructive aspects that mostly influence the conversion efficiency; ii) implement constructive optimisation procedure of the demonstrator/prototype (Visa, Duta et al. 2015). All the experiments were performed by taking into account a wind heat transfer coefficient equal to 5 W/m^2K (i.e. under still conditions).

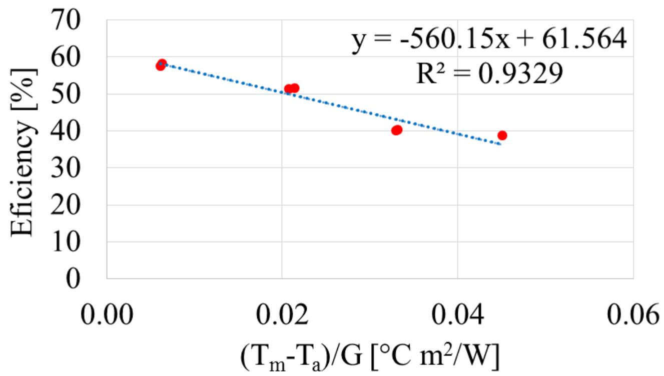

Figure 4.7.17. Thermal characteristic of the prototype with black absorber plate.

The optimization procedure, performed through the simulation model, allow designers and developers to determine the influence of constructive features on the efficiency of the novel collector. Through such sensitivity analysis, the most influencing parameters resulted to be:

- the contact between the absorber plate and the meander tubes (or the air gap);
- the use of clamps, long time before reported as responsible for large thermal losses (Duffie and Beckman 2013), when compared to tubes welded on the plate.

In order to estimate the actual thermal conductivity of the bonds in the demonstrator collector, the conversion efficiency, η, and the heat removal factor, F_R, were modelled for different values of the bond conductance, C_b in Eq. (4.7.27). The modelled η and F_R for the trapeze collector are reported in Figure 4.7.18. Here, the tube-plate bonding has an equivalent thermal conduction value of 1.25 W/m·K, corresponding to the mean experimental efficiency of 60.4%. This value was used in all the simulations in order to estimate the conversion efficiency of the collectors, η, having clamps for bonding the tubes with the plate. The obtained results are presented in
Table 4.7.8.

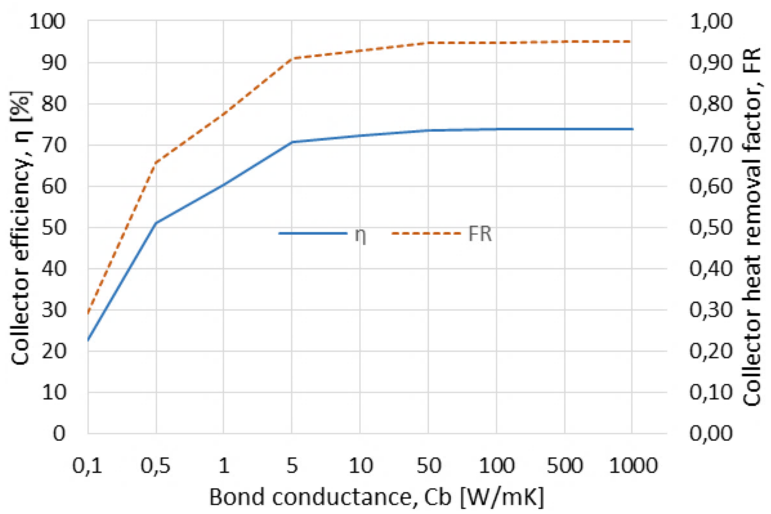

Figure 4.7.18. Modelled conversion efficiency and heat removal factor for the trapeze collector.

Table 4.7.8. Modelled U_L, F_R and η (at G_t 880 and 930 W/m^2 radiation).

U_L	**F_R [-]**		**η [%]**	
[W/m^{2}K]	880 [W/m^2]	930 [W/m^2]	880 [W/m^2]	930 [W/m^2]
3.93	0.781	0.781	60.70	60.89

4.7.6 Simulation of active and passive effects due to the building integration

In order to study the effects due to the building integration of solar collectors on heating and cooling loads and energy demands, a suitable parametric analysis was performed. Such study is based on the simulation model developed for water collectors with a serpentine shaped heat exchanger (as reported in section 4.7.4.2) by taking into account the systems described in section 4.7.2, representative of a similar commercial collector.

4.7.6.1 Building thermal loads and energy demands

In order to calculate the building energy loads and demands, with and without the solar thermal collectors, the algorithm reported on the standard ISO 13790 (Energy performance of building (ISO 2008)) is adopted. Such simulation model was opportunely modified with the aim to take into account the above mentioned solar thermal collector as an integral part of the building envelope. The obtained complete simulation model was implemented in a suitable computer code (written in MatLab). Through such tool the heating and cooling passive effects on the building of the solar collector thermal can be suitably taken into account. In particular, the higher summer cooling energy demand and the lower winter heating energy requirement vs. traditional buildings (without building integrated solar thermal collectors) can be assessed for any selected time interval. Corresponding economic analyses aiming at the investigation of the system feasibility and convenience can be easily achieved.

4.7.6.2 Case study

In order to show the potentiality of the developed simulation code a suitable case study was developed. It regards a non-residential building, consisting of a single thermal zone whose shape and geometry are reported in Figure 4.7.19. The building has a large glazed surface on the south facing wall (i.e. window to wall ratio equal to 55%); the net area suitable for the BISTS installation is of 9.4 m^2 (dark grey surface area reported in Figure 4.7.19). Three main internal heat sources are: light, people and equipment (chosen according to the selected use of the building). All the building features and the considered simulation assumptions are reported in Table 4.7.9.

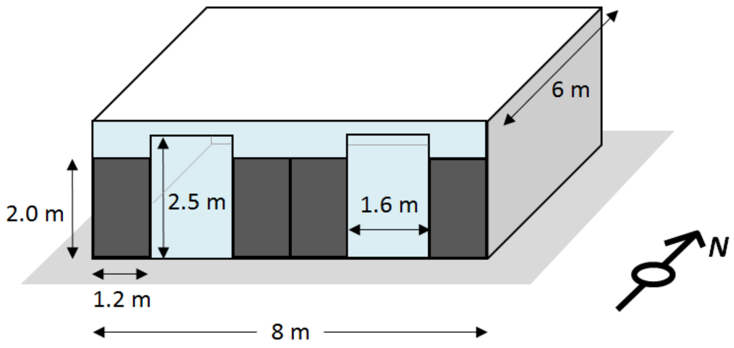

Figure 4.7.19. Case study building shape.

In order to also investigate the influence of the weather conditions on the building integrated solar thermal system, together with the effects of building thermal loads and demands, simulations were performed by taking into account several weather zones representative of various European climates, shown in

Table 4.7.10.

Table 4.7.9. Simulation assumptions.

Parameter	**Value**
Surface to Volume Ratio [%]	1.3
Floor Area [m^2]	48
Volume [m^3]	130
Heating / cooling set point [°C]	20 / 26
Occupancy [person/m^2]	0.06
South/North facing wall area [m^2]	21.6
East/West facing wall area [m^2]	16.2
Glazed surface [m^2]	12
Useful South facing wall area [m^2]	9.6
Air infiltration [vol/h]	1
Internal heat gains [W/m^2]	67
Usage time [-]	8:00 - 18:00

Table 4.7.10. Weather zones.

Weather zone	**Limassol**	**Naples**	**Dublin**	**Freiburg**	**Copenhagen**
HDD [Kd]	800	1335	1370	2966	3757
CDD [Kd]	950	833	774	287	77
ISR [kWh/m^2y]	2000	1825	1529	1470	988
Heating period	from 01/10 to 31/03	from 15/12 to 31/03	from 01/11 to 15/04	from 15/10to 15/04	Always

For each investigated weather zone the simulated U-value of the building envelope (external walls, roof, floor and windows) are reported in Table 4.7.11 (they are taken from the Italian regulation following the requirements of several standards addressing different aspects of the EPBD (CEN Brussels, 2004)). Note that such values depend on the weather area heating degree days, HDD (i.e. the higher the HDD the lower the U-value), reported in

Table 4.7.10. Here, the cooling degree days, CDD, the incident solar radiation, ISR, and the length of the heating season (defined by the HDD) are also reported. The layering layout of the opaque building components is the following:

- for the perimeter wall (from the interior to the exterior): gypsum plaster (thickness, δ, 0.015 m, thermal conductivity, λ, 0.29 W/mK, density, ρ, 600 kg/m^3, and specific heat, c_p, 1000 J/kgK), hollow brick (δ = 0.3 m, λ = 0.247 W/mK, ρ = 775 kg/m^3, c_p = 840 J/kgK) and glass whole (λ = 0.053 W/mK, ρ = 16 kg/m^3, c_p = 920 J/kgK);

- for the roof (from the interior to the exterior) and the floor (from the exterior to the interior): gypsum plaster (δ = 0.015 m, λ = 0.29 W/mK, ρ = 600 kg/m^3, c_p = 1000 J/kgK), glass wool (λ = 0.053 W/mK, ρ = 16 kg/m^3, c_p = 920 J/kgK), hollow slab (δ = 0.24 m, λ = 0.82 W/mK, ρ = 1480 kg/m^3, c_p = 840 J/kgK) and screed (δ = 0.1 m, λ = 0.23 W/mK, ρ = 600 kg/m^3, c_p = 835 J/kgK).

Note that whereas the same construction materials, for each building component (e.g. wall, roof, window), are selected for all the investigated weather zones, to obtain the required U-values different insulation thicknesses are used, reported in Table 4.7.11. Note also that a fixed insulation layer (for each weather zone) of glass wool for a U-value of 0.33 W/m^{2}K (δ = 0.07 m) is assumed for the floor. For example, purposes, in this case study no thermal insulation is modelled between the solar collectors and the wall where they are integrated.

Table 4.7.11. U-values and insulation thickness, δ.

		Zone A	**Zone B**	**Zone C**	**Zone D**	**Zone E**	**Zone F**
Wall	U-value [W/m^{2}K]	0.54	0.41	0.34	0.29	0.27	0.26
	δ [m]	0.02	0.04	0.05	0.07	0.075	0.09
Roof	U-value [W/m^{2}K]	0.32	0.32	0.32	0.26	0.24	0.23
	δ [m]	0.08	0.08	0.08	0.08	0.08	0.08
Window	U-value [W/m^{2}K]	3.70	2.40	2.10	2.00	1.80	1.60

4.7.6.3 Results and discussion

In this subsection, the main results of the parametric analysis carried out on the above described sample building located in the weather zones reported in

Table 4.7.10 are discussed. It is worth noting that the main difference occurring between the Building with solar thermal collectors Integration (BI) and without integration (Reference Building, RB), relies in the thermal loads of the South facing wall. Specifically, for the RB case, in the simulation model procedure the boundary conditions of the South wall are the forcing functions referred to the solar radiation, G_t, and to ambient air temperature T_a. For the BI case, in addition to the above mentioned ones, the boundary condition acting on the collectors area is related to the solar collector back temperature, T_B. The obtained effect due to this temperature is in general higher than the combined forcing functions (G_t and T_a) of the RB case-especially, during the central hours of the day (during both the heating and cooling seasons). As a result, for each investigated weather zone, an averagely higher energy demand for cooling and a lower energy demand for heating (the back of the collector acts as a heating system), are obtained compared to the ones of the RB system.

In order to assess the effective convenience of the BI layout, the total primary energy requirements of the building is calculated by taking into account an air-to-air heat pump / chiller, with a nominal COP / EER equal to 3 and 2.5, respectively. Note that obviously the calculated yearly primary energy demands also depend on the length of the heating and cooling seasons of the considered climate zones. Note also that for each investigated zone the length of the related heating season is reported in

Table 4.7.10, whereas, the duration of the cooling period is scheduled for the remaining months of the year. The obtained results for the calculated yearly primary energy demands, for all the investigated zones and for the BI layouts are reported in Figure 4.7.20.

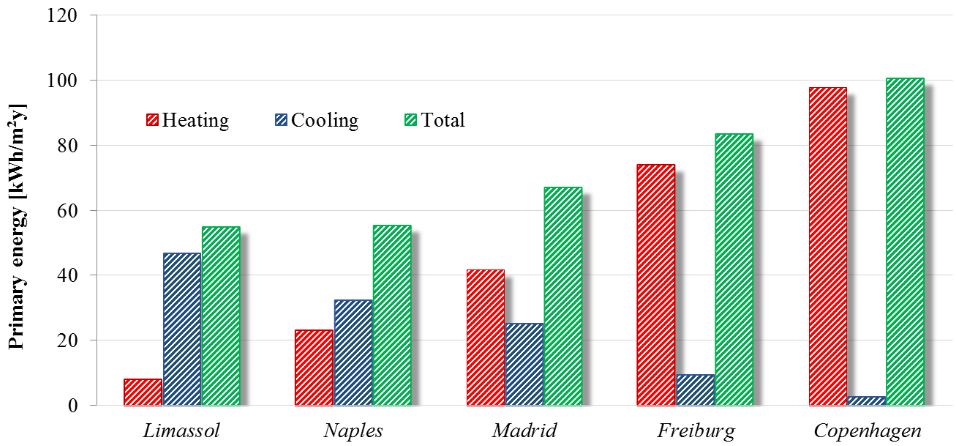

Figure 4.7.20. Primary heating, cooling and total energy demands for the BI layout.

Among the investigated weather zones, the lowest heating and the highest cooling primary energy demands are observed in Limassol, as expected. Conversely, in Copenhagen a zero need of cooling, and a maximum heating demand are detected. The passive effects due to the building integration of solar collectors on the heating and cooling demands can be assessed by comparing the simulation results obtained for the RB vs. the BI layouts. For all the investigated weather zones, comparisons between RB and BI results in terms of heating, cooling and total primary energy demands are shown in Figure 4.7.21. Here, it is possible to observe that during winter, the building integration of solar collectors leads to a heating energy saving effect. In particular, the higher the HDDs, the lower the heating demands. This benefit is inherently balanced by the occurring undesired overheating effect achieved during the cooling season (as expected).

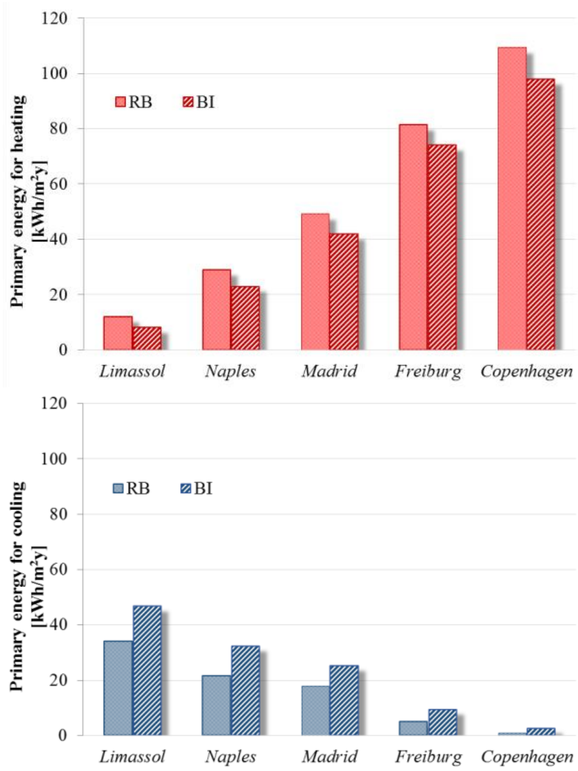

Figure 4.7.21. Primary heating and cooling energy demands for BI and RB layouts.

The building integration of solar collectors leads to a net primary energy savings only in Freiburg and Copenhagen, being the reduction of the heating primary energy higher than the increase of the cooling one (Figure 4.7.22). Conversely, for cooling dominated weather zones, such Naples and Limassol, the over-heating effects due to the building integration configuration of solar collectors lead to an increase of the total yearly primary energy demands (i.e. equal to 18.8% in Limassol and 9.4% in Naples). Finally, in Madrid, the calculated reduction of the heating demand exactly counterbalances the increase of the cooling one.

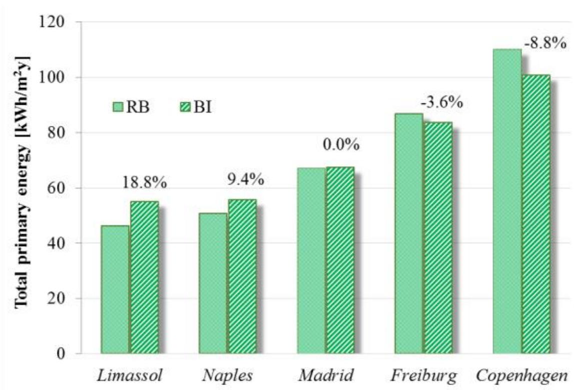

Figure 4.7.22. Total primary (heating plus cooling) energy demands for BI and RB layouts.

REFERENCES

CEN EN ISO 13791 - 13792. Thermal performance of buildings – Calculation of internal temperatures of a room in summer without mechanical cooling. General criteria and validation procedures - Simplified Methods. European Committee for Standardizations, Brussels, 2004.

Duffie, J. A. and W. A. Beckman. Solar engineering of thermal processes Forth Edition., 2013.

Hollands, K. G. T., T. E. Unny, et al., Free convection heat transfer across inclined air layers. Journal of Heat transfer, 1976.

Incropera, F. P. and D. P. Dewitt. Foundamentals of heat and mass transfer Seventh Edition, 2011.

ISO 13790:2008 Energy performance of buildings -- Calculation of energy use for space heating and cooling, 2008.

Kalogirou, S. Solar energy engineering processes and systems. Second Edition, 2014.

Koffi, P. M. E., H. Y. Andoh, et al., Theoretical and experimental study of solar water heater with internal exchanger using thermosiphon system. Energy Conversion and Management, 2008; 49(8): 2279-2290.

Shewen, E., K. G. T. Holiands, et al., Heat transfer by natura convection across a vertical cavity of large aspect ratio. Journal of Heat transfer, 1996.

Visa, I., A. Duta, et al., Design and experimental optimisation of a novel flat plate solar thermal collector with trapezoidal shape for facades integration. Applied Thermal Engineering, 2015; 90: 432-443.

Winterton, R. H. S., Where did the Dittus and Boelter equation come from? International Journal of Heat and Mass Transfer, 1998; 41(4–5): 809-810.

Zhang, H.-F. and Z. Lavan, Thermal performance of a serpentine absorber plate. Solar Energy, 1985; 34(2): 175-177.